Phase Behavior of Colloidal Monolayers on One-Dimensional Periodic and Quasiperiodic Light Fields

Von der Fakultät Mathematik und Physik der Universität Stuttgart
zur Erlangung der Würde eines Doktors der Naturwissenschaften (Dr. rer. nat.)
genehmigte abhandlung

vorgelegt von

Lamiss Zaidouny
aus Al-Klayaa (Libanon)

Hauptberichter: Prof. Dr. Clemens Bechinger
Mitberichter: Prof. Dr. Hans-Reiner Trebin
Tag der mündlichen Prüfung: 26. Januar 2015

Physikalisches Institut der Universität Stuttgart
2015

Contents

Zusammenfassung

In dieser Arbeit beschäftigen wir uns mit dem Verhalten zweidimensionaler, repulsiv wechselwirkender kolloidaler Systeme in Anwesenheit von eindimensionalen Potentialen mit periodischen sowie quasiperiodischen Linienabständen. Experimentell werden diese Potentiale durch eine gerasterte optische Pinzette realisiert. Dabei lassen sich neben der Potentialtiefe auch der Abstand der Linien kontinuierlich variieren. Für den Fall von eindimensional periodischen Liniengittern beobachten wir die Entstehung zweidimensionaler Kristalle mit unterschiedlichen Kristallstrukturen. Diese resultieren aus dem Wechselspiel der repulsiven Teilchenwechselwirkung und der Wechselwirkung mit dem Laserpotential. Für den Fall einer quasiperiodischen Anordnung der Laserlinien beobachten wir mit steigender Linienstärke einen stetigen Übergang von einem eindimensionalen Kristall zu einem Quasikristall. Interessanterweise finden wir bei diesem Übergang eine periodische Übergangsstruktur (periodic average structure, PAS). Solche PAS wurden bereits vor vielen Jahren theoretisch vorhergesagt und sind mit dem quasiperiodischen Liniengitter über eine eindeutige, bijektive Abbildung verknüpft. Unsere Experimente zeigen, dass die Umwandlung von periodischen in quasiperiodische Strukturen bereits durch minimale Teilchenverschiebungen realisiert werden kann. Ferner zeigen unsere Experimente, dass die entstehenden PAS äußerst robust gegenüber der Potentialtiefe und der Teilchendichte sind. Da die kolloidalen Wechselwirkungen rein repulsiv und isotrop sind, belegt dies, dass die Bildung von PAS nicht auf atomare Systeme beschränkt ist, sondern diese auch bei vielen andereren Materialien sowie Längenskalen auftreten sollten.

Introduction

Order in matter has continuously been an interesting phenomenon for many centuries. It started as a mystery about the snow flake six-fold symmetry and lead to the basic rules of crystallography. Although the concept of crystallography describes a periodic crystal as the ground state of matter, this belief shattered when aperiodic structures were discovered. It started when modulated structures (incommensurate or commensurate) were detected in 1960s, till later quasicrystals were discovered in the 1980s [1, 2] leading to a new definition of crystals. In general, ordered structures follow from the self assembly (AS) of particles interacting via specific and local interactions. AS has been observed in a variety of systems ranging from the atomic to mesoscopic scales where liquid to crystal transitions can be induced by gravitational, entropic, magnetic, electrohydrodynamic and convective forces [3, 4].

On the other hand, epitaxial growth of monolayers has been a useful technique for inducing periodic and quasiperiodic order in matter. By this method particles are adsorbed on a surface which transfers its intrinsic structural properties to the deposited monolayer. For example, this found interest in growing silver and Xe films on a quasicrystalline AlPdMn and AlNiCo surfaces respectively [5, 6]. Though diffraction techniques are used to characterize the adsorbate properties, it is still not fully understood how this structure is related to the underlaying surface.

Studying the phase behavior of colloidal suspensions in the presence of periodic and quasiperiodic laser fields can bring insight into new fundamental phenomena based on the principle of thermodynamics and condensed matter physics. Due to the analogy in their physical properties, colloidal systems serve as model for atomic systems and hence provide explanations for basic physical problems. Colloidal suspensions have building blocks that are easily accessible by tuning their interactions, size and shape, surface chemistry and concentration. Colloids can take the form of any state of matter, have mesoscopic size with thermal properties and time scales (ms-s) that can be studied under real space conditions. This allows quantitative understanding of a rich variety of phase transitions in experimental and theoretical studies.

In the first part of this thesis, we study in real space, the phase behavior of colloidal monolayers in the presence of 1D periodic light field potentials. We create such light fields by reflecting a laser beam on a galvano-statically driven mirror which allows the variation of the periodicity without optical

realignments. Previous work in this direction has found attention in freezing and melting phenomena [7], where a 2D liquid transforms, on a 1D interference pattern with periodicity close to the inter-particle distance, into a crystal due to induced thermal fluctuations and melts again into a modulated liquid at strong light fields. In contrast to aqueous systems, here we use an organic suspension of silica particles and bromobenzene. This system has a Debye screening length of about 4.6 µm and results in the formation of crystals with lattice constants up to 20 µm. In contrast to aqueous suspensions, such large distances help to realize a wide range of line spacings relative to the lattice constants. Because the refractive index of bromobenzene is larger than that of the colloids, optical gradient forces lead to the attraction of particles at regions where the intensity is smallest. Depending on the depth and periodicity of the optical potential, we observe the transition of a triangular crystal (formed in the absence of light fields) into a square (or rhombic) structure by passing through an intermediate disordered phase. The latter results from dislocations that appear [8] when optical forces start breaking the crystal symmetry by rapturing pair particle interactions. This is in agreement with observations in 2D vortex lattice of superconductors [9]. At high laser potential strength the colloidal system acquires a crystal symmetry of a square (or rhombic phase) commensurate with the light potential.

In the second part of this thesis, we experimentally study the phase transition of a colloidal monolayer (aqueous suspension) on 1D quasiperiodic light pattern. Such substrates are formed of two or more length scales closely related for example to Fibonacci or Dodecanacci sequences. Upon increasing the laser intensity, we observe a transition from a periodic to a quasiperiodic phase. Interestingly, this transformation proceeds via the formation of an intermediate periodic average structure (PAS) which is related to quasicrystals by 1-1 mapping [10]. We show that PAS can transform to crystals and quasicrystals by minute particle displacements. This in turn provides a mechanism to allow for interesting insights into the relationship between periodic and quasiperiodic order. Although numerical comparison between measured and calculated diffraction patterns provides some evidence for the occurence of PAS [11], periodic average structures have not yet been observed in real space experiments. In contrast to atomic systems, where quasiperiodic order is the sole result of the inter-atomic forces, here quasiperiodic order is imposed by an external potential acting on the colloidal particles. This allows the use of systems interacting with simple and isotropic pair potentials and thus to study the generic conditions under which such phase transitions can occur. At a fixed laser intensity and length scales of the substrate, we measure a complete phase diagram of the colloidal monolayer as function of density. A smooth transition takes place from a 2D triangular crystal at high densities,

passing by 1D periodic phase (PAS) for a range of intermediate densities, to quasicrystalline phase at low particle concentrations. Apparently, the PAS phase is a result of the competing forces of the periodic pair potential and the quasiperiodic light field.

All in all, in this thesis we have studied experimentally the phase behavior of a colloidal monolayer on 1D periodic and quasiperiodic light fields. We learn that a colloidal crystal undergoes a rich variety of order-order or order-disorder phase transformations. Such phases result from the interplay between electrostatic pair-interactions and optical forces. On 1D quasiperiodic substrates we have observed the formation of periodic average structures during crystal to quasicrystal transitions. We conclude that PAS serves as a link between both structures and indicates that such transitions are achieved by minute particle displacements. For different quasiperiodic light fields PAS was observed, meaning that such structures are expected to form in systems where periodic and quasiperiodic forces are present.

Part of this work have been published already:

1. L. Zaidouny, T. Bohlein, R. Roth, and C. Bechinger. Light-induced phase transitions of colloidal monolayers with crystalline order. Soft Matter, 9(38):9230-9236, 2013.

2. L. Zaidouny, T. Bohlein, J. Roth, and C. Bechinger. Periodic average structures of colloidal monolayers. Soft Matter, 10(43):8705-8710, 2014.

1 Periodic and quasiperiodic order

1.1 Introduction

"*A crystal is any solid having an essentially discrete diffraction diagram...*" . This definition given by the International Union of Crystallography in 1992, and generalized to include periodic and aperiodic crystals, came after the discovery of quasicrystals by Daniel Shechtman 1982 [1]. This chapter kicks off with a historical overview on the discoveries of aperiodic structures and then deepens into detailed description of their classes and properties (diffraction patterns, description in space of higher dimensions ...). Aperiodic crystals include two classes: first, quasi-periodic structures (quasicrystals) which do not exhibit periodic translational symmetries [12] and do not obey the crystallographic rules of periodic lattices. Here, we specifically consider the geometrical construction of 1D quasicrystals in higher dimensions. Second, those structures which obey the crystallographic rules like the composite structures (CS) and the incommensurate modulated structures (IMS) [13, 14, 15] within which a class of periodic phases called Periodic Average Structures (PAS) is introduced. Although crystalline and quasicrystalline phases were discovered in metallic alloys, they are also abundant in soft matter systems. In this respect, here we show examples of soft crystals and quasicrystals where particle arrangements are observed on the mesoscopic scale.

1.2 Historical overview of aperiodic structures

Due to its interesting structural symmetry and morphology, the snow flake attracted most attention in crystallography in the seventeenth century. In 1611 Johannes Kepler wrote his *On the six-cornered snowflake* trying to explain its six fold symmetry, while René Descartes in 1634 and Robert Hook in 1665 studied their structures and morphologies. Shortly after the French revolution in the 1790's, René Just Hay described regularly shaped crystals as being made out of smaller symmetrical units, but omitted the icosahedra since the five fold symmetry is not allowed in crystals. From this description the law of rational indices followed. This law states that miller indices have integer coordinates.

Based on the idea that microscopic periodic arrangements of unit cells is the basis of macroscopic symmetry, Auguste Bravais was able to derive 14 classes

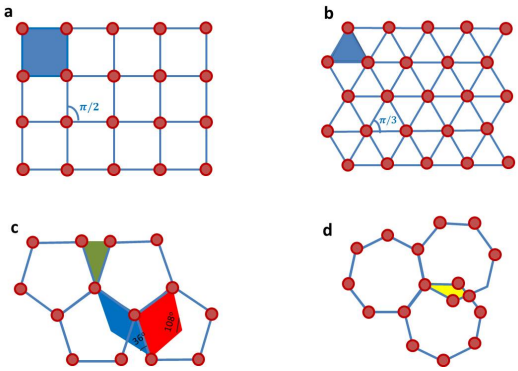

Figure 1.1: ***Two dimensional periodic and quasiperiodic structures***. *A periodic crystal is made by filling the space with one regularly shaped unit cell such as a square a) triangle or hexagon b). In Contrast, filling the space with one unit cell like a pentagon leads to empty regions as shown in green in c) or like a heptagon which leads to overlapped region (yellow) as shown in d). Quasicrystals can be build from two or more unit cells as for example in figure c) where the combination of a thin rhombus (blue) and a thinker one (red) fill the space according to specific matching rules.*

of lattices based on pure geometry. But it was till 1890 when the mineralogist Evgraph Fedorov and the mathematician Arthur Schoenflies derived fully the 230 Euclidean space group symmetry of periodic patterns in three dimensions [16] and till 1912 to experimentally prove the concept of microscopic symmetry after the discovery of X-ray diffraction of crystals by Max von Laue. The latter won in 1914 the Nobel prize for this discovery [17]. That was the beginning of a belief that it is only the periodic arrangement of atoms and molecules that construct the ground state of matter. This means that an ideal crystal can be described by one of the 230 space groups which result from 14 Bravais lattices and 32 point groups known now as the crystallographic rules of symmetry. Note that a space group is a distance-preserving transformation, also called the Eucleadian group of symmetry which includes translation and point space groups. The latter includes rotation, reflections and their combinations.

In this context, a periodic crystal can be built from the periodic stacking of a regularly shaped unit cell that can fill the space by repeating it self upon translation or point rotations with 2,3,4 or 6 fold symmetry, see for example Fig. 1.1(a&b). This rule of construction is not true for 5,7,8,10 or 12 ... etc fold symmetry, since this leaves the space with either empty regions (shown in green) in Fig. 1.1(c) or overlaps (yellow region) as illustrated in Fig. 1.1(d).

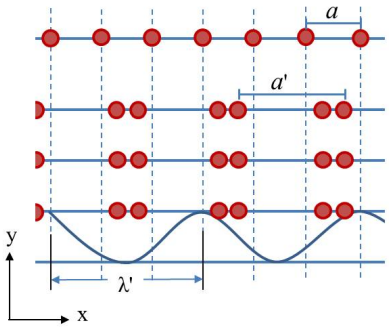

Figure 1.2: *A commensurate modulated crystal with a periodicity* $\boldsymbol{a}'>\boldsymbol{a}$ *is formed when the basic crystal is disturbed by a displacive modulation* $\lambda' = 3\boldsymbol{a}$ *in the x -direction. The conventional crystal shown here is a two dimensional square structure with lattice constant* $\boldsymbol{a}$ *and for simplicity only one chain is shown at the upper part of the figure.*

Therefore, the latter symmetries were forbidden from the crystallographic description of ideal crystals.

The answer for this tiling problem was first solved by Sr. Roger Penrose in 1974 [18]. He constructed a set of two tiles and put them together according to specific matching rules which restricts the ways neighboring tiles are joined [19]. As a result, an aperiodic (non-periodic) tiling which is known now as the Penrose tiling, is formed. Fig. 1.1(c), illustrates a similar construction where two rhombi, one is thin with an angle of 36˚(blue color) and the other is thick with an angle of 108˚(red color), are stacked together to fill the space. Many algorithms [20] and theories [19] were established after this work which widened the scope within which quasiperiodic order is described. But 15 years before the concept of constructing quasicrystals, aperiodic structures with long range order were discovered in their ground state. In 1960s magnetic spin waves showed different periodicities other than their underlying lattice [21]. Another example is Thulium which is also a modulated antiferromagnetic structure, revealed magnetic satellite peaks in the diffraction pattern at a temperature below 56˚K [22]. The spin periodicity is defined as $S(\mathbf{r})=f(\mathbf{q}.\mathbf{r})$, where $\mathbf{r}$ is the position vector of the atom in the crystal, $\mathbf{q}$ is the modulation vector and f has a period 1. Few years later it was observed that the lattice periodicity of a crystal can be destroyed due to displacive waves. In 1964, de Wolff studied the diffraction patterns of distorted structures of anhydrous Na_2CO_3 at room temperature [23] which showed by neutron and

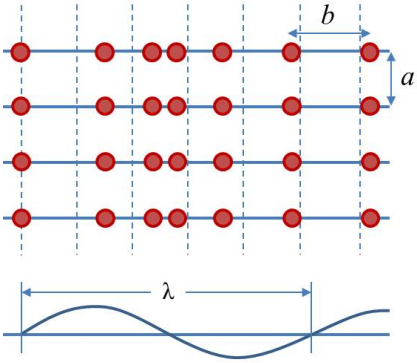

Figure 1.3: *Incommensurate modulated structure where atoms are periodically displaced from the conventional crystal of Fig.2.2, along the direction of the disturbing wave.*

X-ray diffractions that the Bragg peaks are positioned at distances that vary depending on the temperature of the crystal [24]. In this work De Wolff observed structures that are no longer periodic, but rather have satellite peaks with irrational indices (satellites positions are incommensurate with the main reflections). Therefore this aperiodic structure is given the name incommensurate modulated structure (IMS). On the other hand, if the satellite peaks have rational indices (i.e satellite peaks commensurate with the main reflections) then the distorted structure is called a commensurate modulated one (CMS) [14]. The latter was first observed in metastable alloys like Cu-Ni-Fe which were known to have long periods [25, 26] and in copper aluminum metals which were discovered by Sato and Toth 1961 [27].

Another description for IMS and CMS was given by Jamieson et al. 1969, which says that a modulated structure is simply the basic structure plus a modulation with a period λ. If λ fits (or a multiple of) the lattice periodicity of the basic structure of period a then the result is another periodic phase but with a larger periodicity than a (Fig. 1.2), otherwise it forms an aperiodic structure as shown in Fig. 1.3. Incommensurate modulated structures are generally found in all materials; alloys, ionic and molecular crystals, Ferroelectrics, and superconductors. Their origin is frustration or competition among two or more favored periodicities.

If satellite peaks in the diffraction pattern were not taken into account then the structure is rendered as the average structure [14]. Because this structure shares significant symmetrical properties with the basic ones it was a

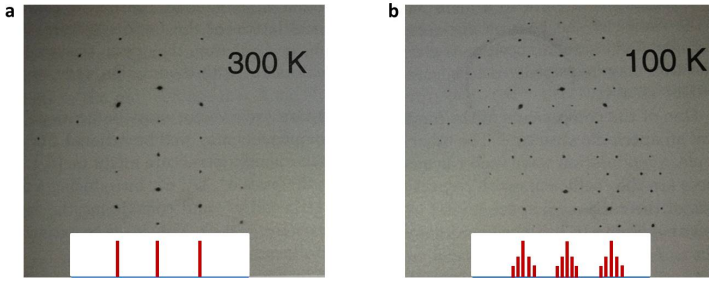

Figure 1.4: *Diffraction pattern of a conventional crystal a), and a modulated structure b). The intensity distribution of reflections is shown in the histogram at the bottom of the each figure. In a) even distribution of intensity are observed with sharp peaks, while in b) several intensity lines indicate the existence of satellite peaks around the main reflection.*

useful concept for understanding the relation between periodic and quasiperiodic ordering [10, 28, 29] and therefore can bring an insight into the process of crystal-quasicrystal transitions [30]. Average structures were observed in atomic systems [11, 31, 32] as well as in colloidal systems [33]. Geometrical description of average structures is discussed in a later chapter.

Another type of crystals whose construction does not fit the 230 group symmetries is the incommensurate composite structures (CS). It is a compound that has a one structure which acts as a host for another one. This composition adds stability to the host structure. In 1980, Janner and Janssen discovered the composite $Hg_{3-\delta}AsF_6$, in which AsF_6 octahedra acts as a host to chains of Hg atoms having an incommensurate periodicity with the host lattice.

Till 1980 the above mentioned two types of aperiodic crystals were found and they cannot be described by any of the 230 space groups of crystallography. In 1982 the first evidence of quasicrystals, was discovered by Daniel Shechtman. He found that the diffraction pattern of a rapidly quenched Aluminum Alloy (AlMn) has quasi-periodic distribution of Bragg peaks with an icosahedral symmetry which is a point group that forbids lattice periodicity in three dimensions. The fairly narrow Bragg peaks in this discovery (Fig. 1.5) revealed a non-periodic atomic arrangement indicating a long range quasiperiodic positional order and lack of translation symmetry. In the same year Levine and Steinhardt predicted theoretically quasiperiodic ordered structures with forbidden space group symmetries. Such study supported the tiling theory established by Roger Penrose in 1974 [18, 34], and the optical experiments

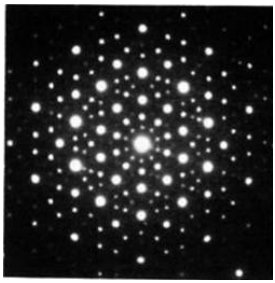

Figure 1.5: *Diffraction pattern of AlMn alloy. Sharp Bragg peaks are observed with a quasiperiodic distribution with 10 fold point symmetry [1].*

made by Mackay in which he illustrated a five fold diffraction pattern for the Penrose tiling.

The difference between quasicrystals and modulated structures is observed in the diffraction patterns where the former is densely filled with sharp Bragg peaks as shown in Fig. 1.5, while in the latter it is possible to identify a lattice with main reflections and satellites as illustrated by Fig. 1.4.

1.2.1 Diffraction patterns of ordered structures

As mentioned earlier, the unit cell of an ordered crystal describes its entire structure with space group symmetries that leave the space invariant under transformations like translation, point symmetry operations (rotation, reflection, inversion) or the combination of both. In 3D the position of an atom is given by

$$\mathbf{r} = n_1\mathbf{a} + n_2\mathbf{b} + n_3\mathbf{c} \tag{1.1}$$

n_1, n_2 and n_3 are integers and $\mathbf{a}$, $\mathbf{b}$ and $\mathbf{c}$ are the basis vectors constituting the unit cell and spanning the whole structure. As a result, the structure is invariant under a symmetry transformation (e.g rotation $\mathbf{R}$ and translation $\mathbf{T}$) and the particle density satisfies the relation

$$\rho(\mathbf{r}) = \rho(\mathbf{R}\mathbf{r} + \mathbf{T}) \tag{1.2}$$

In the Fourier space, Bragg peaks describe the atomic positions in real space through the wave vector $\mathbf{k}$ which is also invariant under Euclidean transformations such that

$$\hat{\rho}(\mathbf{k}) = e^{2\pi i \mathbf{R}\mathbf{k}\cdot\mathbf{T}}\hat{\rho}(\mathbf{R}\mathbf{k}) \tag{1.3}$$

Equation 1.3 leads to a measurement for the intensity of Bragg peaks according to

$$I(\mathbf{k}) = |\sum_j e^{2\pi i \mathbf{k}.\mathbf{r}_j}|^2 \tag{1.4}$$

with r_j being the position of atoms in one unit cell of the periodic crystal (monoatomic crystal in this case). This parameter helps identify a structure by distinguishing satellites that are generally spread around the main reflections and have, in general, weaker intensities. This is illustrated in Fig. 1.4a, where the diffraction pattern of a conventional crystal of bis(4-chlorophenyl)sulfone shows periodic distribution of Bragg peaks with a six fold symmetry at 300°K and transforms under temperature variation into a modulated one. The diffraction pattern of the latter has main reflections with the same distribution as the original but with additional peaks around them which have relatively weak intensities (Fig. 1.4b) and space distribution given by:

$$\mathbf{H} = h\mathbf{a}^* + k\mathbf{b}^* + l\mathbf{c}^* + m\mathbf{q} \tag{1.5}$$

h, k, l and m are integers while $\mathbf{a}^*$, $\mathbf{b}^*$ and $\mathbf{c}^*$ are the basic vectors in the reciprocal space. For a 1D incommensurately modulated structures $\mathbf{q}=\gamma\ \mathbf{c}^*$ is the position vector of the satellites with γ depending on the modulation strength. If γ is an irrational number (i.e the modulation period is not commensurate with the basic lattice constant) then it results in an aperiodic structure. For example the diffraction pattern of modulated structure γ-Na_2CO_3 diffraction pattern which was studied by De wollfs and colleagues [23] showed satellites with indices given by $\mathbf{q}=\alpha\ \mathbf{a}^*+\gamma\ \mathbf{c}^*$ with $\alpha \approx 0.182$, $\gamma \approx 0.318$ and vary depending on the temperature of the crystal [24].

1.2.2 Description in higher dimensions (case of 1D quasicrystals)

De Wolff in 1972 figured that diffraction peaks of a 3D aperiodic structure can be described by four reciprocal vectors (Eq. 1.5) which are related to the three basic lattice vectors in real space. Therefore, it is convenient to describe an n-dimensional crystal with one-dimensional incommensurate modulation as an n+1-dimensional periodic structure called hypercrystal embedded in an abstract space, of which the physical space is a subspace. By this way, a quasiperiodic density function can be obtained by the projection of the lattice sites of the higher dimensional structure into the physical space.

This is simple to understand for a Fibonacci sequence which has two length scales, L for large and S for small segments, with length distributions best explained by the inflation rule $L \rightarrow LS$ and $S \rightarrow L$, and is obtained by the ***projection method***. The latter is illustrated in Fig. 1.6, where an aperiodic

array of atoms in 1D is obtained from a 2D lattice in X and Y which have a density function of the form:

$$\rho(x,y) = \sum_{n,m} \delta(x - na) + \delta(y - ma) \tag{1.6}$$

with a being the lattice constant, n and m are integers and (x,y) are the particle coordinates of the embedded lattice in X and Y directions, respectively [1]. Another frame of coordinates ($X^{\parallel}$,$X^{\perp}$) is introduced with a rotation of angle θ with respect to (X,Y). $X^{\parallel}$ has the most interest since it represents the physical space onto which the quasiperiodic sequence is projected, and $X^{\perp}$ is its orthogonal ally. An acceptance domain, which is a section in the hyperspace, is defined by two thick lines with width D and makes an angle θ' with respect to X-axis Fig. 1.6a in such a way that all its lattice sites are projected onto the physical space. The projection is made along the horizontal and vertical dashed lines thus forming a 1D sequence of L and S segments. If cotθ' is irrational then an aperiodic sequence is obtained. In the specific case where θ'=θ, and cotθ'=τ with $\tau = (1 + \sqrt{5})/2$ then the result is a Fibonacci sequence. Such aperiodic distributions of lattice sites exhibit no regions which have the same global environment although there exists an infinite number of identical local environments. This property of quasicrystals is called local isomorphism (LI). Two quasicrystals are said to belong to the same LI class if the local configuration of unit cells in one occurs in the other. [12].

In the case where cotθ' is an approximation of τ then a different structure called the approximant of the corresponding quasicrystal is obtained. An approximant is characterized by a periodic structure with a large unit cell which has a local atomic distribution (of L and S segments) that "closely approximates" the atomic arrangement of the corresponding quasicrystal. This can be also evident in the diffraction patterns of the approximants that show dominant peaks which have the same positions as those of the associated quasicrystal. The higher the order of approximation the more difficult it becomes to distinguish a quasicrystal from its approximant. If the approximation is a rational number, e.g cotθ'=2/3 then a rational approximant is obtained.

A more general method which is used to construct aperiodic structures, assigns extended objects (atomic surfaces) of length D to the atomic basis of the hyperlattice. This is called the ***section method*** illustrated in Fig. 1.6b where the physical space forms a one-dimansional ***cut*** in the two-dimensional periodic lattice. Again if cotθ is an irrational number then the intersection points between the atomic surfaces and the physical space have an aperiodic distribution. In the case of sequences other than the Fibonacci, for example a

[1] a=b in case of a Fibonacci sequence which requires a square embedded lattice

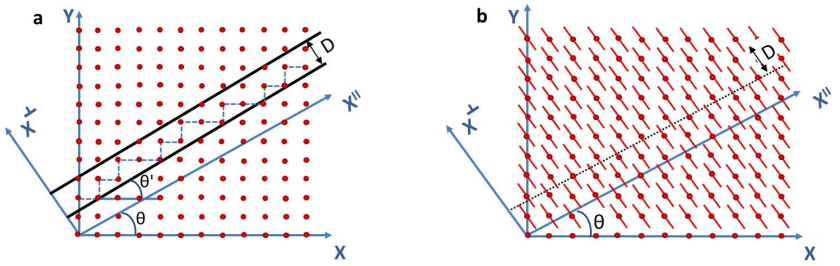

Figure 1.6: *Methods by which a Fibonacci sequence is obtained from a square lattice in higher dimensional space. The projection method in a) requires that lattice points in an accpetance domain which have boundaries indicated by two heavy lines (black) are projected onto $X^{\parallel}$, along the horizontal and vertical dashed lines thus forming L and S segments along $X^{\parallel}$. In b) the section method describes the hyperlattice with lattice points represented by extended objects that intersect $X^{\parallel}$. The dashed line in the hyperspace represents a shift of $X^{\parallel}$ along the $X^{\perp}$.*

Dodecannaci sequence, a rectangular hyperlattice with $\arctan(\sqrt{2}/(\sqrt{3}+1))$ is chosen. This will be discussed in details in chapter 5.

Phasons and phonons

Distortions of a quasiperiodic lattice that cause atomic displacements and translations along one direction or might cause unit cell deformations (physical strain), are called ***phonons***. They can be understood from Fig. 1.6a where atomic displacements occur along the physical space $X^{\parallel}$, leading to a diffraction pattern with broadened peaks. On the other hand, distortions that cause the redistribution of L and S segments while preserving the same quasicrystal physical properties, are called ***phasons***. They can be seen by a rigid shift of either the acceptance domain Fig. 1.6a or the physical space (dashed line in Fig. 1.6b) along $X^{\perp}$.

1.2.3 Dodecanacci sequence

Description of quasicrystals in the hyperspace is considered important in the sense it can be generalized to describe all types of quasicrystals in all dimensions. Therefore, apart from the Fibonacci sequence we discuss the Dodecanacci which can be described by two length scales L and S but with $L/S = \tau_{Dod} = (1+\sqrt{3})/2$. The extension of the Dodecannaci in 2D leads to a Do-

decagonal quasicrystal characterized by a 12 fold rotational symmetry. The

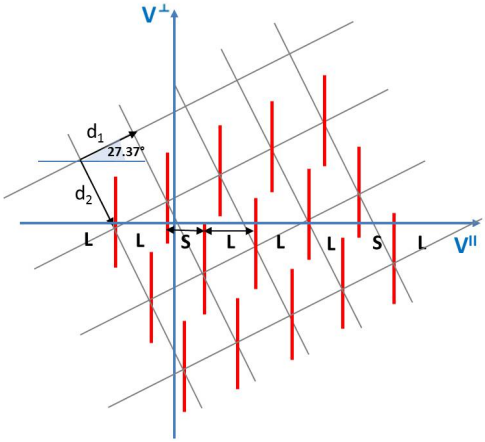

Figure 1.7: *The 2D hyperspace ($V^{\parallel}$,$V^{\perp}$) is spanned by the unit vectors $\boldsymbol{d}_1$ and $\boldsymbol{d}_2$ that define a rectangular unit cell which is rotated by $\theta = arctan(\sqrt{2}/(\sqrt{3}+1)) \approx 27.37°$. The vector $\boldsymbol{d}_1$ is a factor $\sqrt{2}$ longer than $\boldsymbol{d}_2$. The Dodecanacci sequence is obtained by the intersection points of each of the two red vertical bars (hyper-atoms) with the $V^{\parallel}$-axis.*

atomic surfaces lead to an aperiodic sequence when cut with physical space. A shearing of the embedding space parallel to physical space such that the atomic surfaces become vertical leads to the 1D quasicrystals. In the simple case of a one-dimensional sequence embedded periodically in two dimensional space, a square lattice is used as the support of the atomic surfaces as shown in Fig. 1.6b. In that case, the frequency of the tiles and their length fraction has to be equal. For the one-dimensional quasiperiodic structure discussed here and described in Fig. 1.7, this requires a rectangular lattice (See also [19] for the general case). The basis vector $\mathbf{d}_2$ has to be $\sqrt{2}$ longer than the basis vector $\mathbf{d}_1$, and the fraction of N_L/N_S : L/S is 2. The length of the atomic surface can be chosen as $L+S$, and the length of the tiles as L and S. The inclination angle of the supporting rectangular lattice with respect to the physical space must be $\theta = 27.368$ or $arctan(\sqrt{2}/(\sqrt{3}+1))$.

The Dodecanacci sequence is derived from a dodecagonal square-triangle tiling. Such tilings are not unique with respect to tile arrangements and vertex frequencies; many different constructions exist. For the present realization we refer to the tiling variant given by Hermisson et al. [35]. If the vertices of this tiling are projected onto a line parallel to a tile edge, a sequence with 3

distances is created: L of length $(\sqrt{3}+1)/2 = 1.366$, S of length 1, and L-S of length 0.366. Since the latter distance is very short it can be eliminated (the position of the particles fluctuate, thus would smear out the distance anyway). It turns out that the short L-S-distance is always neighbored by two S-distances. This allows us to move the vertices at the end of the short distance, where the occupancy is lower, to the other end. Therefore creating a new L,S-sequence instead of the S,L-S,S-sequence. The new quasiperiodic sequence contains only L and S distances with a relative frequency of $N_L/N_S = (\sqrt{3}+1) : 1$. A simple formula to generate the sequence was given by Socolar et al. [36]. The position of the N-th vertex is given by:

$$x_N = S(N + \alpha + N/\rho * int(N/\sigma + \beta)) \tag{1.7}$$

with $L = S(1 + 1/\rho)$ and $N_L/N_S = 1/(\sigma - 1)$, σ is an irrational number, α and β are arbitrary parameters, int is the integer part.
In general, 1D quasiperiodic sequence can be extended into two and three dimensions, and can be described by periodic lattices in the hyperspace as explained before. For example dodecagonal and octagonal quasicrystals are described by a hyperlattice of dimension four while an icosahedron is embedded with a six dimensional crystal. On the other hand, a planar quasicrystal which is a formed of the periodic stacking of quasi-periodic monolayers can be described by a dimension $\phi(n)$ called Eulers totient function, where n is the symmetry order of the quasicrystal. $\phi(n)$ is the number of positive integers which are less than n and has no common divisor with it besides 1. As an example, a dodecagonal quasicrystal has $n = 12$ fold symmetry and therefore $\phi(12)$=4.

In this specific case where the hyperspace is a rectangular lattice with $d_2 = \sqrt{2}d_1$, then $tan\theta = 1/(\sqrt{2}\tau_{\mathrm{Dod}})$ for $\tau_{\mathrm{Dod}} = L/S = (1+\sqrt{3})/2$ such that $L = d_1 cos\theta$ and $S = \sqrt{2}d_2 sin\theta$. In this context the rational approximants defined earlier by $cot\theta$ can be proportional to the ratio of two successive Dodecanacci numbers D_{n+1}/D_n such that $D_n = D_{n-1} + D_{n-2}/2$ with $D_0 = 0$ and $D_1 = 1$. In this case, the value of $cot\theta$ increases for increasing values of n and the rational approximate approaches τ_{Dod} for the limit of D_{n+1}/D_n as $n \longrightarrow \infty$.

1.3 Quasiperiodic order in soft matter

Twenty five years after their discoveries, stable quasicrystals where known to exist only in binary and ternary metallic alloys [1, 37] with mainly icosahedral symmetry (more than a hundred different type) [38] and fewer decagonal and other symmetries [39]. So far the stability of these structures formed at the atomic scale has no unified explanations concerning their energy and entropy

[40, 41]. Therefore, it has been an advantage to observe similar structures on a larger scale in soft matter systems where the building blocks are microscopically visible (large than 100nm) and easily accessible (e.g. tunable pair interactions, particle size, surface properties, concentration, etc.). Soft quasicrystals were first experimentally witnessed in dendrimer liquid crystals [42] and ABC star-shaped polymers [43]. One-component quasicrystals were predicted in theory to be thermodynamically stable in charged-stabilized colloidal suspensions using perturbation theory [44] and in systems with isotropic pair potentials with more than one length scale [45, 46, 47, 48, 49, 50]. Experimentally soft quasicrystals have been observed in mesoscopic and colloidal systems under specific conditions like variation of temperature, concentration [51], light potential [52, 33] particle interaction [53, 54]. So far stable soft quasicrystals are observed to have mostly 12-fold symmetry and in few cases 10, 14, 18 and 24-fold quasicrystals [51, 50, 47]. In particular colloidal quasicrystals are of major interest due to their self assembly in a rich variety of phases (gas, liquid, crystal, glass and also quasicrystals). Therefore they serve as a model system to examine fundamental physical and chemical properties of crystalline and quasicrystalline structures which are useful in many applications and development of devices. For example, colloidal quasicrystals can be used in photonic devices since they have length scales which are an order of magnitude of the wavelength of visible light.

1.3.1 Colloidal quasicystals in the meso-scopic scale

Micelles are examples of mesoscopic-sized (1-1000nm) colloids that can order into periodic assemblies in aqueous solutions [55]. Recent studies on the block copolymer $PI_{30} - PEO_{120}$ showed that micelles can self assemble into quasicrystalline structures with 12-fold and 18-fold symmetries [51]. In this study, a temperature-induced phase transition from an FCC to the two quasicrystals was observed in situ by time-resolved synchrotron SAXS [2] diffraction experiments. Fig. 1.8 shows for a micellar solution, which had a 15% concentration and was cooled under oscillatory shear, a diffraction pattern with six additional peaks forming Q12 phase after 10 secs and proceed with a splitting to form 18 peaks for Q18 after 50 secs.

Each of the different phases were stable within a concentration range of $10 - 25\%$) and temperature range of $15 - 25℃$ [51] which is in agreement with the theoretical prediction of colloidal quasicrystals with soft interaction potentials [44]. The nature of the transition is explained to have been achieved by small rearrangements of the micelles positions since the corresponding

[2] small angle X-ray scattering

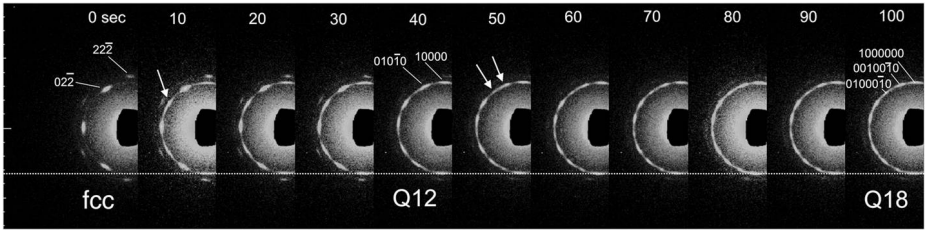

Figure 1.8: *Time-resolved diffraction patterns from a microfocus synchrotron SAXS. Frames recorded for 10 s show the temperature-induced transition from the FCC phase to the Q12 and Q18 phases which proceed by appearance of six additional peaks at after 10s (Q12) and splitting of the new peaks into further six reflections after 50 s. Arrows indicate newly developed peaks and the dotted line indicates a constant length scale during the phase transition [51].*

quasiperiodic tilings can be scaled to a periodic one through the periodic average structure (PAS) [10]. This mapping of the quasiperiodic structures onto periodic is a theoretical model developed by Steurer et al. (1999) and meant to investigate crystal-quasicrystal phase transitions observed experimentally in metallic alloys [11, 31, 56]. The theoretical concept of PAS will be explained in chapter 5.

1.3.2 Stable quasicrystals with two-length scale interaction potentials

Soft colloids similar to dendritic micelles [42] which have a core surrounded by a soft shell (shoulder) have been modeled by Dotera et. al. [50] as two dimensional disks with two-length scale pair interaction potential. As the shoulder-to-core ratio λ is changed within a range of 1.2-2, a family of quasicrystals with 10-, 12-, 18- and 24-fold rotational symmetries are observed. This is illustrated in Fig. 1.9, where snaps shots of the real space and corresponding diffraction patterns of high and low density (HD and LD) quasicrystals are shown. Due to this pair interaction the local packing density initiates three particle assemblies with core-to-core or shoulder-to-shoulder interactions forming either isosceles: short (S) and long (L) or equilateral: collapsed (C) or expanded (E) triangles (Fig. 1.9c). A phase diagram of the quasicrystalline phases formed at different packing fractions is plotted as a function of shoulder-to-core ratio in Fig. 1.9d.

It was found in this study that the stability of the dodecagonal quasicrystal (Fig. 1.9) depends on the relative number of squares and triangles and not on the structure of the tiling. Meaning that the minimum free energy required for

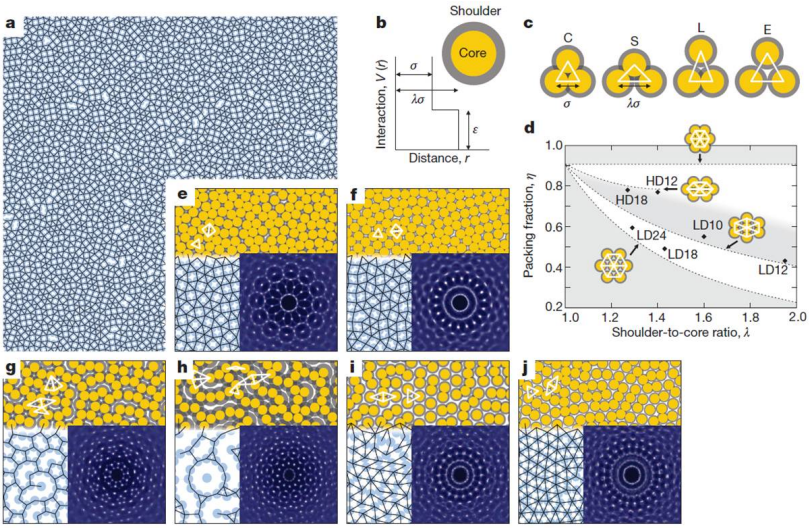

Figure 1.9: *Real space and diffraction patterns. a) A snapshot of a random square-triangular tiling of a highly dense dodecagonal quasicrystal HD12 with* $\lambda = 1.40$*, temperature* $\Theta = k_B T/\varepsilon = 0.278$ *and packing fraction* $\eta = 0.77$*. b) Plot of the pair interaction versus distance. c) Geometrical construction of the packing triangles. d) Phase diagram of the quasicrystalline phases. Dashed line represent two pairs of hexagonal and rhombic phases. e) HD12, f) HD18 (*$\lambda = 1.27$*,* $\Theta = 0.208$*,* $\eta = 0.780$*), g) LD10 (*$\lambda = 1.6$*,* $\Theta = 0.133$*,* $\eta = 0.550$*) and h) LD12 (*$\lambda = 1.95$*,* $\Theta = 0.154$*,* $\eta = 0.430$*), i)LD18(*$\lambda = 1.43$*,* $\Theta = 0.0885$*,* $\eta = 0.49$*) and j) LD24 (*$\lambda = 1.29$*,* $\Theta = 0.098$*,* $\eta = 0.595$*) phases [50].*

a random free-defect dodecagonal phase is obtained at a density for which the triangle-to-square ratio is ideal [57]. Consequently, a high density dodecagonal quasicrystal is assumed to be stable at high and low temperatures. This hints that the other quasicrystals can be long-lived metastable states for a range of temperature from high to intermediate [50].

1.3.3 Conclusion and outlook

The intriguing nature under which stable quasicrystals are observed has become less ambiguous as more theoretical and experimental studies are performed. But so far experiments to demonstrate stable quasicystals with two or more potential length scales has failed. Therefore, we propose in this thesis an experimental model which studies the phase behavior of a two dimensional

system of charged-stabilized colloidal particles in the presence of a one dimensional quasiperiodic light field. The latter is composed of two potential length scales whose frequencies and ratios match those of well known quasiperiodic squences e.g Dodecanacci, Fibonacci, etc. In the presence of pair particle interaction and light potentials, it would be then interesting to study the minimal requirements for a two dimensional quasicrystal to be formed. Such an experimental model is expected to bring insight into the nature of crystalline-quasicrystalline (or approximants) transitions and consequently understand the geometrical structure that relates periodic crystals to quasicrystals.

2 Colloidal suspensions

The giant atoms: colloids, have interesting physical properties that made them a model analogous to atomic systems, except that colloids can be examined in real space and their individual trajectories can be easily accessible. Our experiments make use of charged colloidal monolayers for studying their phase behavior in the presence of light field potentials. Therefore, this chapter starts with an overview on colloids, their properties, then discusses suspensions in quasi-2D, experimental tools used to prepare colloidal monolayers, inter-particle interactions and their response to external fields. Examples illustrating the behavior of colloidal monolayaers in the presence of light (optical trapping) are introduced.

2.1 Physical properties

Colloids are microscopic particles that can be suspended in solvents like water, oils or alcohols etc. Their size ranges typically between 1 nm and 10 µm which is considerably smaller than the macroscopic scale but larger than atoms. Therefore, in contrary to atomic systems which require complex analysis through diffraction patterns which result in average quantities in the reciprocal space (e.g structure factor), colloids are large enough to be visualized in real space under optical video microscopy. Colloids are also small enough to exhibit Brownian motion which is a very important property since it gives colloids a life of random movement explained as thermal fluctuatios originating from collisions with the solvent molecules. Thus colloids can be found in suspensions as randomly distributed (liquid, gas phase) or having well defined average positions (crystals). The particle kinetics can then be studied statistically by employing Boltzmann distributions and therefore identify the phase behavior of the suspension under certain conditions of temperature, pressure, radiation, etc. For this reason colloidal suspensions are found very useful in soft matter systems which are distinguished from hard materials by their thermal and elastic properties. For example, colloids are found in a variety of industrial products like glues, gels, paints, foods, pharmaceuticals, cosmetics and liquid crystals. They can be also found in biological systems like DNA, viruses and membranes. Therefore a colloidal suspension serves well as a model system in which the structure is observed and phase transitions investigated. Such studies bring insight to the thermal stability of materials

whether they are soft or hard.

2.1.1 2D colloidal systems

Three dimensional structures are very stable and can provide more information about their kinetics and phase transformations when compared to two dimensional systems. But the latter are more easier to visualize and more practical under experimental studies. Therefore 2D colloidal suspensions serve as a test bed for many-body statistical physics since they can provide direct and *insitu* observation of their phase behavior. In our experiments we study the phase behavior of a monolayer of charged colloids in the presence of light field, for example, liquid to crystal (chap. 3), crystal-crystal (chap. 4) and crystal to quasicrystals transitions (chap. 5) are investigated. Therefore two important interactions we deal with and discuss in this chapter: particle-particle interaction which is purely electrostatic and repulsive, and particle-light interaction. Without any external field, a confined 2D colloidal suspension can be defined by its number density ρ and its pair interaction. Therefore in charged colloidal systems pair electrostatic repulsion plays an important role in the stability of the suspension against aggregation and particles distribution which determine the phase of the monolayers. That is, for strong electrostatics (or a large number density ρ) a crystal phase with a hexagonal structure is formed, while for weak electrostatic (or low ρ) a liquid phase is expected.
Two types of colloidal systems were used in our experiments, both consisting of mono-dispersed spherical particles with size mean deviation less than 5%. The first suspension consists of polystyrene particles having a diameter of 3.9 µm and carboxylate-COOH end group. This suspension is used to investigate freezing and melting (chap. 3) and quasicrystal-crystal transitions (chap. 5) phenomenon. In studying the crystalline order transitions in our experiments we used a different suspension consisting of silica spheres of size 3.7 µm and freely suspended in bromobenzene. Such a suspension is very critical to prepare and therefore requires more understanding. Details will be discussed later in chap. 4.

2.1.2 Brownian motion and diffusion

The Brownian motion that a colloid experiences when present in a medium, makes it just like an atom but with a larger scale, hence the name big atoms [58]. Thus for a colloid to diffuse its own diameter σ, it requires a relaxation time τ_c known as the self diffusion time and is expressed as:

$$\tau_c = \frac{\sigma^2}{6D_0} \tag{2.1}$$

D_0 is the diffusion coefficient in the limit of an infinite particle dilution, and is given:

$$D_0 = \frac{k_B T}{3\pi\eta\sigma} \tag{2.2}$$

$k_B T$ is the thermal energy of the particle with $k_B = 1.38 \times 10^{-23} J/K$, T is the medium temperature expressed in Kelvin and η is the viscosity of the solvent. From the above equations the relaxation time for an atom at room temperatures is $\tau_a \approx 1\,\text{ps}$ and a colloid in our experiments is $\tau_c \approx 1\,\text{s}$. The latter value means that a colloidal suspension needs a macroscopic time scale in order to crystallize. This time window is large enough to a make a detailed time-resolved study for the crystallization kinetics which is impossible in atomic systems.

2.1.3 Thermal energy distribution

Due to the hydrodynamic effects that colloids encounter, their motion might be damped leading to a linear thermal diffusion with respect to time as described in equation 2.1. For an atomic gas, atoms perform a ballistic motion for short range distances (less than the mean free path). But in any case whether colloids or atoms, for a system of many particles the thermal energy can be described by the same statistics due to their Brownian motion. The type of motion is a result of the solvent molecules colliding with the present colloids which are continuously provided by momentum and thermal energy causing each colloid to diffuse and fluctuate during the time course of its trip through space. As a consequence the evolution of a particle velocity in time and position is well described by Boltzmann distribution function $p(x, v, t)$ in one dimension such that:

$$p(v) = [\frac{m}{2\pi k_B T}]^{\frac{1}{2}} exp[-\frac{E_K}{k_B T}] \tag{2.3}$$

knowing that v is the particle velocity, m is its mass and $E_K = mv^2/2$ is its kinetic energy. In the presence of an external field (gravitational, light field, ...etc) particles positions are described by the Virial theorem and therefore the positional distribution is given by:

$$p(x) = p_0 exp[-\frac{E_{pot}}{k_B T}] \tag{2.4}$$

$E_{pot} = E_K + E_{ext}$ with E_{ext} being the total energy resulting from the presence of external fields. In all of the experiments we deal with kinetic energy much smaller than E_{ext} and therefore E_K is neglected. Here we express energy

in units of k_BT rather than joules J. Therefore, at room temperature of $T = 298K$, $1k_BT = 4.115 \times 10^{-21}J$.

In conclusion, 2D colloidal assemblies can provide insight to the physics which is not accessible directly in atomic systems. In particular the kinetics observed in colloids at equilibrium provide information about atomic many-body system interacting with similar inter-particle potentials.

2.1.4 Correlation function in charged colloidal monolayers

The thermal statistics that can be collected from tracking colloidal particles and recording their coordinates through the course of time, is best explained by the correlation function. This function measures the probability to find at the same time two particles at a certain distance apart from each other. For a canonical ensemble of N particles, a circle of maximum radius r_{max} is made around each particle (reference) and the center to center distance to N other particles within this radius is measured [59]. In our experiments in which we use 2D colloidal systems the two particle probability distribution $p(r_1, r_2)$ is extracted. r_1 and r_2 represent the position of two particles and therefore we make use of the pair correlation function $g(r_1, r_2)$ such that:

$$g(r_1, r_2) = \frac{p(r_1, r_2)}{p(r_1)p(r_2)} \tag{2.5}$$

For a homogeneous isotropic system, $g(r_1, r_2)$ depends on the absolute value $r = (r_1 - r_2)$ and can then be written as $g(r)$ To avoid boundary conditions for finite sized systems, measurements of $g(r_1, r_2)$ are made for the central region of each frame. Due to local density fluctuations, the density $\rho = N/\pi r_{max}$, N and $g(r_1, r_2)$ depend on the individual frames and reference particles and therefore are averaged over N and number of recorded frames.

The pair correlation function is a very useful quantity in characterizing the structure of a colloidal system, e.g by extracting thermodynamical properties like the isothermal compressibility K_T which takes into account the fluctuation of particle number N around its mean value such that:

$$K_T = \frac{<\Delta N^2>}{k_BT\rho < N >} = \frac{1}{k_BT}\int (g(r_1, r_2) - 1)dr_1dr_2 - \frac{1}{k_BT\rho} \tag{2.6}$$

The thermal compressibility is related to the pressure of the system from which the particle-particle interaction is estimated. This will be discussed further in details in chap. 4 where the density functional theory (DFT) is employed to determine the electrostatic repulsion forces between highly charged silica sphere suspended in an organic solvent.

The electrostatic force can be also calculated from Ornstein-zernike equation [60] which is related to the total correlation function $h(r) = g(r) - 1$ and the direct correlation function $c(r)$. The latter is a measure of the correlation between two particles, excluding any interaction with all other particles. To be able to employ this method, a diluted system is considered which wipes out the effect of many-body particles that rise up at high densities. This method is used in chap. 5, to calculate the pair interaction between highly charged polystyrene sphere suspended in water.

2.1.5 Phase transitions and KTHNY-theory

During phase transitions, the correlation function is the order parameter which predicts under which conditions a certain transition happens. For example, lowering the temperature for a three dimensional system leads to a first order phase transition from liquid to crystal due to spontaneous formation of nucleation clusters. A change in the correlation between particles follows, indicating a structural change. A liquid has a weak correlation function that decays to one after a fairly short distance (no long-range positional order). Upon crystallization the correlation increases and $g(r)$ does not decay to zero due to the periodic arrangement of lattice sites.

However, in 2D systems the stability of the crystal phase is not as strong as in 3D systems since in the former case, less neighboring particles are present leading to thermal fluctuations of short (liquid) or quasi-long (crystal) range order [61, 62]. According to the KTHNY theory [63, 64, 65, 66] [1], large thermal fluctuations provoke a crystal to melt into the liquid state through the creation of thermally excited pairs of defects (dislocations or disclinations). In a 2D crystal a pair of dislocations may appear and combine but impose a negligible effect, such that the crystal keeps an orientational order $g_6(r)$ and a quasi-long translational order with $g(r)$ expected to decay algebraically for large distances according to:

$$crystal \qquad g(r) \propto 1 + r^{-\eta}, \quad 0<\eta<1 \tag{2.7}$$

$$g_6(r) = constant \tag{2.8}$$

Upon increasing the temperature of the system, the crystal starts melting. This transition happen through the formation of a hexatic phase which is characterized by a short translational order with $g(r)$ expected to decay exponential and a long range orientational order such that:

$$Hexatic \qquad g(r) \propto 1+e^{-\zeta r}, \quad 0<\zeta \tag{2.9}$$

[1] Kosterlitz and Thoules proposed in 1972 the defect mediated theory which was extended by Haperlin, Nelson and Young

$$g_6(r) \propto 1 + r^{-\eta_6}, \quad 0<\eta_6<1 \qquad (2.10)$$

ζ and η represent the inverse of the correlation length which is defined as the distance beyond which the correlation between two particles is lost. In the

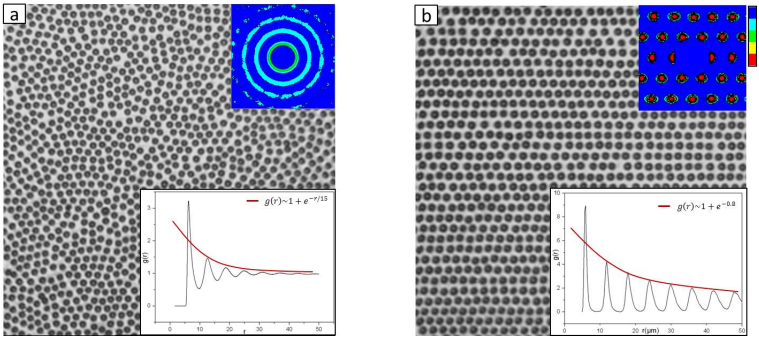

Figure 2.1: *Snap shot of a colloidal monolayer in a liquid phase shown in a) and crystal phase shown in b). In a) the particles prefer random distribution thus the pair correlation function $g(x, y)$ (upper right inset) shows concentric rings with the inner radius identical to the mean particle distance. The corresponding $g(r)$ decays exponentially for large distances as shown in lower right inset. b) shows a triangular periodic distribution of the particles, and this periodic ordering is verified by the algebraically decaying $g(r)$ (lower inset) and the hexagonal probability distribution. The color bar is associated with $g(x, y)$ and provides the probability to find a particle at a certain position, highest probability is indicated in red and the lowest in blue.*

second melting phase, the hexatic crystal which contains few dislocations, but has most of its particles surrounded by six nearest neighbors, transforms into the liquid phase accompanied by appearance of disclinations. The latter are particles that have five or seven nearest neighbors that break the orientational order in the system. Therefore the order parameters of an isotropic liquid become:

Liquid

$$g(r) \propto 1+e^{-\zeta r}, \quad 0<\zeta \qquad (2.11)$$

$$g_6(r) \propto 1 + r^{\zeta_6}, \quad 0<\zeta_6 \qquad (2.12)$$

In our experiments, we observed the colloidal monolayer with N particles recorded for 1000 frames with a rate of 1 frame per second. In order to identify the structure of the colloidal sample, we extract beside $g(r)$, the pair correlation function $g(x, y)$ and the density distribution $\rho(x, y)$ average over

all N and all number of frames recorded. Fig. 2.1 shows snap shots for the sample in the liquid and solid phases with the corresponding $g(r)$ and $g(x, y)$. x and y being the particle coordinates in the sample plane.

2.1.6 Pair interaction in charged colloidal suspensions

Colloids suspended in a medium interact among each other through various types of potentials. This pair potential can be of a long-range or short-range electrostatic, van der Waals or dipole-dipole nature [67]. Colloids act as hard spheres in the absence of these interactions. They can be also tunable by external fields, such as light [68, 69, 70] or magnetic radiation [71, 72, 73]. This ability of controlling colloids gives them a major advantage when compared to atomic systems. In our experiments, we use suspensions with charged colloids which interact via long range coulomb potentials.

In general, charged colloids form a stable suspension with high monodispersity when they have repulsive forces that are strong enough to overcome the attractive van der Waal forces which lead to aggregates and collapse of the suspension. At a distance of 100 nm and less van der Waal forces become important. The mechanism behind the colloidal stabilization depends on the charge of the colloids and the ion concentration in the solvent. The number of ions in the suspension plays an important role in screening the colloids from each other and therefore predicts at which distance (Debye screening length) the pair interaction decays significantly. Colloids obtain their charge by the dissociation of ions (counter ions) from their surface, leaving them with charges that are opposite in sign. But for an ion to exist in a medium it needs enough energy to be dissociated and introduced into the solvent [74] according to:

$$\frac{U_{ion}}{k_{\mathrm{B}}T} = \frac{(Ze)^2}{4\pi k_{\mathrm{B}}T\varepsilon_0\varepsilon_m d_{ion}} = Z^2\lambda_B\frac{1}{d_{ion}} \approx 1 \tag{2.13}$$

Z is the surface charge (monovalent species $Z = 1$), e is the elementary charge, $\varepsilon_0 = 8.854 \times 10^{-12} Fm^{-1}$ is vacuum permittivity, ε_m is the relative dielectric constant of the solvent and d_{ion} is the diameter of the ion. ε_m is the characteristic parameter of the solvent that indicates polarity of its molecules. The more polar the solvent is, more molecules can dissociate ions from the surface of the colloids. λ_B is called the Bjerrum length and it is the distance between two electrons at which the electrostatic potential is equal to $k_{\mathrm{B}}T$. Water has a high static polarity with $\varepsilon_w = 80$ giving $\lambda_B = 0.7\,\mathrm{nm}$ at room temperatures and therefore it is a convenient medium that provides enough energy to dissolve ions in it. On the other hand, non polar liquids e.g. oil has a low polarity $\varepsilon_m < 5$ and $\lambda_B \approx 28\,\mathrm{nm}$ leading to $U_{ion} \gg k_{\mathrm{B}}T$ which leaves

colloids uncharged with no electrostatic repulsion and giving room to van der Waal forces to dominate and result in colloidal aggregation. Suspensions in organic solvents will be discussed later in chap. 4. For polystyrene colloids

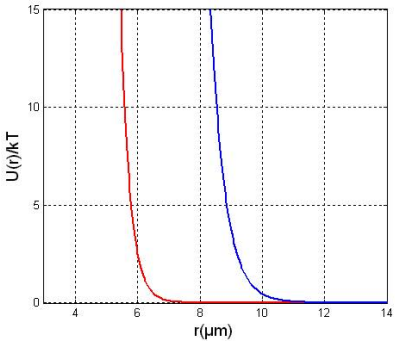

Figure 2.2: *The electrostatic pair potential is plotted as a function of distance. The two curves correspond to two different suspensions of polystyrene spheres in water. The red curve represents a potential with a prefactor* $A = 10^9$ *and* $\kappa^{-1} = 500\,nm$ *and it falls to zero at a distance much smaller than the blue curve. This indicates that the electrostatic interaction is lost at shorter distance than the blue curve which has* $A = 10^9$ *and* $\kappa^{-1} = 320\,nm$.

suspended in water the particles are left negatively charged due to the dissociation of the sulfate (or cyrboxylate) group which release the hydrogen ion H^+ into the water and then form an electric cloud around the colloids. Besides the 20 million dissociated ions per colloid present in water, ions arise from the self-dissociation of water molecules, added salts and from the surface of the sample cell which acquires a negative charge OH^- through the dissociation of the silanol groups [75].

Screened Yukawa potential

Due to the presence of this complex bed of ions, it would be impossible to determine the pair potential on the molecular level and therefore this many body system requires coarse-grain theoretical approximation in which the colloidal coordinates and the effective force between them are the only parameters taken into account. Assuming that the medium is continuous the ion concentration in the solvent obeys the Boltzmann distribution:

$$n_i = n_{i0} exp(-\frac{Z_i e \phi(r)}{k_B T}) \tag{2.14}$$

This is the ion concentration at a point in the solvent and has an electric potential energy $\phi(r)$ for ion species i with valence Z_i and have n_{i0} as an ion concentration at the bulk. The average density distribution of all ions in the system is the average sum of cations and anions in the solvent and is given by:

$$\rho(r) = \sum_i Z_i e n_i = \sum_i Z_i e n_{i0} exp(-\frac{Z_i e \phi(r)}{k_B T}) \tag{2.15}$$

In our approximation we focus on the electrostatic interactions between the micro ions and the colloidal particles and this interaction is best described by Poisson equation:

$$\bigtriangledown^2 \phi(r) = \frac{\rho(r)}{\varepsilon_0 \varepsilon_m k_B T} \tag{2.16}$$

The combination of equations 2.15 and 2.16 lead to the Poisson-Boltzmann relation:

$$\bigtriangledown^2 \phi(r) = \frac{1}{\varepsilon_0 \varepsilon_m} \sum_i Z_i e n_{i0} exp(-\frac{Z_i e \phi(r)}{k_B T}) \tag{2.17}$$

The non-linear Poisson-Boltzmann equation can be solved in the limit of low potential i.e $Z_i exp(\frac{\phi(r)}{k_B T}) \ll 1$, which allows to linearize the exponential in spherical coordinates according to the Debye-Hückel theory, where only the second term in the series expansion is considered. The linearized equation then becomes:

$$\bigtriangledown^2 \phi(r) = \kappa^2 \phi(r) \tag{2.18}$$

where $\kappa = \sqrt{\frac{e^2}{\varepsilon_0 \varepsilon_m k_B T} \sum_i n_{i0} Z_i^2}$ is the inverse Debye screening length. Therefore κ^{-1} indicates the ionic strength in the suspension and the distance beyond which the electrostatic interaction between colloids is lost. In our experiments, the typical Debye screening length for polystyrene in water is in the range of 100 nm to 500 nm (see chap. 3 & chap. 5), while for silica particles suspended in bromobenzene where particle-particle interaction is of a long range nature, κ^{-1} reaches several micrometers (see chap. 4).

The solution of equation 2.18 describes the pair potential and leads to determine the ionic distribution through equation 2.16. Knowing $\phi(r)$ the pair electrostatic potential $U(r)$ is expressed by:

$$U(r) = \frac{A}{r} e^{-\kappa r} \tag{2.19}$$

with the pre-factor $A = \frac{(Z^*e)^2}{4\pi\varepsilon_0\varepsilon_m}(\frac{exp(\kappa(\sigma/2))}{1+\kappa(\sigma/2)})^2$. Z^* is the effective surface charge, σ is the diameter of the particle and r is the center to center particle distance. $U(r)$ is expressed in units of k_BT.

Equation 2.19 is the Yukawa screened coulomb potential which represents the electrostatic part of the derjaguin-Landau-Vervey-Overbeek (DLVO) theory [76].

In our experiments the determination of κ and A cannot be achieved by measuring the ion concentration directly from the solvent. We rather extracted the pair correlation function g(r) to which the potential $U(r)$ is related. By fitting a simulated $g(r)$ to the experimentally measured $g(r)$, κ and A were estimated. Two different simulation methods were used to make the fitting, the DFT (done at Institute of theoretical statistical physics and soft matter, Tübingen University) and the inversion of the $g(r)$ (Institute of computational physics (ICP), Stuttgart University). The second method involves inverse Monte Carlo simulations (IMC) procedure for a diluted suspension, otherwise an inversion technique based on the Ornstein-Zernicke (OZ) equation [77] is employed. This relation relates the fast Fourier transform (FTT) of the total correlation function $h(r)$ to the Fourier transform of the direct correlation function $c(r)$ via $\hat{c}(k) = \hat{h}(k)/(1+\rho\hat{h}(k))$ with $\hat{h}(k) = \int drh(r)e^{-i\kappa r}$.

In case of an aqueous suspension, the pair potential between colloids is represented in Fig. 2.2 for two samples with different ionic strengths. The red curve decays faster than the blue one as a function of distance. This indicates that the red curve corresponds to a suspension with a higher ion concentration and a shorter Debye screening length than that of the other sample.

2.2 2D colloidal assemblies on 1D periodic templates

In particular, $2D$ colloidal assemblies have been attracting attention due to their versatile structural behavior which is known in solid state physics. When Freezing and melting in 2D systems were studied by KTHNY in the 1970s (see section 2.1.5), they developed their theory without taking into account the effect of substrate field potentials. This study brings insight into the nature of phase transformations in the presence of external fields. Understanding the many-body statistical physics of this phenomena is useful in surface science, for example paramagnetic-to- ferromagnetic transitions in thin films where thermal fluctuations show their significance in low dimensional systems [78, 79]. In addition colloidal assemblies on substrate surfaces has great technological importance [63, 4] in development of new materials, e.g $2D$ and $3D$ photonic crystals [80, 81]. Colloidal liquid-crystal transitions can be induced

by gravitational [4], magnetic [82], electrohydrodynamic [83], convective [84] and entropic [3] fields. They can also be spontaneously formed in thermal equilibrium [85].

2.3 Colloidal interaction with external light fields - optical trapping

Colloidal spheres can be manipulated by light, electric and magnetic fields. We focus on colloid-light interaction where optical tweezers are employed with tunable parameters like, intensity and spatial distribution of the potential wells. For example, using interference light beam [7, 86, 87] or galvano-statically driven mirrors [88], acousto-optic deflectors (AOD) or holographic optical tweezers [2] (HOT) patterned potential landscapes can be created [89]. This light field serves as a substrate potential upon which the phase behavior of a colloidal monolayers are studied. Laser beams can also be used to create thermal gradients (thermophoresis in artificial active swimmer) which cause particles transport similar to bacteria in living bodies [90, 91]. Other types of optical tweezers include acousto optic modulators which have been used in studying the statistical and stochastic properties of particles at the micro scale, by trapping one or more colloids in a ring-like light potential [92]. The

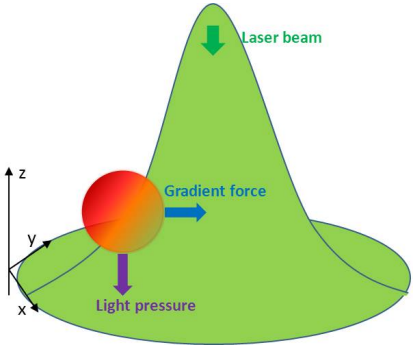

Figure 2.3: *Cross-section of the laser beam which has a Gaussian intensity distribution. A colloidal particle (red circle) with $\varepsilon_m < \varepsilon_c$ experiences a gradient force pulling it towards the center of the beam. At the same time the colloid scatters part of the incident photons resulting in a radiation pressure in the direction of propagation of the laser beam.*

[2] The HOT technique uses a single collimated laser beam which splits into several by using a computer-based diffractive optical element (DOE)

concept of optical trapping by light radiations stem from the fact that colloids are dielectric materials that can be polarized by the electric field component [93]. When a colloid with a dielectric constant ε_c is suspended in a medium, it experiences light radiations with two effects acting on the it: optical gradient force and radiation pressure. In our experiments we use transparent colloids that are not thermally affected by absorption of laser light at wavelengths $\lambda = 320\,\text{nm}$ and $\lambda = 488\,\text{nm}$. The two forces are illustrated in Fig. 2.3 for a laser beam with a Gaussian intensity distribution.

2.3.1 Gradient forces

When a dielectric particle is subject to light, it becomes polarized and acquires a dipole moment:

$$d = (\varepsilon_c - \varepsilon_m)V_c E_c \tag{2.20}$$

with V_c being the volume of the sphere, and E_c is the electric field vector induced in the colloid by the light field. The above equation is a result of the difference in electronic field strength induced in the colloid and the solvent such that:

$$E_c = \frac{3\varepsilon_m}{\varepsilon_c + 2\varepsilon_m} E_m \tag{2.21}$$

Combining equations 2.20 and 2.21 we can give the expression of the polarization energy gained by the colloid in the presence of the light field:

$$U_{grad} = -\frac{d \cdot E_m}{2} = -\pi\varepsilon_0\varepsilon_m \frac{\sigma^3}{4}\left(\frac{\varepsilon_c - \varepsilon_m}{\varepsilon_c + 2\varepsilon_m}\right)E_m^2 \tag{2.22}$$

From this relation we conclude that for a particle to be trapped in the highest intensity regime of the laser field then $\varepsilon_c > \varepsilon_m$ ($\varepsilon \sim n^2$), e.g polystyrene particles ($n_p = 1.53$) suspended in water ($n_w = 1.33$) and used in our experiments which will be discussed in chapters 3 and 5. While in the case of silica particles ($n_s = 1.42$) suspended in bromobenzene ($n_{BrB} = 1.68$), $n_s < n_{BrB}$ they will prefer the minimum intensity regions (inverse tweezing) [88]. Equation 2.22 is valid for a particle with size less than or equal to the beam diameter.

2.3.2 Radiation pressure

Light pressure acts on the colloid in the same direction as the propagation of light, that is along the pointing vector $\vec{S} = \vec{E} \times \vec{B}$ with $\vec{E}$ and $\vec{B}$ being the electric and magnetic vectors respectively. When the light beam hits the surface of the colloid, part of it is transmitted through and the other is reflected but the combination of the two parts does not yield the same momentum as

that of the incident beam. This results in scattered momentum at the colloidal surface due to the difference in index of refraction of the two media (colloid and solvent). The magnitude of this radiation force depends on the size of the particle and the intensity of the laser beam according to:

$$F_{scatt} = 2\pi\alpha^2 I w^2 \tag{2.23}$$

with $\alpha = \frac{\varepsilon_c}{\varepsilon_m} - 1$ and w is the waist of the laser beam. The intensity I of the trapping beam can be calculated at the sample plane by measuring the power P_L.

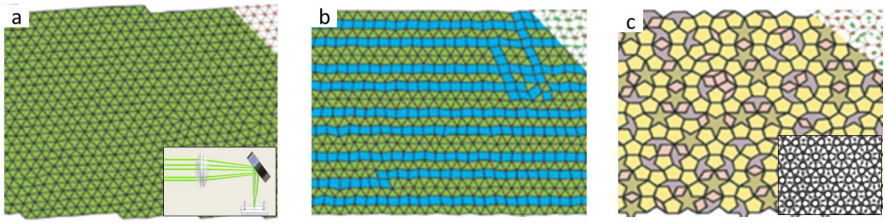

Figure 2.4: *Phase transition of a colloidal crystal of charged polystyrene spheres suspended in water as a function of the laser power P_L .a) At $P_L = 0$ a crystalline phase in the absence of the laser field is formed. The inset shows a sketch of the 5 interfering beams at the colloidal sample plane. b)At $P_L = 2W/m^2$ and $\kappa^{-1} = 160\,nm$ an Archemidian-like tiling forms with particles distributed in squares (blue) and triangles (green). c)At $P_L = 2W/m^2$ and $\kappa^{-1} = 10\,nm$ the system transforms into a quasicrystalline phase with a 10-fold symmetry and tilings composed of pentagons (yellow), rhombuses (pink), crowns (violet) and pentagonal stars (brown). The inset shows the substrate created with a quasiperiodic light distribution; white spots for the high intensity areas [94].*

2.4 Colloidal phase transitions in the presence of light field potentials

As mentioned earlier, light patterns can be formed by two or more interference beams. Two beams produce a periodic line pattern formed of parallel lines, 3 interfering beams give a 2D land scape of triangularly distributed lattice sites and 5 beams give a 2D quasiperiodic distribution of lattice sites. Due to gradient forces acting on colloidal particles, light patterns act like potential surfaces [68, 95, 96]. For example a colloidal monolayer subject to a

quasicrystalline decagonal light surface, undergoes a phase transformation to adapt with the quasiperiodic order. This is illustrated in Fig. 2.4 which shows different colloidal phases at different light intensities. In the abscence of light the triangular crystal is formed (Fig. 2.4a) which then changes at moderate light strength into an Archimedian-like phase which is periodic in one dimension and quasiperiodic in the other [52]. Due to the competition between the colloid-colloid repulsive and the colloid-substrate interaction, particles are driven to form squares and triangles Fig. 2.4b. At intensities high enough the light trapping forces dominate and particles follow the laser lattice sites as shown in Fig. 2.4c. The phase transition illustrated here, is a result of an interplay between inter-particle repulsive forces and external optical fields. therefore this phenomena cannot be explained by KTHNY-theory, since it is only true in the case of 2D systems without any external light fields.

3 Experimental setup

In this chapter we explain how colloidal monolayers and 1D light patterns are created. We emphasize on the advantages of our experimental setup over light interference technique which is limited to creating periodic laser lines which has a sinusoidal wave function in one dimension and a periodicity that requires frequent adjustments by optical realignment. On the contrary, the technique used here, creates not only periodic patterns but also non-periodic ones with two or more line spacings. Moreover, this technique has *insitu* control parameters e.g line spacings and intensity are easily accessible.

In our experiments, a 2D colloidal monolayer is prepared in order to study its phase behavior in the presence of a 1D light field potential. In a sample cell, charged colloids are confined and subjected to a periodic or a quasiperiodic light pattern which is created by scanning a light beam. As a result of two competing forces, colloid-colloid electrostatics and colloid-light trapping forces, the monolayer undergoes phase transformations. We explain how the light field strength is measured experimentally and we show a real time phase transition as a function of the laser intensity.

3.1 Colloidal monolayers

We prepare a sample with a quasi-2D colloidal phase of charged particles that are suspended in a solvent that could be water or an organic liquid. Gravity localized particles close to the bottom surface of the cell. Particle fluctuations in the third dimension are suppressed due to sample charged surfaces, resulting in a colloidal monolayer. Each colloidal phase is then characterized by its density ρ as well as the electrostatic strength encountered by the particles among each other. Therefore, preparing a stable $2D$ colloidal monolayer requires a certain density range and number of ions present in the solvent. For example, at a constant ion concentration, a crystal is formed at high densities while a liquid phase forms at lower concentrations.

3.1.1 Preparation

An aqueous suspension of polymer-synthesized particles with a diameter of $3-4\,\mu m$ are purchased from microparticle GmbH company (Berlin). A $100\,\mu L$ of the suspension is then transfered to a micro-tube, where the water is removed

by centrifuging (2000 rounds/2min) and replaced several times by highly de-ionized water. This step increases the electrostatic repulsion between particles. In case of polystyrene particles ($\sigma = 3.9\,\mu m$) a density above $0.0265\,\mu m^{-2}$ creates a crystalline phase. The solution prepared is then injected into a quartz cuvette cell (Hellma) which is connected to a de-ionization circuit that maintains water at a minimum conductivity of $0.06\,\mu S/cm$, with S standing for $Siemens = ohm^{-1}$. Fig. 3.1a is a picture taken for this circuit which contains three reservoirs, one for the conductivity meter, and another is full with resin particles with diameter ranging between $0.3 - 1.2\,mm$. The latter serves as an ion exchange reservoir with negatively charged resins carrying OH^- and H^+ which maintains ionic equilibrium and minimal water conductivity [97, 98]. The third reservoir which connects the sample cell to the whole circuit, is used to inject the colloidal suspension into the cell.

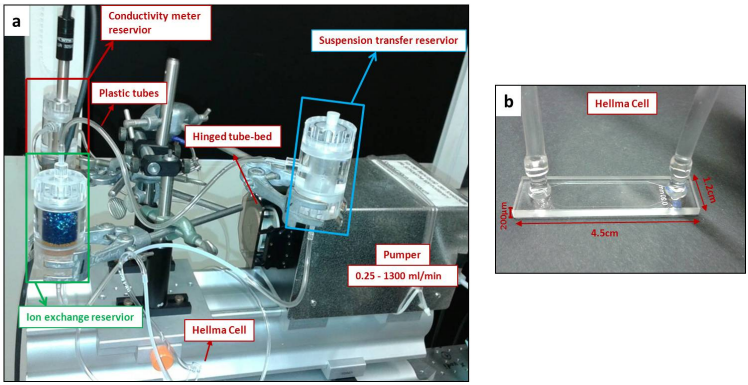

Figure 3.1: *The de-ionization circuit. a) parts of the circuit connected by plastic tubes. The sample cell is directly connected to a reservoir (left side in picture a)) in which the suspension is injected. Enlarged picture of the sample cell with its dimensions is shown in b).*

3.1.2 Confinement

After injecting the suspension, the tubes at the terminals are closed by two clamps and particle are left to sediment under gravitational forces which localize them about 100 nm above the negatively charge bottom plate of the sample cell. As a result, a 2D dimensional structure is formed with out-of plane fluctuations less than 5% of particles diameter. If the density of the suspension is very high then colloids buckle and additional layers would be formed. To avoid this, polystyrene suspensions are prepared with densities $\rho < 0.035\,\mu m^{-2}$, and

injected into a sample cell of depth 200 µm which is small enough to suppress convection that might rise from temperature gradients.

3.2 Real time observations

The colloidal sample is illuminated by a white light source and visualized by a CCD camera (camera 1) through a long-distance microscope objective (Nikon, 20x, NA=0.4). Since the self diffusion time of a colloid is around $1s$ and its size is in the order of several micrometers, it is then possible to use digital video microscopy [99]. We track the particles in a field of view of $300 \times 250\,\mu m^2$ which is large enough to contain up to 1000 particles. Real time visualization allows to observe the time evolution of the particle distributions and to calculate their radial pair correlations. By using Fourier transform of the latter we analyze the reciprocal space.

3.2.1 Phase characterization, real and reciprocal space

In our setup, we have also made a real time reciprocal space observation (online diffraction pattern) by sending a focused argon ion Ar^+ laser beam ($\lambda = 488\,nm$, Coherent Inc., USA) through the central region of the samples field of view. The scattered light is then collected by a polarizing beam splitter, a focusing lens and a camera chip (camera 2) similar to the one used for the real space observation. Fig. 3.2 shows a schematic diagram of the experimental setup, including the optical elements, the path of the Verdi laser ($\lambda = 532\,nm$), the argon ion beam and the light field created at the sample cell. A polarizing beam splitter (PBS) is situated below the sample, minimizing the laser received by camera 1 to 10% of the its intensity at the sample. The same PBS reflects the Ar^+ beam up into the sample where the light is scattered by the colloids and collected by a lens standing in front of camera 2. Due to the difference in the refraction indices of polystyrene particles and water, the argon ion laser scatters on the surface of the colloids and corresponding diffraction patterns can be observed.

3.3 Creation of 1D light patterns

A laser beam with wavelength $\lambda = 532\,nm$ and diameter of 3 mm is emitted from a Nd:YAG solid-based source (Coherent, USA), which then passes through a collection of optical elements illustrated in Fig. 3.2 and eventually forming a one dimensional pattern at the sample cell. The pattern could be made periodic or quasiperiodic in the direction perpendicular to the lines (Fig.

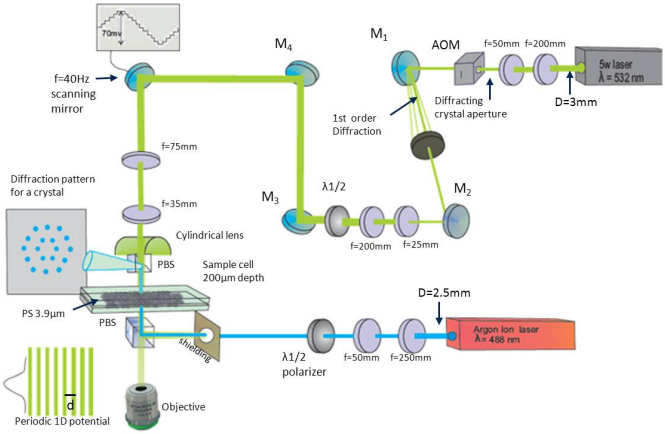

Figure 3.2: *Schematic diagram of the experimental setup. The laser beam of* $\lambda = 532\,nm$ *is used to create the pattern at the sample cell. It passes through several telescopes, an acousto-optic modulator (AOM) then reflects at the galvanostatically driven mirror to continue to the sample plane creating a light pattern. Images of the colloids and the light pattern are collected by the objective situated below the sample cell. Following the* Ar^+ *laser beam a diffraction pattern of the colloidal structure is collected on a screen situated on the other side of the sample.*

3.3). In the set up there are a number of elements that play an important role in creating the desired patterns with tunable spacial distribution and laser intensity. A very important optical tweezer is the Acousto Optic Modulators (AOM). It is able to create light patterns that have spatially varying intensities (in our experiments we used only patterns with the same intensity for all lines). The AOM is a piezoelectric crystal-based devise which is fed by an external radio frequency driver in order to create a diffraction pattern with a tunable frequency. Only the first order, which has 80% of the laser intensity at the source, is considered and transmitted to the colloidal sample cell (the central beam is omitted since it has no time-dependent variation).

As a result of optical forces such light patterns act on colloids as one dimensional potential landscapes [100]. Experimentally, such light fields were created by deflection of a laser beam by the rotating mirror and imaging its pivot point by a telescope to a cylindrical lens. The latter forms the initial spherical cross-section of the laser beam (about 3 mm diameter) into a line with half width of 3.25 μm which is then imaged into the sample plane (Fig.

3.3a and Fig. 3.3b). In order to create arbitrary line patterns with generally non-sinusoidal shapes, we have scanned the line focus in jerky leaps across the sample plane. This is achieved by application of a step like voltage protocol to the scanner as schematically shown in Fig. 3.3d. Such protocols are characterized by the time interval Δt, which corresponds to the resting time of the laser beam being set to about 400 µs in our experiments. The height of the steps ΔV determines the spacing between adjacent laser lines which was varied between approximately 6 -12 µm. As a result, the laser line starts from $x = 0$, goes to one end $(+x)$ in one direction then follows back the same path in the opposite direction $(-x)$ passing by $x = 0$ again. By this it forms a complete cycle by making continuous jumps with the same distance $\boldsymbol{d}$. The repetition time of each cycle was set to $t = 0.025s$ $(40Hz)$. During that time the colloidal particle diffuses over a distance L determined from the mean square displacement $L^2 = \langle x \rangle^2 = 2Dt$, with $D = k_{\mathrm{B}}T/6\pi\eta R$ the diffusion coefficient (with R the radius of the particle, η the viscosity of the solvent, T the temperature, and k_{B} the Boltzmann constant). Under our experimental conditions, we obtain values for L which are less than 2% of the half width of the optical trap. Accordingly, our light potentials can be regarded as quasi-static. The telescope implemented directly after the scanning mirror as shown in Fig. 3.3a is used to decrease the angle of incidence of the beam at the concave surface of the cylindrical lens. The cylindrical lens has a focal length $f = 9.7\,\mathrm{mm}$, hight $H = 10\,\mathrm{mm}$ and length $L = 12\,\mathrm{mm}$. The accuracy of the line position is determined to about 0.03 µm. Note that, when the scanning mirror and the AOM are synchronized they create light fields with time-dependent intensities.

3.4 1D periodic light potentials

A periodic line pattern exemplified in Fig. 3.3b creates light forces whose strength varies in the x-direction while stays constant in the y-direction. A pattern with 31 lines are created with a periodicity $\boldsymbol{d}$ which can be varied independently of the laser beam half width ($w = 3.25$ µm). Such patterns have been intensively used to understand liquid-crystal transition [7, 98] of aqueous suspensions of polystyrene particles and will be explained in more details in this chapter. The formed monolayer have average inter-particle distances $\boldsymbol{a}$ that are of the same order as the periodicity of the imposed interference pattern. While the light potential forces particles to make registrations along the high intensity regions, the repulsive forces maintain the inter-particle separations. Experimental results under these conditions are discussed later in details for a variable laser potential strength V_0 and the case for a fixed V_0

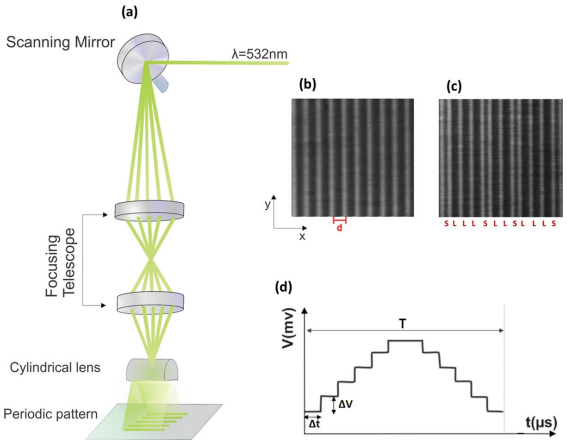

Figure 3.3: *(a) Detailed schematic sketch of the experimental setup with a laser beam which is first reflected on a galvanostatically driven mirror and then directed through a telescope to a cylindrical lens ($f = 9.7\,mm$). (b) Snapshot of the periodic light pattern taken at the sample position characterized by a period* $\boldsymbol{d}$*. (c) Snapshot of a quasiperiodic pattern characterized by two length scales L and S. In (b) and (c) the white lines indicate the high intensity regions. (d) Typical step-like voltage input supplied to the mirror which leads to the intensity pattern shown in (b).*

while $\boldsymbol{d}$ is varied (chapter 5).

3.4.1 Light potentials

In the plane of the colloidal sample, each laser line forms a 1D potential well with Gaussian laser distribution in the x direction. Therefore, for a whole patterns of 31 lines, the light potential has a potential strength $V(y) = const$ and $V(x) = f(x)$. With V_0 being the colloid-light interaction which is expected to vary linearly as a function of laser power P [101, 102].

Experimental characterization of the light potential

In our experiments V_0 increases linearly with the laser intensity I which is provided at the laser source. We measure V_0 by tracking the particle position as a function of time. This is achieved by preparing a diluted colloidal suspension where inter-particle interactions are neglected and particles fluctuations are affected only by the optical trap. Since the laser beam has a Gaussian

intensity profile, we focus our study using the central part of the pattern in order to avoid any significant reduce in the intensity along the y-direction. By

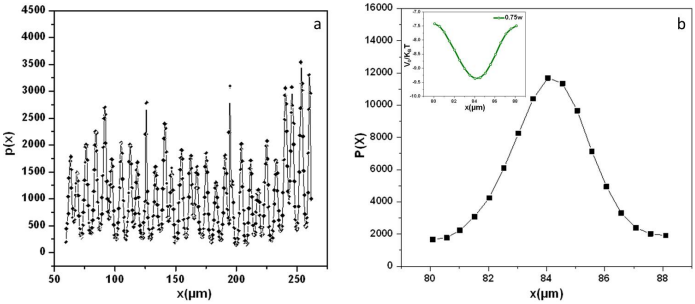

Figure 3.4: *Experimental measurement of the laser potential at a power of* $0.75\,W$. *a) is a plot of the average particle density distribution p(x) for a diluted Polystyrene suspension* ($\sigma = 3.9\,\mu m$) *with a number density of* $0.002/\,\mu m^2$. *b) Plot of* $P(x)$ *which is the sum of all p(x) of all potential wells shown in a). The inversion of the Boltzmann relation yields the profile of the average potential well (inset of b) of a each laser line with* $2V_0$ *being the peak to peak voltage. The black squares indicate the experimentally measured data.*

measuring the average particle density distribution $\rho(x, y)$ in the presence of a light pattern and projecting it in the direction perpendicular to the laser lines, we can evaluate the average particle density distribution $p(x)$ as it is shown in Fig. 3.4a. We can then find $V(x)$. For better statistics, we section $p(x)$ of each potential well and add them up to form the total probability density $P(x)$ shown in Fig. 3.4b. The colloidal particles are considered at thermal equilibrium in the presence of a scanning laser beam (quasi-static pattern as described in section 3.3), we can employ Boltzmann statistics:

$$P(x) \propto exp(-\frac{V(x)}{k_B T}) \qquad \Longrightarrow \qquad V(x) \propto -k_B T ln P(x) \tag{3.1}$$

Inverting $P(x)$ according to equation 3.1 we obtain the potential well profile (inset of Fig. 3.4b) with a peak to peak amplitude of $2V_0$ and a half width of $4\,\mu m$ which is larger than the actual half width of the optical trap due to the finite size of the particles [98].

We determine for different laser potentials $V_0 < 3k_B T$ ($P \leq 1$ W), the corresponding potential profiles which are plotted in Fig. 3.5a. At these potential strengths [1], particle fluctuations are important and the shape of the

[1] Potential wells with strength $V_0 > 3k_B T$ cannot be experimentally measured here, since

potential well results from the particle positions visited during the time of measurement. Plotting V_0 as a function of the laser power shows a linearity (Fig. 3.5b) which is in good agreement with equation 3.1 of Loudiyiet al. It should be pointed, that in general, for a periodic light pattern non-sinusoidal potential cross-sections are obtained, and the similarity with a sine function at a certain spacing $\boldsymbol{d}$ might be obtained as a result of the Guassian intensity distribution of the laser line.

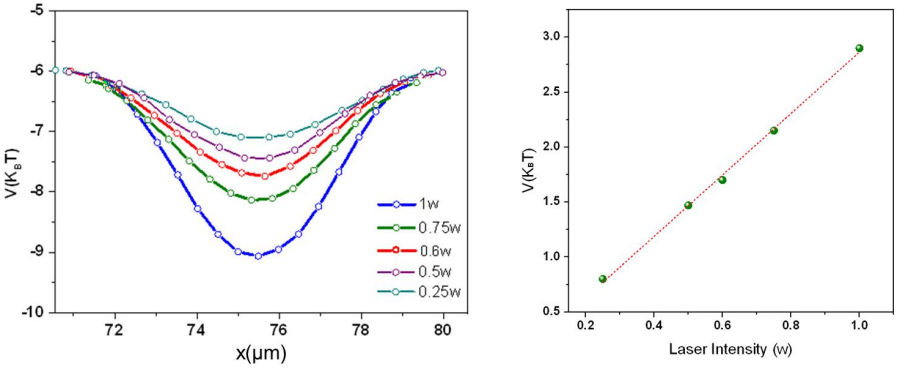

Figure 3.5: *Colloid-light interaction as a function of the laser power for polystyrene particles ($\sigma = 3.9\,\mu m$) in water. a) Laser potential cross-section for $0.25\,W$ (light green), $0.5\,W$ (purple), $0.6\,W$ (red), $0.75\,W$ (green) and $1\,W$ (blue). b) Experimental data are indicated by full circles and the dashed line is a linear fit corresponding to eq. 3.2 of Loudiyi et al. [98].*

3.4.2 Laser-induced periodic ordering

In this section we show how a periodic ordering is induced in the colloidal monolayer in the direction perpendicular to the light potential which has a periodicity $\boldsymbol{d}$ slightly larger than the average particle distance $\boldsymbol{a}$ of the colloidal monolayer. As a result, a suspension of polystyrene particles ($\sigma = 3.9\,\mu m$ and $\rho = 0.016/\,\mu m^2$) which forms a liquid phase in the absence of light field, transforms gradually into a one dimensional periodic phase ($1D$ crystal) as V_0 increases. This is illustrated in Fig. 3.6 for a sample of $N = 1400$ particles ($a = 7.8\,\mu m$). At weak laser potential the interplay of the optical and electrostatic forces imposes a slight order in the x-axis while maintaining significant

the potential well barrier becomes much higher than the thermal fluctuation energy of the particle

thermal fluctuations preventing particles from making local registrations in the potential well. When potential strength is increased above $10k_BT$ trapping forces dominate and particles follow the potential wells forming decoupled strings. The latter is a result of suppressed thermal fluctuations in the direction perpendicular to the strings and enhanced fluctuations along them, thus forming a periodic modulated liquid state with a periodicity commensurate with the substrate. This change in fluctuations strength along and perpen-

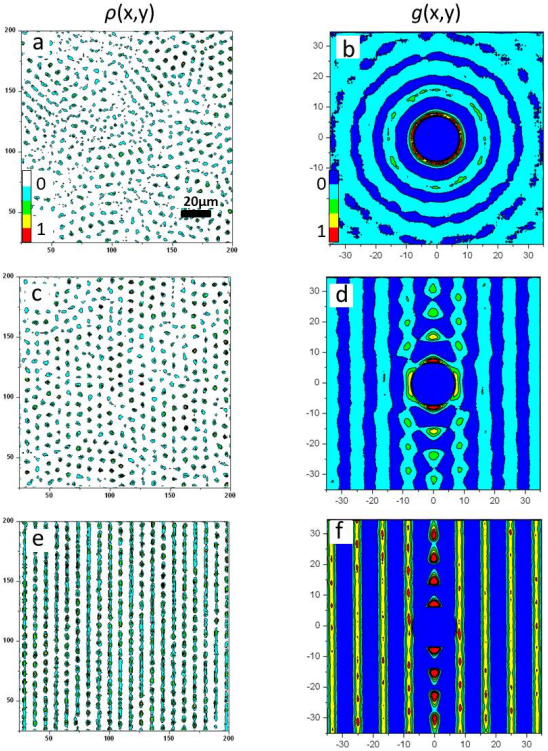

Figure 3.6: *Contour plots of the average density distribution $\rho(x, y)$ and the pair correlation function $g(x, y)$ at different substrate potential strength V_0 and $\boldsymbol{d} = 8.2\,\mu m$. (a,b) is the initial phase $V_0 = 0k_BT$, (c,d) $V_0 = 3k_BT$ and (e,f) $V_0 = 12k_BT$.*

dicular the particle strings is clearly seen in the average particle distribution $\rho(x, y)$ and $g(x, y)$ in Fig. 3.6. As the light potential strength increases from $V_0 = 3k_BT$ (Fig. 3.6(c,d)) to $V_0 = 12k_BT$ (Fig. 3.6(e,f)) the particle density lines become narrower.

It must be emphasized that a periodic ordering is not necessarily induced by a periodic substrate potential. Quasiperiodic patterns can also induce a periodic ordering with a periodicity incommensurate with the substrate but related to the imposed quasiperiodic length scales. This is exemplified for 1D quasiperiodic patterns in chapter 5, and for 2D substrates which where illustrated in the section 2.4 of the previous chapter. Up to now, the created light fields give the same results as the interference pattern [7, 86].

3.4.3 Advantages over interference patterns

Compared to light potentials modulated by two interfering laser beams [7, 103, 104] this method allows *in situ* control of the spacial distribution of potential wells without any optical realignment. In addition this method allows the creation of periodic and non-periodic light patterns. This is exemplary shown in Fig. 3.3c where we created a quasiperiodic pattern with line spacing following a Dodecanacci sequence [105, 35] being closely related to 12-fold quasicrystals. This sequence is comprised of two length scales, L and S with $L/S = (1 + \sqrt{3})/2$. Another advantage of this method over interference patterns is creating periodic but non-symmetric patterns. The latter is achieved by replacing even step-like voltage protocol shown in Fig. 3.3d (corresponding to a single distance of the scanned laser lines) by an uneven step function applied to the voltage controlled mirror (corresponding to two distances including a small one in the order of 1 µm).

3.5 Freezing and melting of colloidal monolayers on 1D periodic light fields

In this section we test the scanning tweezing technique we use to create 1D light patterns. This is done by performing an experiment on a colloidal monolayer of highly charged particles and comparing the results to a well known phenomena in which phase transitions are observed in the presence of an 1D interference light pattern.

We expect a phase transition from a liquid to crystal followed by a reentrant melting into a liquid as a function of the light potential strength. This results from the interplay between the pair particle and light-particle interactions under the conditions that the periodicity $\boldsymbol{d}$ of the light pattern is close to the mean particle distance $\boldsymbol{a}$ of the suspension.

Theoretical studies by Chakrabarty et al. (1985) showed a phase diagram where this phenomena is observed for a certain range of the colloidal density $\kappa \boldsymbol{a}^{-1}$ against the light potential strength. This is illustrated in Fig. 3.7 in

the colored regime where a liquid freezes into a crystal and then melts again for large light potential strengths and particle densities around $\kappa \boldsymbol{a}^{-1} = 0.07$. Here, we give an overview of the early work done in this field, experimetally and theoreticaly, and then explain in details our experimental results which have been observed before for the interference pattern. From this test we conclude that the scanned beam in our present setup creates a quasi-static light potential pattern but with more advantages (mentioned in section 3.4.3)over interference patterns.

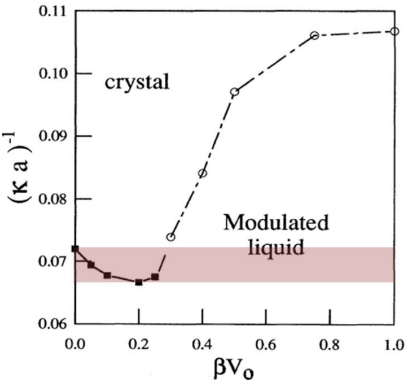

Figure 3.7: *Phase diagram as a function of* $\kappa \boldsymbol{a}^{-1}$ *against* βV_0 *with* $\beta = 1/k_B T$ *as obtained by MC simulations. Filled squares denote first-order transition points, whereas open circles correspond to continuous transition points in the colored regime. These data are used from ref [106]. The area in light red shows the induced freezing and melting regime.*

3.5.1 Earlier studies on colloidal monolayers in the presence of periodic light field

The first experiments in this direction have been carried out by Chowdhury, Ackerson and Clark [7], who demonstrated that a colloidal liquid freezes into a hexagonal crystalline state by application of an optical interference pattern of periodically spaced lines. When they tuned the distance of the laser lines to $\boldsymbol{d}=\boldsymbol{a}\sqrt{3}/2$ with $\boldsymbol{a}$ being the mean particle distance, they observed a phase transition from a liquid into a hexagonal phase as the laser intensity was increased (laser-induced freezing) [7].

Later, it has been demonstrated that a further increase of the laser intensity can lead to reentrant behavior from a hexagonal phase to a liquid. This is in agreement with theoretical and numerical studies [87, 101]. The reentrant

melting is expected in systems with short range interactions where phonon fluctuations are suppressed in the direction perpendicular to the substrate, leading to a decoupling of the colloidal strings [86, 101]. This study was further expanded by Radhovsky, Nelson and Frey when they theoretically found novel phases for different commensurabilities between the substrate and the suspension [107]. For example, if $\boldsymbol{d}=\boldsymbol{a}\sqrt{3}/4$, a locked smectic (LSm) phase is observed where particles, though locked in every second line, preserve strong correlations in the direction transverse to the substrate [107]. Experimental study with interference light field patterns showed agreeable results which are presented in details in reference [108].

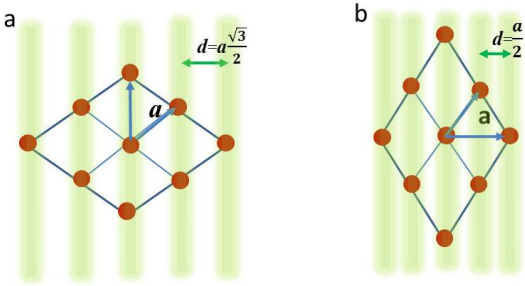

Figure 3.8: *Local particle density distribution showing two orientations along the laser lines. a) triangular distribution (triangular I phase) at laser line spacing* $\boldsymbol{d}=\boldsymbol{a}\sqrt{3}/2$. *The laser lines are shown in green. b) triangular II phase (rotated triangular I) can be formed at* $\boldsymbol{d}=\boldsymbol{a}/2$.

3.5.2 Experimental results

We present the experimental realizations of liquid-crystal-liquid transitions for charged polystyrene spheres, with diameter $\sigma = 3.9\,\mu m$ and suspended in water (preparation described in section 3.1.1), in the presence of a periodic light pattern. A schematic sketch in Fig. 3.8, shows the possible crystal orientation induced for two commensurate periodicities $\boldsymbol{d}=\boldsymbol{a}\sqrt{3}/2$ and $\boldsymbol{d}=\boldsymbol{a}/2$. The transition in the second case is difficult to achieve due to the restriction on the periodicity of the light pattern which cannot be less than $5\,\mu m$ else it results in an overlap of the potential wells. To solve this problem we use organic solvents which have lower ionic strength and particles that can exhibit larger mean distances (this will be the subject of chapter 4).

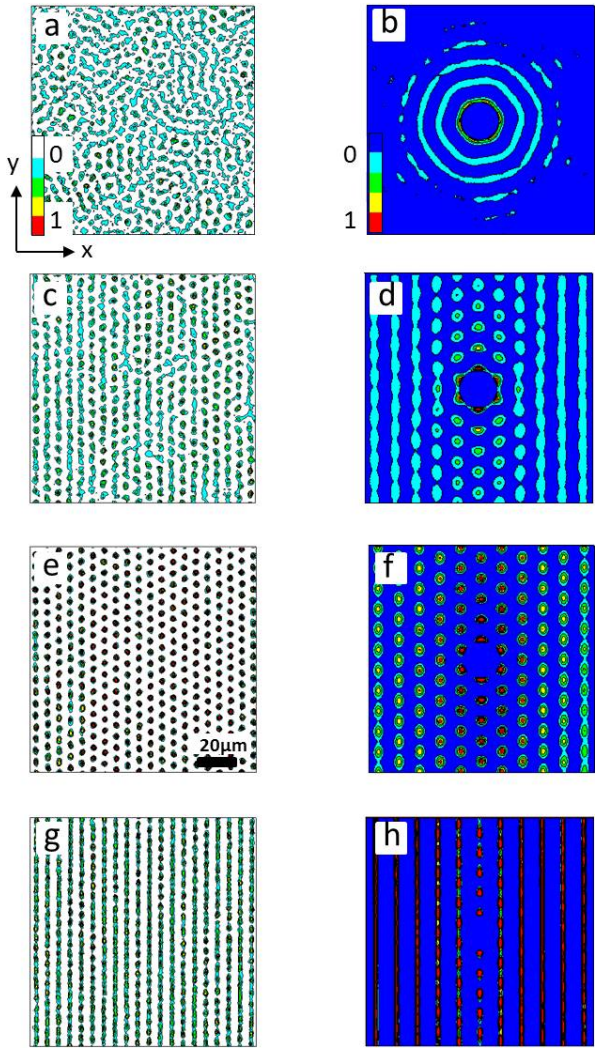

Figure 3.9: *Contour plots for $\rho(x, y)$ presented in the left column and $g(x, y)$ in the right column for a colloidal sample at a particle density $\rho = 0.024/\,\mu m^2$, $\boldsymbol{d} = 6\,\mu m$. (a,b) liquid phase at $V_0 = 0$, (c,d) modulated liquid (ML) at $V_0 = 0.75 k_B T$, (e,f) triangular I crystal (freezing state) at $V_0 = 3 k_B T$. (g,h) a modulated liquid at $V_0 = 12 k_B T$.*

Liquid-crystal-liquid transition as function of substrate potential strength

In the following we show the different phases by analyzing the pair correlation function $g(x, y)$ and the particle density distribution $\rho(x, y)$ of a sample cell with $N = 1000$ particles and density $\rho = 0.0240/\,\mu m^2$ ($\boldsymbol{a} = 6.6\,\mu m$). Each experiment lasted 16 minutes and was recorded with a rate of 1 fps. At this density, the sample forms a liquid phase in the absence of light field. Fig. 3.9 shows how this phase evolves when the light field strength is increased. At weak potential strength of $V_0 = 0.75 k_B T$ (Fig. 3.9 c,d) we observe a modulated liquid (Light-induced melting LIM) where particles start to feel the optical forces and make ordering in the x -direction. At $V_0 = 1.5 k_B T$ the particles order is now transfered along the potential wells and a two-dimensional triangular crystal phase (Light-induced freezing LIF) is formed. This is shown in Fig. 3.9(e,f) where, at this stage, the interplay between optical forces and coulomb pair interactions drive the particles to make ordered registrations along the potential wells. The mechanism behind this transition has been explained in details in Ref [101] and briefly states that gradient forces push the particles to follow the laser lines and form periodically spaced strings, which enhance thermal fluctuations between particles sitting in adjacent lines. At a laser strength of $V_0 = 12 k_B T$, a reentrant melting (LIM) into a modulated liquid is observed. This is illustrated in Fig. 3.9 (g,h) where now the potential wells are strong enough to decouple the particle strings by suppressing thermal fluctuations in the transverse direction (x-axis) and enhancing those along the potential wells [86, 101]. A comparison of the thermal fluctuations, perpendicular and along the potential wells, between the freezing and reentrant melting

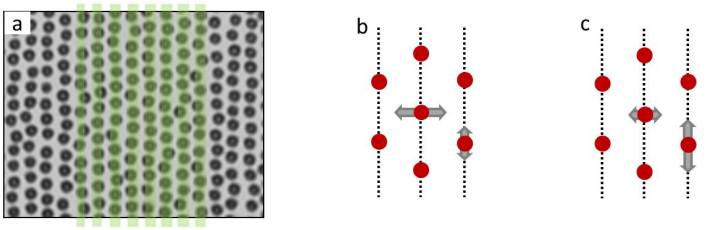

Figure 3.10: *A snap shot of the crystal phase is shown in a) with particles positioned on the potential wells (green lines). In b) and c) fluctuation strength are represented by arrows and the potential wells by dashed lines. In b) the fluctuations are stronger in the direction perpendicular to the laser lines, leading to 2D triangular I crystal. In c) fluctuations strength reverse and become stronger along the potential wells causing decoupling of particle lines and melting of the crystal into a modulated liquid.*

states is illustrated in Fig. 3.10. In this figure an over lay of the observed crystal phase and the laser potential wells (green lines) is sketched, showing an alignment of the particles but with out-of-line fluctuations due to the strong correlation of adjacent lines. This indicates qualitatively, a quasi-long range order along the colloidal strings of the induced crystal phase.

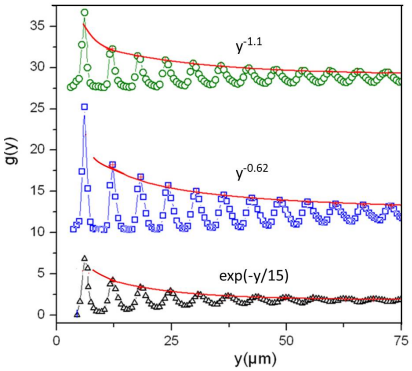

Figure 3.11: *Pair correlation function g(y) of particles along the laser lines for* $V_0 = 0.75k_BT$ *(triangles),* $3k_BT$ *(squares), and* $12k_BT$ *(circles). Solid lines are fits to each envelope of the curves.*

A more quantitative evidence for the different phases mentioned here can be extracted from g(y), i.e the pair correlation function along the laser lines. This parameter has been also used in Ref [86, 108] to these phases. Therefore, g(y) is illustrated in Fig. 3.11 where a modulated liquid at weak potentials (lower curve) shows a short range correlation and finally decays to 1 (triangles) at large distances. The envelope of this curve can be fitted with an exponential function with decay length of 15 µm (solid line). At the intermediate potential, shown in the middle curve (squares), g(y) decays much slower with an envelope fitted to an algebraic decay such that $g(y) = 1 - y^{-\eta}$ (solid line) with $\eta = 0.62$ is the correlation length. This is in agreement with 2D crystals which are characterized by quasi-long range order and pair correlations decaying algebraically as a function of distance [62, 65]. The upper curve of Fig. 3.11 shows that for a potential depth of $V_0 = 12k_BT$ the pair correlation becomes weaker along the lines and it can be fitted to an algebraic decay with exponent $\eta = 1.1$ which is larger than the theoretical upper limit for a crystal [109, 110], thus indicating a modulated liquid.

3.5.3 Phase diagram for liquid-crystal transition

The same phase behavior discussed above is expected for a range of particle densities in which coulomb interactions between neighboring particles are significant. Therefore, an experimental observation of the phase behavior of a colloidal monolayer (aqueous suspension of polystyrene spheres), is made at different densities, i.e $\kappa \boldsymbol{a}^{-1}$ and studied for different light potential strengths [111].

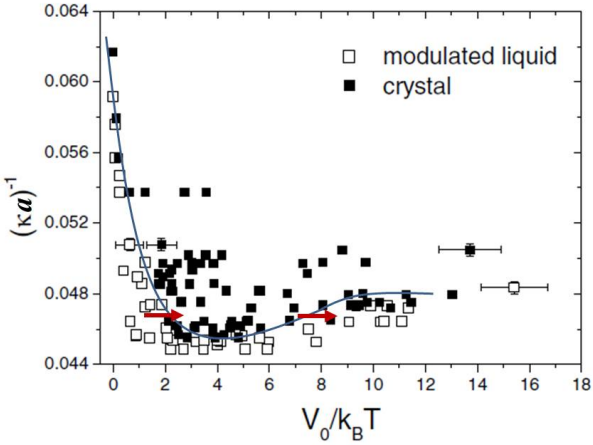

Figure 3.12: *Phase diagram as a function of $\kappa \boldsymbol{a}^{-1}$ versus the light potential strength V_0. Symbols denote experimental data [101] for the modulated liquid (open squares) and the crystal (full squares). The solid line is a guide for vision [101]. Red arrows indicate LIF and LIM phases we discussed in Fig. 3.9.*

This is illustrated in Fig. 3.12, where for a relatively small range of $\kappa \boldsymbol{a}^{-1}$ between 0.0045 and 0.0048, one observes the sequence of transformations: isotropic liquid - modulated liquid - crystal - modulated liquid. Other wise a crystal cannot be melted (high $\kappa \boldsymbol{a}^{-1}$) and a liquid stays a liquid without passing through the freezing state (low $\kappa \boldsymbol{a}^{-1}$).

3.5.4 Conclusion and outlook

In conclusion, we are able with this laser tweezing technique to produce quasi-static light fields similar to interference patterns and reproduce the same results previously done in refs [7, 86, 108]. Therefore, we have experimentally revisited the crystallization and melting behavior of a 2D colloidal suspension

in the presence of a periodic light pattern with a periodicity $\boldsymbol{d}=\boldsymbol{a}\sqrt{3}/2$. Other commensurate light patterns like $\boldsymbol{d}=\boldsymbol{a}\sqrt{3}/6$ or $\boldsymbol{d}=\boldsymbol{a}\sqrt{2}/2$ would lead to similar phase diagrams but with particles filling second or third lines respectively. Radhovskiy, Nelson and Frey [107] had theoretically predicted a full phase digram for freezing and melting phenomena in the presence of different pattern commensurabilities. Experimentally it would be interesting to investigate the phase behavior in the presence of such patterns with particles filling each line. This can be achieved for a colloidal suspension with strong repulsive forces and long range order where then, larger particle spacings would allow the light pattern to be used. We discuss such experiments in the next chapter where we used silica particles suspended in bromobenzene and had more that 20 µm mean particle distance.

4 Laser-induced crystalline order transition

We present measurements on the phase behavior of a suspension of colloidal crystals interacting with periodic substrate potentials which are created by scanning one laser beam. In order to realize a wide range of line spacings relative to the lattice constant, we use a suspension of silica particles in bromobenzene. This colloidal system has a Debye screening length of about 4.6 µm which results in the formation of crystals with lattice constants up to 20 µm. Because the refractive index of bromobenzene is larger than that of the colloids, optical gradient forces lead to the attraction of particles at regions where the intensity is smallest, therefore the process we call inverse tweezing. Depending on the depth and periodicity of the optical potential, we observe the light-induced assembly of colloids into triangular, rhombic, square phases in addition to ordered-disordered phase transitions.

4.1 Motivation

Phase transitions in two-dimensional systems have attracted considerable attention, because such systems are of great technological importance [4, 112]. Often, the transition between a liquid (disordered) and a crystalline (ordered) state is induced by variations in the particle pair potential [113, 77]. In addition, structural phase transitions can be also triggered by external periodic fields which enhance the long-range positional order. While the latter is obvious for two-dimensional substrate potentials which localize the particles at well-defined positions in the sample plane [114, 115, 52], it is less obvious that also a one-dimensional, periodic substrate potential can induce two-dimensional order in a colloidal system. The first experiments in this direction have been discussed in section 3.5.1. In contrast to the above experiments where the initial phase (i.e. the phase formed in the absence of a light pattern) was a colloidal liquid, here we investigate the response of a charge-stabilized colloidal crystal with lattice constant $\boldsymbol{a}$ to a one-dimensional light field with periodicity $\boldsymbol{d}$. To obtain a large range of $\boldsymbol{d/a}$, we have used a colloidal suspension in an organic solvent which has low polarity and therefore large Debye screening lengths much larger than those observed in aqueous solutions. Depending on the intensity, periodicity and even the width of the light field, we observe a phase diagram rich in a variety of different colloidal phases with triangular, rhombic, square, and disordered transient phases.

4.2 Materials and methods

4.2.1 Colloidal suspensions of silica particles in bromobenzene

In our experiments we use charged silica spheres with diameter $\sigma = 3.72\,\mu m$ and a polydispersity less than 5% suspended in an organic solvent namely bromobenzene (C_6H_5Br). These colloids were purchased as an aqueous suspension from Microparticles GmbH with size of standard deviation $SD = 0.08\,\mu m$ and mass concentration of 5% w/v. These silica spheres are hydrophilic and when placed in contact with water acquire a negative charge due to the dissociation of the silanol group according to:

$$SiOH \rightleftarrows SiO^- + H^+ \tag{4.1}$$

with SiO^- being the colloidal surface charge and H^+ as counter ions [75, 116].

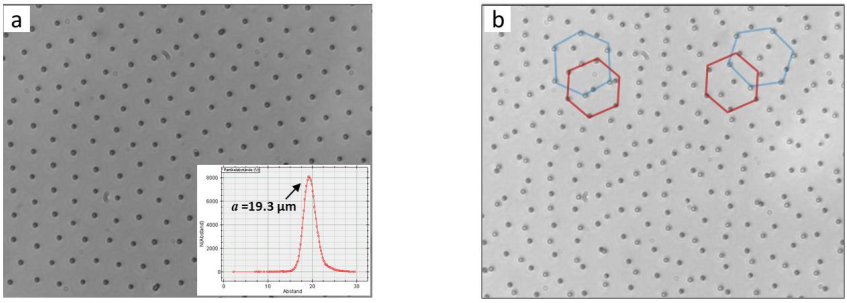

Figure 4.1: *Snap shots of colloidal silica spheres suspended in bromobenzene. At a density a)* $\rho = 0.0055/\,\mu m^2$ *a monolayer is formed with particles imaged as full circles at the focal plane of the objective. The mean particle distance* $\boldsymbol{a}$ *is determined from the bond length distribution which is plotted in the inset. In b) where* $\rho = 0.008/\,\mu m^2$ *a second layer is formed with particles positioned out of focus and displayed as rings. The red and blue hexagons indicate the particle arrangement in the lower and upper layers respectively.*

Before the colloids are transferred to bromobenzene, the following steps have to be done carefully to ensure monodispersity and stability of the colloids. First, a 100 µL sample is prepared in a glass micro tube where the original solvent is replaced by highly deionized water with an ionic conductivity of $0.06\,\mu S/cm$. This process helps to decrease the number of ions in the solvent, thus enhancing the electrostatic stability of the suspension. Next, the suspension is centrifuged for 2 minutes at 2000 *rpm* to separate the water from

the particles. The water is then taken out and replaced by deionized water. This step is repeated several times before the suspension is sonicated for few minutes. Sonication helps to release coagulated particles occurred due to the centrifugation process and therefore insures monodispersity in the suspension. Then, the water is evaporated from the suspension under vacuum conditions at room temperatures. After this process, only a thin adsorbed layer is left on the surface of silica particles [75, 117]. We add 1 mL of bromobenzene to the dried sampled and place it in an electrical shaker for several hours to separate particles that aggregated during the drying process. At this stage sonication is avoided since this may cause the degradation of bromobenzene into its constituents, i.e. benzene and bromine [118]. After the bromobenzene suspension is left for half an hour, aggregates sediment towards the bottom where they can be easily removed. Finally, around 100 µL of the aggregate-free suspension is injected into a sample cell (Hellma) which consists of a fused silica cuvette with 200 µm height. The cell is then sealed tightly to avoid contact with air since the air will significantly increase the ionic concentration in the solvent as a function of time. In a closed cell, the suspension maintains its properties for a period of two months.

Bromobenzene is an organic solvent with a refractive index $n = 1.56$ and a polarity close to the limit of that of apolar liquids [119]. Since the density of silica particles is larger than that of bromobenzene, then particles sediment toward the bottom surface of the cell. For particle densities in the range of $\rho = 0.004 - 0.006/\,\mu m^2$ the colloidal system forms a two-dimensional charge-stabilized crystal. Due to the large Debye screening length (see below) the particles form a triangular crystal with lattice constants up to 20 µm as shown in Fig. 4.1a. The mean particle $\boldsymbol{a}$ is determined from the bond length histograms. Bond-lengths were caculated based on a Delaunay triangulation that identifies the bonds between each particle and its nearest neighbor. Because the out of phase fluctuations account to less than 100nm, the system can be considered as effectively two-dimensional. Samples with particle densities beyond $0.006/\,\mu m^2$ are observed to build additional layers of triangular crystals. A snap shot of a sample of two layers is shown in Fig. 4.1b where the particles of the layer close to the bottom surface are in the focal plane of the camera objective (full circles) while the particles of the second layers are distinguished by rings due to their positions above the focal plane.

4.2.2 Pair interaction determined by density functional theory (DFT)

In order to determine the pair interaction of our experimental system, we prepared several low density samples ($\rho = 0.002/\,\mu m^2$) and measured the pair correlation function g(r). A direct inversion of g(r) for two-dimensional sys-

tems is not possible due to the finite size of the system and particle density fluctuations during the course of measurement which results in statistical errors and deviation of g(r) from 1 at large distances. Therefore, some model density functional theory (DFT) calculations [120] were carried out at the institute of theoretical statistical physics and soft matter (Tübingen University), for a two-dimensional system of disks that interact via a hard-core Yukawa potential of the form:

$$\frac{U(r)}{k_{\mathrm{B}}T} = \frac{A}{r}e^{(-\kappa r)} \qquad r > \sigma \tag{4.2}$$

with $U(r) = \infty$ for $r < \sigma$, $A = (Z^*)^2\lambda_B(\frac{e^{\kappa\sigma/2}}{1+\kappa\sigma/2})^2$. Here, r is the center-to-center particle distance, Z^* the effective surface charge, λ_B the Bjerrum length, κ the inverse screening length and σ the diameter of the particles. In the case of bromobenzene (dielectric constant $\varepsilon = 5.6$) the Bjerrum length is 10nm.

A recently developed DFT [121] is used for the hard disk reference system and a perturbation theory treatment for the soft Yukawa repulsion [122]. The Yukawa parameters were obtained by combining two observations: First, from the experimental particle trajectories we obtained the average number density and the number particle fluctuation in a sub-volume of our system. From this it is possible to estimate the compressibility of the fluid [122] as described by equation 2.6 which is valid in a grand canonical ensemble where the sub-volume system is coupled to a particle reservoir [1]. Now comparing the measured to the computed g(r), the latter determined from test particle route DFT calculations, we obtained the Yukawa parameters, under the constraint of the above obtained compressibility. Best agreement between experiment and theory was found for $\beta A = 186\,\mu\mathrm{m}$ and $\kappa^{-1} = 4.6\,\mu\mathrm{m}$ which leads to an effective surface charge $Z^* = 128$. Due to the small value of the effective surface charge, a variation of the particle density within the range discussed here does not measurably change the ionic strength. It should be also mentioned, that the contribution of the colloidal monolayer to the overall counterion concentration is rather small since the height of our sample cell is much larger than the particle size.

If the particle density in this system is increased, the DFT results in a freezing transition to a crystal which has a lattice constant of 14 µm which

[1] On the other hand the compressibility is related to the pressure in the system by the relation: $\frac{\partial p}{\partial \rho} = \frac{1}{\rho\chi_T}$ which is useful since the DFT has an analytical form of $\rho(r)$. DFT approach results then in a relation that combines the two Yukawa parameters A and κ. This estimation of χ_T is very helpful to search for good parameters.

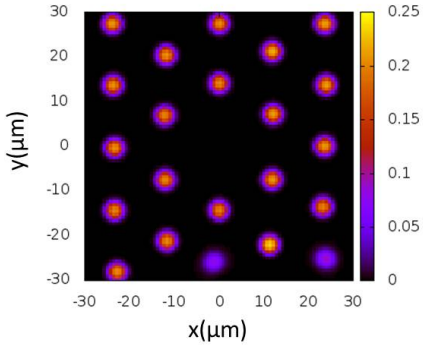

Figure 4.2: *Pair correlation function $\rho(x, y)$ of a crystal obtained with DFT for $A = 186\,\mu m$ and $\kappa^{-1} = 4.6\,\mu m$. The center of the plot represents a fixed particle. The color code indicates the probability distribution of finding a particle at a certain distance from the center. This probability ranges between minimum (black) and maximum (yellow) (private communication with R. Roth at the statistical and soft matter theoretical physics, Tübingen, Germany 2013).*

is in a good agreement with the experimentally observed crystals studied in this chapter. From the particle trajectories the pair correlation functions $\rho(x, y)$ are obtained by DFT and compared to the experimentally calculated one (Fig. 4.2). This is another check test that the DFT routine used here is reliable and accurate. Note that the DFT calculation is performed in the so called test-particle route. This means that one particle is fixed at the center of the coordinate system where this particle becomes an external potential for the rest of the system. In this potential the density profile $\rho(r)$ is obtained and $g(r)$ is calculated through the relation $g(r) = \rho(r)/\rho$. This explains the missing particle at the center of the $g(x, y)$ plot in Fig. 4.2.

4.2.3 Light substrate potentials and inverse tweezing

Light patterns described in section 3.3 are used here, but since the refractive index of bromobenzene is larger than that of silica ($n = 1.42$) as listed in table 4.1, the colloidal particles will be expelled from the high intensity regions and attracted towards locations where the laser pattern has its smallest intensity. This inverse tweezing process is illustrated in Fig. 4.3a. The regions with minimal light constitute the substrate potential with a period $\boldsymbol{d}$ which in this case determine the width of the trapping potential wells presented by gray

	C_6H_5Br	H_2O	SiO_2
n	1.56	1.33	1.42
$\rho(g/cm^3)$	1.49	1.00	1.8
ε	5.45	80	–
η x 10^{-3} $(Pa.S)$	1.124	0.894	–

Table 4.1: *Physical properties of bromobenzene, water and silica particles.*

lines in Fig. 4.3b.

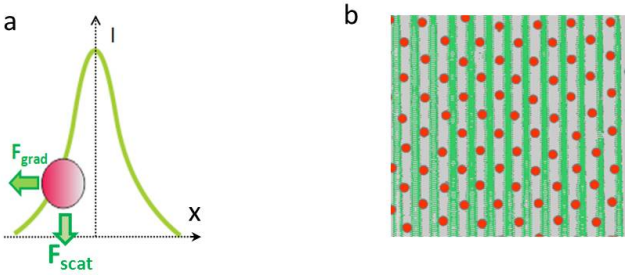

Figure 4.3: *Inverse tweezing: a) light gradient forces of the Gaussian beam kicks silica spheres out of the high intensity regions and b) is an overlay of a crystal with colloids (full red circles) with the substrate potential of minimum (gray regions) and high intensity light (green).*

In our experiments we work with $\boldsymbol{d}$ between $6 - 18\,\mu m$ and a repetition time of one cycle of the scanning mirror is t=0.025s. During that time the silica particle diffuses over a distance $L = \sqrt{2Dt}$, with a diffusion coefficient of $D = 0.104\,\mu m^2 s^{-1}$ in bromobenzene and yields a diffusion distance $L = 0.071\,\mu m$ which is less than 2% of the half width of the optical trap. Therefore, the substrate potentials discussed here can be regarded as quasi-static. To have a quantitative estimate about the particle-light interaction, we measured the particle density distribution of a highly diluted colloidal suspension ($\rho = 0.0003/\,\mu m^2$) in the presence of the light potential. Evaluating the particle probability distribution in the direction perpendicular to the laser lines, and employing the Boltzmann statistics we obtain the depth and width of the laser potential acting on the particles as shown in Fig. 4.4. The half width of the interaction potential in the inset of Fig. 4.4 is $4.1\,\mu m$ which is somewhat larger than the actual half width of the optical line due to the fi-

nite size of the particles [98]. As expected [100, 98], the potential amplitude V_0 increases linearly with the laser intensity. As a result of inverse tweezing

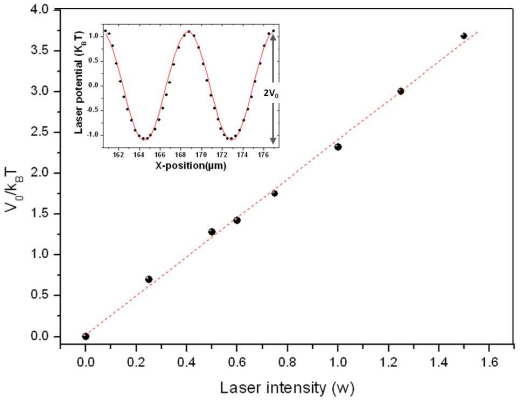

Figure 4.4: *Amplitude of the laser potential acting on colloidal particles of* $3.72\,\mu m$ *diameter as a function of the incident laser intensity. The symbols correspond to the measured data and the dashed line is a linear fit which indicates the linear relationship between* V_0 *and the laser intensity. The inset shows a part of the cross-section of the potential for a line spacing* $\boldsymbol{d} = 8.2\,\mu m$*. It should be emphasized, that in general non-sinusoidal potential cross-sections are obtained. The similarity with a sine function shown here is a result of the Gaussian intensity distribution of the laser line and the specific line spacing chosen.*

mechanism a colloidal monolayer of this suspension is expected to undergo phase transformations as a function of the substrate potential strength and the periodicity $\boldsymbol{d}$.

4.2.4 Phase characterization

To distinguish between different structural phases obtained in our experiments we determined the particle-center coordinates by means of digital video microscopy [99] and a particle-tracking algorithm in order to calculate the corresponding pair correlation functions $g(x, y)$. Fig. 4.5 shows a schematic illustration of the central region of $g(x, y)$ together with the trapping potential indicated by dashed vertical lines. From the distances v and u of the central particle to its nearest neighbors perpendicular and along the laser lines respectively, we define the order parameter $\xi = u/v$ which allows us to distinguish different structural phases according to table 4.2.

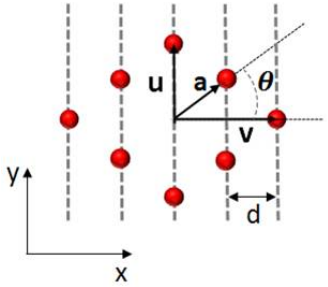

Figure 4.5: *Center region of the $g(x, y)$ illustrating the average nearest particle distance v and u along the x and y axes respectively, with an average particle distance a along symmetry lines making angle $\theta = tan^{-1}(\xi)$ with the x-axis.*

Crystal phase Parameter	$\boldsymbol{d/a}$	$\xi = u/v$	$\theta = tan^{-1}(\xi)$
Triangular I	0.86	0.554, 0.600	29°, 31°
Rhombic I	0.85, 0.72	0.600, 0.965	31°, 44°
Square	0.71	0.965, 1.036	44°, 46°
Rhombic II	0.69, 0.51	1.036, 1.000	46°, 59°
Traingular II	0.5	1.660, 1.804	59°, 61°

Table 4.2: *Characterization of different crystalline phases by different order parameters as defined in the text.*

4.3 Results and discussions

4.3.1 Observation of phase transitions from triangular to rhombic and square phases

The experiments discussed in the following were performed with samples having a particle density $\rho = 0.0057/\,\mu m^2$. Each experiment lasted for 16 minutes and was recorded with a rate of 1 fps. In the absence of the external potential, at this density the system forms a spontaneous crystal with random orientation and a mean lattice constant of about 13.5 µm. Fig. 4.6 shows the corresponding snap shots as well as the particle densities and pair correlations when the periodicity of the laser pattern was set to values between $6 - 12\,\mu m$. Each measurement started with a spontaneous crystal ($V_0 = 0$) and the intensity was slowly increased to $7.2 k_B T$. Due to this protocol, the particles can initially exchange between potential lines and the obtained structures corre-

spond to equilibrium phases. In Fig. 4.6(a,b,c) the periodicity is tuned to the triangular commensurate case $\boldsymbol{d/a} = 0.86$. At $V_0 = 1.5k_BT$ the crystal aligns accordingly and eventually forms a perfect triangular I structure at $7.2k_BT$. Fig. 4.6(d,e,f) correspond to $\boldsymbol{d/a} = 0.77$. According to the above definition of phases, under such conditions a rhombic I phase with $\xi = 0.83$ is obtained. Fig. 4.6(g,h,i) correspond to the square commensurate phase where $\boldsymbol{d/a} = 0.71$. Further decrease of the line spacing to $\boldsymbol{d/a} = 0.63$ leads to the rhombic phase II Fig. 4.6(j,k,l) and finally, for $\boldsymbol{d/a} = 0.5$ a rotated triangular crystal (triangular II phase) is obtained as shown in Fig. 4.6(m,n,o).

The reason for the formation of the different phases is the counter play between optical trapping forces and the repulsive pair potential. While the optical forces align the particles along the potential lines at a given distance $\boldsymbol{d}$, the strong electrostatic particle repulsion leads to a registration between adjacent lines. It is important to realize, that due to the constant total particle density in the sample cell, the particle line density will change upon variation of the line spacing $\boldsymbol{d}$. For example, during the transition from the triangular I to the square phase, i.e. upon decreasing the distance $\boldsymbol{d}$, the particle density along the lines will decrease. Note, that the length of the laser lines in y-direction is about 3mm being much smaller than the extension of the sample cell which allows the exchange of particles in that direction.

The different phases can be also clearly distinguished by analysing their bond-length histogram. Bond-lengths were calculated based on a Delaunay triangulation [123, 124] that identifies the bonds between each particle and its nearest neighbor. Fig. 4.7 shows such normalized histograms for the different phases taken at $V_0 = 7.2k_BT$. Both, the triangular I and the triangular II phases show a single peak corresponding to six-fold coordinated particles at distance $\boldsymbol{a}$. In contrast, the rhombic I and II phases show a decrease in the amplitude of the first peak and a rise of a second one at a larger distance. The first peak corresponds to 4-fold coordinated particles at distance $\boldsymbol{a}$ and the second peak corresponds to 2-fold coordinated particle at distances between $\boldsymbol{a}$ and less than $\boldsymbol{a}\sqrt{3}$. For the square phase, also two peaks are observed, one corresponding to the four nearest neighbors at distance $\boldsymbol{a}$ and a second peak at distance $\boldsymbol{a}\sqrt{2}$. Due to the quasiperiodic order in two-dimensional systems, in general the second peak of the bond-length histograms is slightly broader than that of the first peak.

4.3.2 Disoredered intermediate phase during crystal-crystal transition

In Fig. 4.8 we have investigated how the square phase gradually forms for a period $\boldsymbol{d} = 9.58\,\mu\text{m}$ with increasing the laser intensity. Starting from a randomly oriented spontaneous triangular crystal at zero light intensity as

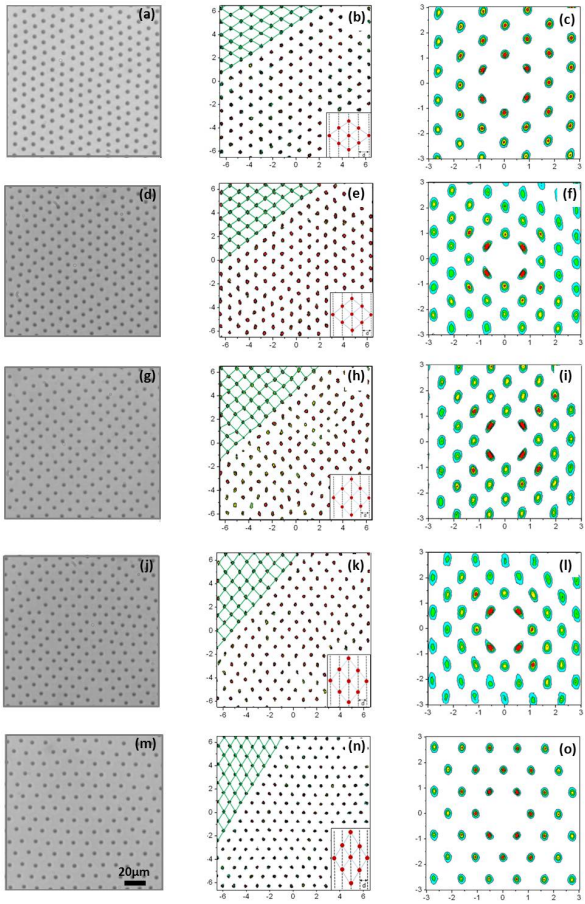

Figure 4.6: *Snap shots for the different phases are shown at the left while contour plots of the average density distribution function* $\rho(x, y)$ *are shown at the middle and pair correlation function* $g(x, y)$ *are shown at the right for a potential strength of* $V_0 = 7.2 k_B T$. *[a,b,c] triangular I phase at a periodicity* $d = 11.6\,\mu m$ *and* $\xi = 0.588$, *[d,e,f] rhombic I phase at* $d = 10.4\,\mu m$ *and* $\xi = 0.830$ *[g,h,i], square phase at* $d = 9.58\,\mu m$ *and* $\xi = 0.995$, *[j,k,l] rhombic II phase at* $d = 8.5\,\mu m$ *and* $\xi = 1.217$, *[m,n,o] triangular II phase at* $d = 6.75\,\mu m$ *and* $\xi = 1.681$. *Green lines in* $\rho(x, y)$ *help to visualize the structure of each phase. All length scales are normalized by the lattice constant* $\boldsymbol{a}$ *of the initial phase.*

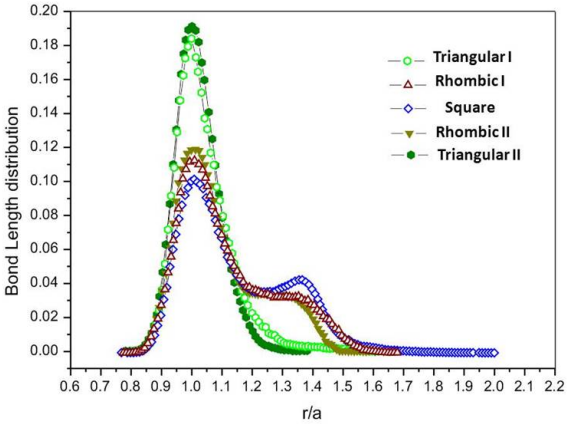

Figure 4.7: *Bond length distribution for the five phases at* $7.2k_BT$*. Triangular I (light green) and triangular II (dark green) show single peaks while rhombic I (red), rhombic II (brown) and square phase (blue) show two peaks.*

shown in Fig. 4.8(a,b), we observe at $V_0 = 2.4k_BT$ an intermediate phase as shown in Fig. 4.8(c,d). By looking particularly at the pair correlation function, which indicates the probability to find a particle at a certain distance from another one, a ring is observed around the center.

This is a signature of a disordered state which is a result of dislocations that appear [8, 125] when optical forces start breaking the crystal symmetry by rapturing pair particle interactions. This can be clearly seen in the Delaunay triangulation represented in Fig. 4.9 where the light potential disturbs the triangular particle bonding and introduces dislocations constituting mainly of 5- and 7- fold coordinated nearest neighbors as indicated by green and red particles respectively. This observation is in agreement with experiments on 2D vortex lattice of superconductors [9, 126] and numerically examined 2D particle systems [127] on 1D periodic substrates, where the substrate potential strength drives the systems into a disordered state.

On the other hand the light potential rather causes local registrations with 4-fold coordinated nearest neighbor particles which (colored by pink in Fig. 4.9b) give rise to the four peaks in the first ring of $g(x, y)$ in Fig. 4.8d. Increasing the potential strength localizes the particles in the potential wells and enhances their positional order which finally restores symmetry of a perfect square phase (Fig. 4.8(e-h)).

As already pointed out, the creation of potential landscapes by a scanned

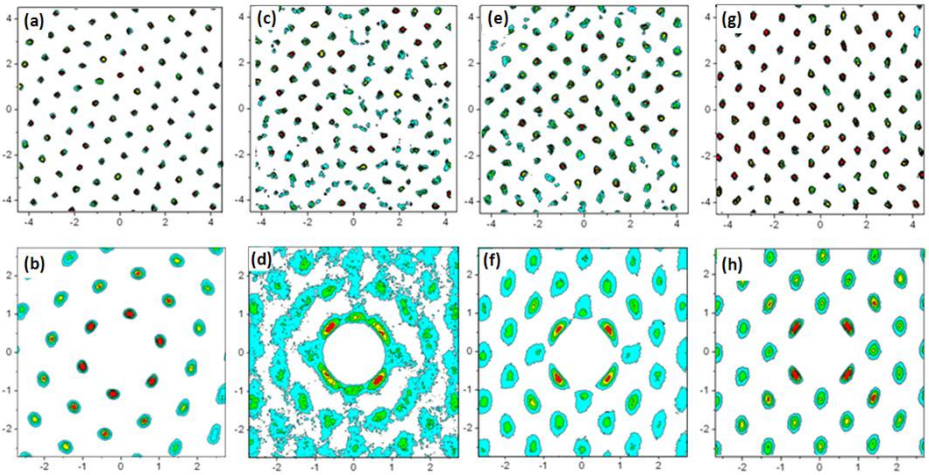

Figure 4.8: *$\rho(x, y)$ and $g(x, y)$ are shown at the top and bottom respectively at a fixed periodicity $\boldsymbol{d} = 9.58\,\mu m$ and different potential strengths for a randomly oriented triangular crystal. (a,b) at $V_0 = 0$, (c,d) a disordered state at $V_0 = 2.4k_BT$, a square phase shown in (e,f) at $V_0 = 3.6k_BT$ and (g,h) at $V_0 = 7.2k_BT$. All length scales are normalized by the lattice constant $\boldsymbol{a}$ of the triangular crystal.*

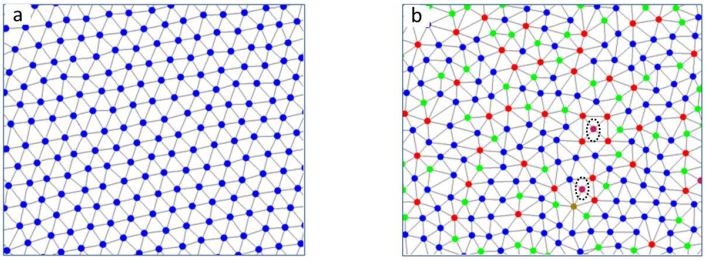

Figure 4.9: *Delaunay triangulation for a) a triangular phase, initially formed at zero light field, indicating particles (blue) bonding with 6 nearest neighbors. b) a disordered phase showing additional types of bonds per particle with 5 (green full circles), 7 (red full circle) nearest neighbors. Particles with 4 bonds (pink full cirlces) are marked by black dashed circles for clarity and indicate here motifs for the square phase.*

laser line offers several advantages compared to interference patterns. This includes the creation of non-periodic particle-light potentials as mentioned in

section 3.4.3 (Advantages over interference patterns), and also periodic but non-symmetric patterns. The latter is achieved by replacing the even step-like voltage protocol shown in Fig. 3.3d (corresponding to a single distance of the scanned laser lines) by an uneven step function applied to the voltage controlled mirror (corresponding to two distances including a small one in the order of 1 µm). This is exemplarily shown in Fig. 4.10a, where we create a non-symmetric particle-light interaction potential with periodicity of 18 µm and a width of the potential wells of 11.5 µm. Applying this potential with strength

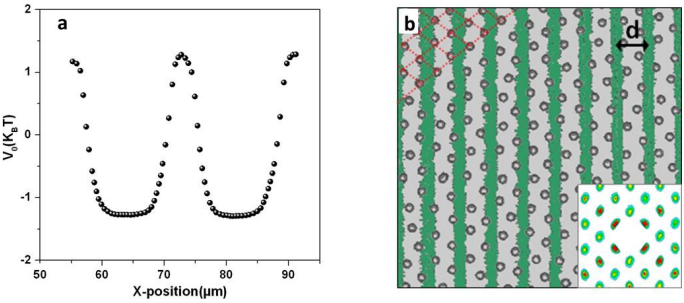

Figure 4.10: *a) Part of a non-symmetric potential cross-section for a periodicity of* $18\,\mu m$ *and a width of the potential wells of* $11.5\,\mu m$*. b) snapshot of colloidal particles superimposed to the potential pattern with potential wells (grey) and laser lines (green). The potential depth was set to* $8k_BT$*. Red lines show the colloidal structure and the inset with the corresponding g(x,y) gives* $\xi = 0.85$ *indicating a rhombic I phase.*

of $6k_BT$ or above to a colloidal crystal of lattice constant $\boldsymbol{a} = 12.5$ µm results in the formation of a rhombic I phase. In contrast to Fig. 4.6(d,e), however, here two rows of particles are trapped within a single optical potential line where they are arranged in a zig-zag pattern due to their electrostatic repulsion. Similar to above, a change in the periodicity of the light potential will result in a square phase.

We show in a phase diagram for samples with different densities ($\rho = 0.004$ - $0.006/\,\mu m^2$), the crystal-crystal transition as a function of the substrate periodicity and potential depth. It can be seen from Fig. 4.11 that the transition to a new crystalline order was achieved through a disordered phase as it was described in the previous section.

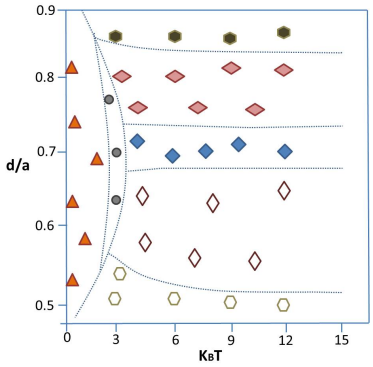

Figure 4.11: *a) Phase diagram as a function of* $\boldsymbol{d/a}$ *verses the light potential strength. For* $V_0 < 2k_BT$ *a random triangle phase exists (orange triangles). Above* $2k_BT$ *a disordered phase occurs (gray full circles) leading to ordered crystals at further higher light potentials: triangular I (full hexagons), rhombic I (full diamonds), square phase (full square), rhombic II (empty diamonds) and triangular II (empty hexagons).*

4.4 Conclusion and Outlook

We have reported on the creation of colloidal crystalline phases in one-dimensional periodic potential landscapes. In order to realize a wide range of line spacings relative to the lattice constant, we use a suspension of silica particles and bromobenzene. Because the Debye screening length of the system is about 4.6 µm it results in the formation of crystals with lattice constants up to 20 µm. In the presence of the laser pattern, the crystals are stabilized by the competition of optical and electrostatic forces and thus strongly depend on both the periodicity and the laser intensity of the light field. By using scanning optical tweezers, such potential landscapes can, in contrast to interference patterns, be controlled in situ without realignment of optical components.

As for future plans, it would be interesting to understand how would an initially formed liquid or crystal monolayer interact and evolve for a range $\boldsymbol{d/a}$ larger or smaller than that discussed above. In addition, inverse tweezing with quasiperiodic light potentials is also applicable for such colloidal systems. It would be also interesting to understand how such colloidal monolayers respond to an external one dimensional quasiperiodic ordering for a wide range of $\boldsymbol{L/a}$ and $\boldsymbol{S/a}$.

5 Phase transitions of colloidal monolayers on 1D quasiperiodic light fields

Here we report on the structural transformation of a periodic crystal induced by an external quasiperiodic order under real space conditions. This is achieved by subjecting a charge-stabilized two-dimensional colloidal monolayer to a one-dimensional quasiperiodic substrate potential. Upon increasing the laser intensity, we observe a transition from a periodic to a quasiperiodic state. Interestingly, our experiments show that this transition proceeds via the formation of an intermediate periodic average structure (PAS) which is related to the quasiperiodic lattice by a bounded 1-1 mapping [28, 29, 10]. Because PAS can transform to crystals and quasicrystals by minute particle displacements, they provide a mechanism to allow for interesting insights into the relationship between periodic and quasiperiodic order. We report on the formation of PAS in the presence of the Dodecanacci and Fibonacci light patterns for a wide range of the particle density and the substrate distance parameter S.

5.1 Motivation

Although *periodic* crystals and quasicrystals, both exhibit long-range positional order, their atomic configuration is markedly different [1]: In contrast to a periodic arrangement, quasicrystals are created by the aperiodic distribution of atoms [18, 128, 129]. In view of these striking differences regarding their intrinsic order [12], the experimental observation of phase transitions between quasicrystals and crystals (or their corresponding approximants) upon variations in temperature [130, 131, 132] or pressure [133], exposure to electron beams [134, 32] or small changes in the sample conditions [135], is surprising. In particular, it is not obvious what atomic movements are required to allow for such phase transitions. Periodic average structures (PAS) have been suggested as a possible solution to this problem because they are related to quasicrystals by a 1-1 mapping [28, 29, 136] and can provide an explanation how atoms can change between periodic and quasiperiodic positions by particle displacements smaller than the smallest atomic bond length [11]. Although numerical comparison between measured and calculated diffraction patterns provides some evidence for the occurrence of PAS [11, 130], periodic average

structures have not yet been observed in real space experiments.

5.2 Relation between crystals and quasicrystals in atomic systems

A relation between both structures has manifested itself in a variety of physical phenomena involving quasicrystal to crystal (or their approximants) transitions [137, 135, 131, 134], surface structural transitions of quasicrystals [138], or quasicrystal-crystal interfaces [139, 140]. Bendersky et al. 1987 studied the relation between the hexagonal phase of $\mu - Al_4Mn$ and the icosahedral ones. When stable icosahedral quasicyrstals were first discovered in Zn-Mg-rare earth alloys [141, 142], similarities with the hexagonal structures of a Zn-Mg-Sm alloy were observed by electron diffraction experiments [56]. This analysis shows that a twofold axis of the icosahedral phase corresponds to the sixfold axis of the hexagonal phase [143].

5.2.1 Quasicrystals to crystal transformations in metallic alloys

Quasicrystal to crystal phase transitions can occur in metallic alloys under temperature variations [144, 131, 145], pressure [133], Argon ion (Ar^+) irradiation [146, 147], e^- irradiation [134, 30], high energy ball milling [148] and slight change in composition [32]. Under any of the above mentioned conditions, transitions from 2D or 3D to 1D quasicrystals are also observed. Nature of these transitions are suggested to involve atomic diffusion along side their displacements [149, 150]. The commonly used techniques to identify phases are : X-ray diffraction (XRD), transmission electron microscopy (TEM), scanning electron microscopy (SEM) and selected area electron diffraction (SAED).

Quasicrystal-crystal transformation under temperature variations

Since the discovery of the first quasicrystal, it has been unclear whether they are thermally stable or not. But what is for sure, is that quasicrystals are susceptible to temperature variations and undergo phase transformations into their approximants, periodic crystals, or to ordered/disordered quasicrystals [150]. The procedure under which these transformations occur involves annealing, quenching, melt-spinning and other cooling techniques. These transitions obtained a general interest due to their kinetics associated with atomic diffusion and displacements [150]. In some cases a reversible phase transition is expected since the higher entropy of quasicrystals could stabilize them at higher temperatures while periodic crystals are favored at low temperatures [135]. For example, the rare earth icosahedral metal $i - ZnMgY$ shows a

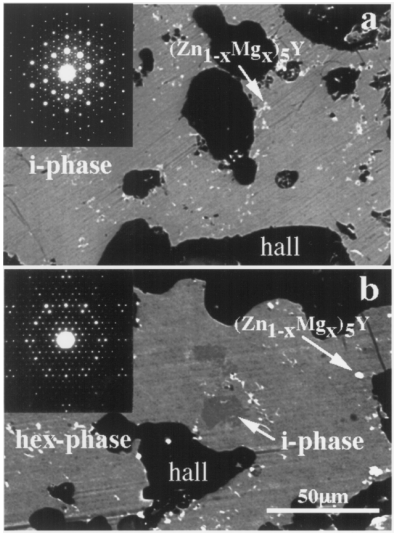

Figure 5.1: *SEM images of the two phases obtained for $Zn_{65}Mg_{25}Y_{10}$ alloy annealed at a) 873˚K for 20hr where an icosahedral phase exists and b) 773˚K for 72hr where a hexagonal phase dominates. The small white regions indicate $(Zn_{1-x}Mg_x)_5Y$ particles with $x = 0.1 - 0.2$. The inset for each figure shows the X- ray diffraction pattern of the corresponding phase [131].*

high structural perfection and stability [151, 152] more than the icosahedral aluminum alloys which are the best known stable quasicrystals. Single X-ray experiments show that $i-ZnMgRE$ has distinguished atomic structures which are significantly different from other icosahedral metallic phases [153], therefore it has been interesting to study under specific conditions, different quasicrystalline structural behavior and in particular $i-ZnMgRE$ alloys. Fig. 5.1 shows a reversible phase transition of $Zn_{65}Mg_{25}Y_{10}$ induced by subsequent annealing between $i-ZnMgY$ (20hr at 873˚K) and the hexagonal phase $h-ZnMgY$ (72hr at 773˚K) [131]. At 750˚K a coexistence phase was observed [154]. This transition is accompanied by a slight change in composition. Interestingly, the hexagonal phase is structurally related to the quasiperiodic phase and not through the latter approximants.

Radiation-induced decagonal to crystalline transformations

Even though quasicrystal-crystal transitions are smoothly induced by heat treatments (mentioned above), it is hard to draw a clear description about the phase stability due to their slow atomic diffusion at low temperatures. $Al_{62}Cu_{20}Co_{15}$ which was found by He et al. (1988) [155] to exhibit a stable decagonal structure at room temperature transforms under electron beam irradiation [156], into an fcc crystal. This type of experiment was then used

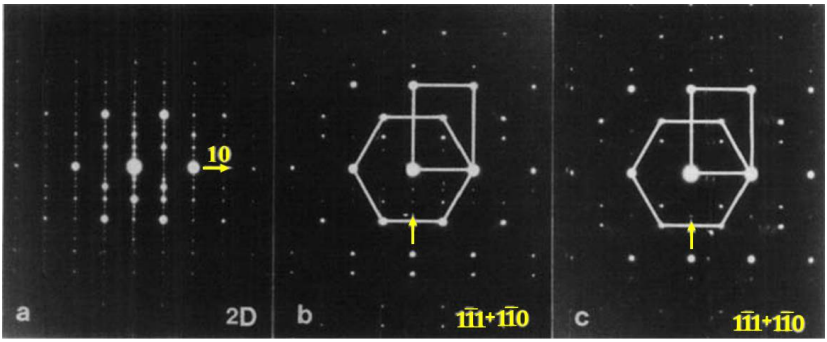

Figure 5.2: *Diffraction images along a twofold axis 2D of $Al_{62}Cu_{20}Co_{15}Si_3$, showing: a) a quasi periodic distribution of brag peaks in the direction perpendicular to the indicated arrow (without radiation), b) a bbc structure after 15 minutes of radiation, and c) a CsCl structure after 30 minutes of exposure. The latter structure is evident from the additional spots (pointed by the arrow) and can be identified as the (100) superlattice reflections of the CsCl-type ordered phase [147].*

intensively by Audier et al. 1991, Zhang et al. 1992, and J.Reyes-gasga 1993, to study at room temperature, the phase transformations of Al-Cu(CO) alloy and in particular $Al_{62}Cu_{20}Co_{15}Si_3$ [1]. This technique proved to be successful in inducing quasicrystal to crystal transitions for an electron beam operating at 400keV. This is strong enough to radiate fast particles and accelerate phase transformations by producing atomic defects which in turn act as diffusion carriers [147]. Zhang and Urban in 1992 verified by a simultaneous electron diffraction and high resolution electron microscope that $Al_{62}Cu_{20}Co_{15}Si_3$ undergoes a series of changes from decagonal to a bcc, then to a CsCl ordered structure during 30 minutes of radiation. Diffraction patterns are illustrated in Fig. 5.2 and real space images in Fig. 5.3 for two symmetrically different twofold directions. Note that the CsCl is the Cesium chloride structure and

[1] silicon atoms enhance the formation of the decagonal phase (Daulton and kelton, (1991))

can be used as a presentation of a cubic structure for a thermally stable and ordered equi-atomic alloy. It is sketched in the inset Fig. 5.3b as two simple penetrating cubic structures. In the study carried by J.Reyes-Gasga (1993)

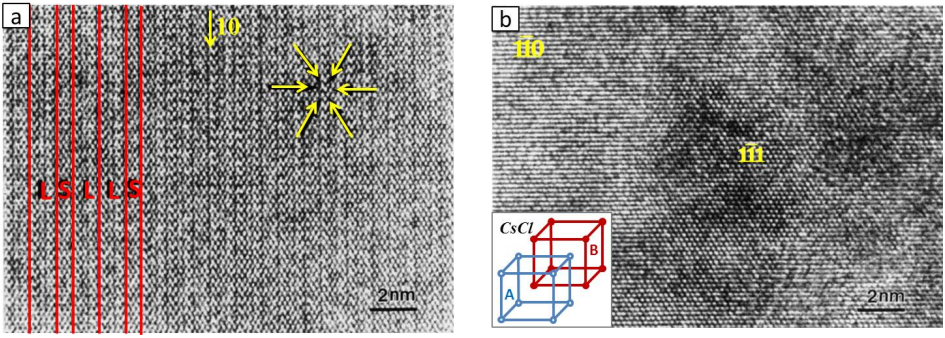

Figure 5.3: *High resolution lattice images along a twofold axis of* $Al_{62}Cu_{20}Co_{15}Si_3$. *a) a decagonal phase before irradiation where the particles form strings distributed in a Fibonacci sequence with L and S distances (red lines). An area indicated by arrows shows the pseudo-hexagonal lattice which is typically seen in such an orientation. Along the 10 fold axis a periodic stacking of layers can be recognized. b) the CsCl-ordered phase obtained after 30 minutes of bombardment, shows the coexistence of the two oriented domains* $(1\bar{1}0)$ *with parallel fringes and* $(1\bar{1}1)$ *with hexagonal lattice. The inset describes the bcc structure of CsCl as a superposition of two cubes A and B [147].*

and colleagues for $Al_{62}Cu_{20}Co_{15}Si_3$, the same phase transition, under the same irradiation technique were established within 6 minutes. And they render these transformations to the atomic displacements described by phasonic movement or flip-flop [157]. According to this model, at high temperatures atoms make displacements that are large enough to drive them smoothly into other equilibrium positions, that is to say each atom has an equilibrium position that makes a phasonic "flip-flop". This can be evident from the broad diffraction peaks observed during quasicrystal-crystal transitions [134].

5.2.2 Orientational relationship between periodic and quasiperiodic structures

As a result of the HREM, STM and X-ray diffraction experiments carried on the phase transformations of Al-Cu(Co) alloys, Song et al. figured in 1996 the relationship between the decagonal phase of $Al_{62}Cu_{20}Co_{15}$ (d-phase) and

the CsCl-type ordered structure. He compared the lattice orientation and the atomic distances along the two and tenfold axes of the *d*-phase to those in the periodic one [158]. Based on these comparisons, the CsCl-type fits nicely as the periodic average structure (PAS) of the $Al_{62}Cu_{20}Co_{15}$ decagonal quasicrystal. The PAS theory was well explained by Steurer et al. in 2000 and described as a link between periodic and quasiperiodic structures in general [150]. The PAS constitutes the core of this chapter and its extension from metallic systems into soft materials and in particular colloidal suspensions [33].

5.3 Periodic average structures in colloidal systems

In this chapter here, we experimentally demonstrate the transition between a PAS and a quasicrystal in a colloidal system under real space conditions. Such soft quasicrystals have recently received considerable attention as model systems to understand the stability and structure of quasicrystals [50, 46, 52, 49, 51]. In contrast to atomic systems, where quasiperiodic order is the result of the interatomic forces, here quasiperiodic order is imposed by an external potential acting on the colloidal particles. This allows the use of systems interacting with simple and isotropic pair potentials and thus to study the generic conditions under which such phase transitions can occur. Since most theoretical studies on PAS have been performed in one-dimensional systems [29, 10], in our experiments we consider a colloidal monolayer which is subjected to a one-dimensional quasiperiodic substrate potential. We consider a substrate potential in accordance with Dodecanacci and Fibonacci sequences as will be described in the following section.

5.3.1 Experimental materials and methods

Our experiments were performed with an aqueous suspension of highly charged polystyrene spheres with diameter $\sigma = 3.9\,\mu m$ and functionalized -COOH surface groups (Microparticles GmbH, Berlin). Gravity localizes the particles about 100 nm above the negatively charged bottom plate of the sample cell, where they form a two-dimensional monolayer with out-of-plane fluctuations less than 5% of the particle diameter. The particles interact via a screened Coulomb potential $u(r) = A \cdot \exp(-\kappa r)/r$. This type of pair potential [76] has been demonstrated to be also applicable when the particles are confined close to a wall [159, 160]. The prefactor A and the Debye screening length κ^{-1} have been determined by comparison of pair correlation functions which have been obtained experimentally and by two-dimensional numerical simulations [161] performed at the institute for computational physics (ICP, Stuttgart

University). From this, results $A \approx 10^{10}\ k_{\mathrm{B}}T \cdot \mu\mathrm{m}$ and $\kappa^{-1} = 360 \pm 40\,\mathrm{nm}$, respectively. To achieve such large screening lengths ions were removed from the sample by pumping the suspension through a circuit containing an ion exchange resin [97].

Substrate potentials with one-dimensional quasiperiodic order were created by a scanned optical line tweezer [88] which interacts with the particles due to optical gradient forces [68] and thus serves as a substrate potential [95] whose strength V_0 is set by the laser intensity I. The patterns were formed by reflection of a laser beam of a frequency doubled Nd:YAG laser ($\lambda = 532\,\mathrm{nm}$) on a single-axis galvanostatically driven mirror (Scanlab) whose position was controlled by the voltage of a programmable frequency generator. Afterwards the circular cross section of the beam is expanded to a line of 3 mm length and half width $w = 2.5\,\mu\mathrm{m}$.

Line patterns comprised of 40 parallel lines were achieved by application of appropriate signals to the mirror which result in a quasiperiodic step-wise motion of the laser line. The time duration for an entire mirror cycle was set to $T = 0.025$ s, which ensures, that the light pattern can be considered as a quasi-static potential for the colloidal particles [88]. In our experiments, we have chosen patterns corresponding to a Dodecanacci series SLLLSLLSLL... which is formed by the quasiperiodic sequence of two length scales L and S with $\mathrm{L/S} = \tau_{\mathrm{Dod}} = (1 + \sqrt{3})/2$. For further information about the Dodecanacci model and other 1D quasiperiodic sequences we refer to the literature [105, 35]. Particle positions were recorded via digital video microscopy at frame rates of 1 Hz and determined with an accuracy of about ± 50 nm by digital video microscopy. Two-dimensional particle density distributions and pair correlation functions were obtained by averaging over 1000 frames. The substrate potential is obtained from the probability distribution of a highly diluted colloidal suspension. Under equilibrium conditions, this distribution is given by the Boltzmann distribution from which the shape and the depth of the quasiperiodic substrate potential are obtained.

5.3.2 1D quasiperiodic light fields

1D quasiperiodic patterns are created with two or more length scales S and L, and have specific ratios among their lengths and frequencies. This is done by creating a wave form (Fig. 3.3d) with uneven potential steps (ΔV) by a special software (Arb Express, Textronic) or using a Lab view program and sent to the scan lab mirror. For example, a Fibonacci or a Dodecanacci line pattern requires two steps with a length ratio of $L/S = 1.62 \pm 0.05$ or 1.37 ± 0.05 respectively. We have chosen to use these two patterns in our experiments in order to study the response of the colloidal monolayer in the presence of

a quasiperiodic ordering and to mainly understand under which conditions a higher dimentional quasicrystal might be formed on a 1D quasiperiodic substrate potential.

Therefore, we design one dimensional patterns based on length distributions found in a quasiperiodic structure. The Fibonacci sequence for example, forms the basic geometry in a decagonal quasicrystal (Penrose tiling) and the Dodecanacci sequence is found in the Dodecagonal quasicrystal which has a 12-fold rotational symmetry.

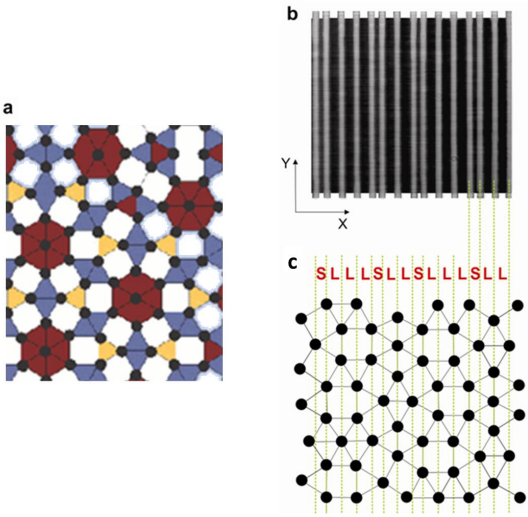

Figure 5.4: *Dodecanacci sequence model. a) Dodecagonal Square-triangle tiling with particle vertices* 3^6 *and* $3^3 \cdot 4^2$*, squares in white and triangles in blue, yellow and red. b) snap shot of the light pattern at the sample plane with high and zero intensity regions presented in white and black respectively. c) is a schematic diagram of an overlay of the light pattern (light green) and the particles (full black circles).*

Creation of the Dodecanacci light pattern

The Dodecannaci sequence we use in our experiments has been derived from a square-triangle tiling. Section 1.2.3 in chapter one explains how can this sequence be realized in a more general way. Here, we take the square-triangle tiling with particles sitting at their common vertices with 3^6 (vertex common for 6 triangles) and $3^3 \cdot 4^2$ (vertex common to 3 triangles and 2 squares) as

shown in Fig. 5.4a. Then we take the particle distribution and construct a line pattern made of two length scales L and S with $L/S = (1 + \sqrt{3})/2$ which covers 98% of the particles as shown in Fig. 5.4c. Based on this line sequence we experimentally create the wave form with corresponding potential steps and sent it to the scanning mirror. The result is a light pattern with a sequence of SLLLSLLSLL... shown in Fig. 5.4b which is a snap shot taken at the sample plane in the absence a colloidal suspension (white lines represent the high intensity regions). An infinite Dodecanacci sequence might contain 4 consecutive Ls but one of them could be exchanged with an S without interfering with the sequence order.

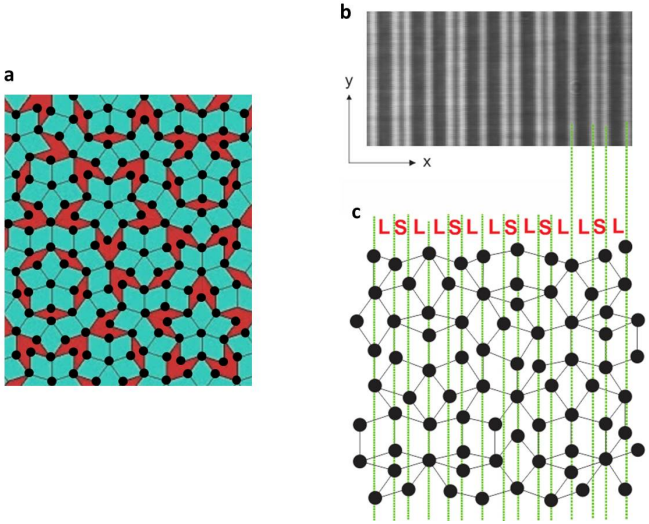

Figure 5.5: *Fibonacci sequence model. a) Penrose tiling with particle vertices (black full circles) thin and fat rhombuses in red and green respectively. b) snap shot of the light pattern at the sample plane with high and zero intensity regions presented in white and black respectively. c) is a schematic diagram of an overlay of the light pattern (green) and the particles (full black circles).*

Creation of the Fibonacci light pattern

This sequence is generated by the inflation rule (section 1.2.2) staring by one length scale L, such that $L \to LS$ and $S \to L$, therefore a sequence of LSLLSLLSLSLL... is generated with no more than two consecutive Ls. Similar

to the model approached for the Dodecanacci line pattern, a Penrose tiling made of thin and fat Rhombuses shown in Fig. 5.5a can be used as a model to construct a line pattern that tries to cover the particles sitting at the vertices. The line sequence with L and S spacings and their ratio $L/S = (1+\sqrt{5})/2$ carries about 95% of the vertices (Fig. 5.5c). Based on this model we create our Fibonacci light pattern as shown by a snap shot taken at the sample cell and illustrated in Fig. 5.5b.

5.4 Results and discussions

5.4.1 Crystal-quasicrystal transition with increasing potential depth of a Dodecanacci line pattern

Fig. 5.6 shows the particle density distribution of a colloidal monolayer in the presence of a dodecagonal line potential with L = 8.0 µm and S = 5.9 µm for increasing substrate potential strength. Particle positions have been determined by digital video microscopy. The experiment has been performed at a mean particle distance of $a = 7.2\,\mu\mathrm{m}$ ($\rho = 0.018\,\mu\mathrm{m}^{-2}$). At such particle distances, a liquid state is observed for $V_0 = 0\ k_\mathrm{B}T$ (Fig. 5.6(a)). For

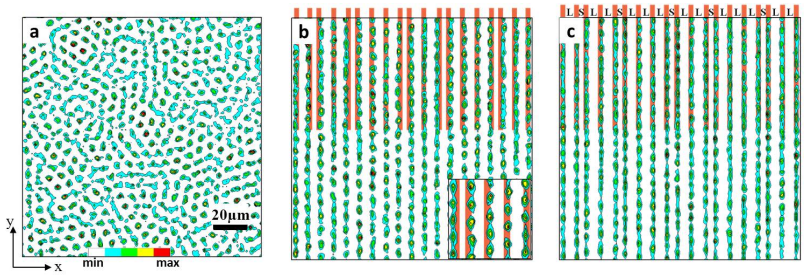

Figure 5.6: *Contour plots of the two-dimensional average colloidal density distribution in presence of a one-dimensional quasiperiodic substrate potential ($L = 8.0\,\mu m$, $S = 5.9\,\mu m$) and for increasing strength (a) $V_0 = 0\ k_BT$: isotropic liquid, (b) $V_0 = 1.2\ k_BT$: one-dimensional periodic crystal with lattice constant $d \approx 7.5\,\mu m$. The inset corresponds to a magnified area and shows how the colloidal strings are shifted in x-direction relative to the quasiperiodic substrate potential (c) $V_0 = 16\ k_BT$: one-dimensional quasicrystal. The vertical red lines correspond to the potential minima of the substrate potential (for clarity, those lines are only shown in the upper part of the figures).*

$V_0 = 1.2\ k_\mathrm{B}T$, the particles arrange in strings along the y-direction, i.e. par-

allel to the imposed quasiperiodic light potential (Fig. 5.6(b)). It should be realized, however, that the colloidal strings do not exactly follow the quasiperiodic substrate potential but are laterally shifted by $0.5-1.5\,\mu m$ (corresponding to about 20% of the mean particle distance) relative to the substrate potential. These shifts are visualized by imposing the potential minima as red lines on Fig. 5.6. Clearly, the colloids form a string pattern with *periodic* spacing with lattice constant $d \approx 7.5\,\mu m$. Only when V_0 is increased to a much higher value, i.e. 16 k_BT, the colloids resemble the quasiperiodic substrate pattern and form a one-dimensional quasicrystal (Fig. 5.6(c)). The average shift of particles in the x-direction was calculated from the average particle density distribution $\rho(d)$ which is plotted in Fig. 5.7 for several laser potential strengths. At $V_0 = 1.2\ k_BT$ (brown curve) and $V_0 = 3\ k_BT$ (blue curve) $\rho(d)$ show equidistant peaks which corresponding to colloidal strings. As V_0 increases the peaks start shifting to closer or farther distances reaching S and L at 16 k_BT respectively.

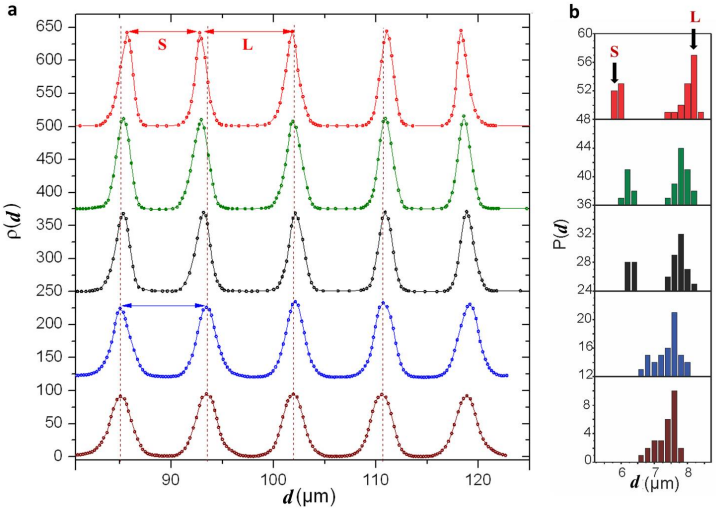

Figure 5.7: *Average particle density distribution $\rho(d)$ (a) and the line particle distance distribution $P(d)$ (b) as a function of the laser potential strength. It shows an equidistant peak-peak distance for the lowest two potential strengths $V_0 = 1.2\ k_BT$ (brown curve) and $V_0 = 3\ k_BT$ (blue curve) (dashed line presents the position for the peaks). The peaks shift from the dashed line at $V_0 = 6.5\ k_BT$ (black curve) and $V_0 = 9\ k_BT$ (green curve) till d becomes S or L at $V_0 = 16\ k_BT$ (red curve).*

The probability distributions $p(d)$ of the particle's lateral next neighbour distance d is plotted in the Fig. 5.7b. Peak to peak distance histograms for the different laser potentials of the corresponding curves are shown in a).

5.4.2 Characterization of 1D periodic structures

To understand the formation of a periodic colloidal structure in the presence of a *quasiperiodic* substrate potential, we first investigated how the spacing between colloidal strings depends on the particle number density ρ. During these experiments, the potential strength was kept at $V_0 = 1.5\ k_\mathrm{B}T$. Fig. 5.8 shows probability distributions $p(d)$ for mean particle distances $6.5\,\mu\mathrm{m} < a < 8.2\,\mu\mathrm{m}$ or densities $0.011\,\mu\mathrm{m}^{-2} < \rho < 0.022\,\mu\mathrm{m}^{-2}$. Despite some broadening

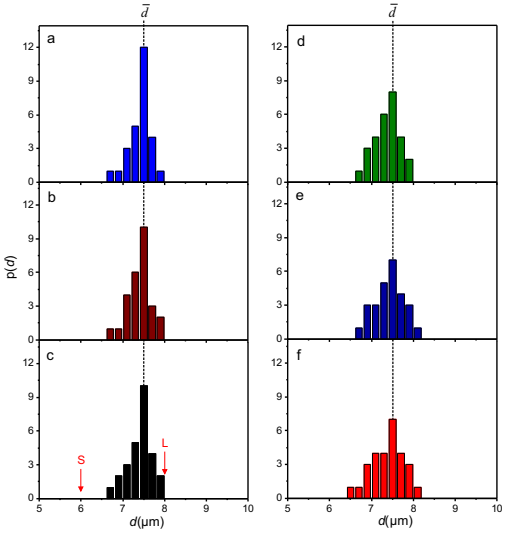

Figure 5.8: *Measured lateral distance distributions between particles in neighbouring colloidal strings for increasing mean particle distance (a) $a = 6.5\,\mu m$, (b) $6.8\,\mu m$, (c) $7.2\,\mu m$, (d) $7.6\,\mu m$, (e) $8.0\,\mu m$ to (f) $8.2\,\mu m$. The quasiperiodic light potential is set to $V_0 = 1.5\ k_BT$ with $L = 8.0\,\mu m$ and $S = 5.9\,\mu m$. Despite broadening of the distributions, the maxima, i.e. the lattice constant of the one-dimensional colloidal crystals, remains identical at $\bar{d} \approx 7.5\,\mu m$.*

of the distributions, the maxima remain at $\bar{d} = 7.5 \pm 0.1\,\mu\mathrm{m}$, independent of the particle density. This suggests, that the emerging periodic structure is not the result of particle interactions only. As will be shown in the following, the

lattice constant of the observed structures is in quantitative agreement with the PAS corresponding to the quasiperiodic substrate potential.

5.4.3 Theoretical approach for constructing periodic average strutures

Generally, quasicrystalline structures can be obtained by a lower-dimensional section of a higher-dimensional periodic crystal [13, 14, 19]. However, when such hypercrystals are projected under an oblique angle onto the physical space, this yields a discrete *periodic* structure, i.e. the periodic average structure, with lattice constant P_{av} [10] (Fig. 5.9).

Periodic average structures (PAS) of a Dodecanacci sequence

The PAS is a modification of the higher-dimensional description of incommensurately modulated structures (IMS) introduced by Janner, Janssen, and de Wolff in the 1970s [13, 14]. IMS have an aperiodic diffraction diagram with satellite peaks which can be embedded in a periodic higher-dimensional space. On transformation to physical space this leads to a periodic average structure, produced by vertical projection of oblique acceptance domains which determine the position of the atoms [162, 30]. On the other hand, the acceptance domains lead to an aperiodic sequence when cut with physical space. A shearing of the embedding space parallel to the physical space such that the acceptance domains become vertical (red bars in Fig. 5.9) leads to the standard PAS picture for quasicrystals. Now the higher-dimensional bands of the PAS are oblique (green bars). In the simple case of a one-dimensional sequence embedded periodically in two dimensional space, a square lattice is used as the support of the acceptance domains. In that case, the frequency of the tiles and their length fraction has to be equal. For the one-dimensional quasiperiodic structure discussed here and described in Fig. 5.9, this requires a rectangular lattice (See also Socolar *et. al.* [19] for the general case). The basis vector $\mathbf{d}_1$ has to be $\sqrt{2}$ longer than the basis vector $\mathbf{d}_2$, and the fraction of $N_L/N_S : L/S$ is 2. The length of the acceptance domains can be chosen as $L + S$, and the length of the tiles as L and S. The inclination angle of the supporting rectangular lattice with respect to the physical space must be then $\phi = 27.368^{\circ}$ or $arctan(\sqrt{2}/(\sqrt{3}+1))$.

Because the resulting PAS corresponds to a bounded 1-1 mapping onto the quasicrystalline structure [28], it provides a natural link between structures having periodic and quasiperiodic order. The construction of a PAS for a Dodecanacci sequence is schematically illustrated in Fig. 5.9 and demonstrates how the transition between both structures is achieved by local and minute particle displacements [11, 10, 163, 32]. The unique mapping between the

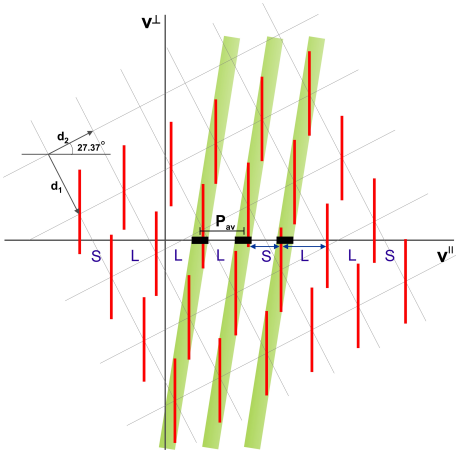

Figure 5.9: *The 2D hyperspace* $(V^{\parallel},V^{\perp})$ *is spanned by the unit vectors* $\boldsymbol{d}_1$ *and* $\boldsymbol{d}_2$ *that define a rectangular unit cell which is rotated by* $\phi = \sqrt{2}/(\sqrt{3}+1) \approx 27.37^{\circ}$. *The vector* $\boldsymbol{d}_1$ *is a factor* $\sqrt{2}$ *longer than* $\boldsymbol{d}_2$. *The Dodecanacci sequence is obtained by the intersection points of the red vertical bars (hyper-atoms) and the* $V^{\parallel}$*-axis. When the hyperatoms are projected in oblique direction on the* $V^{\parallel}$*-axis, as shown by green bars, this leads to periodically spaced regions (black bars) which constitute the corresponding one-dimensional periodic average structures with periodicity* P_{av}.

quasiperiodic sequence and the periodic average structure requires, that the number of vertices remain identical. Therefore, $(N_L + N_S)P_{\mathrm{av}} = N_L L + N_S S$ with N_{L} and N_{S} the frequency of L and S segments, respectively [10]. Because for a Dodecanacci sequence $N_L : N_S = 2\tau_{\mathrm{Dod}}$ [163], one obtains

$$P_{\mathrm{av}} = 2\mathrm{S}(2 - \tau_{\mathrm{Dod}}). \tag{5.1}$$

5.4.4 Experimental verification of periodic average structures of quasicrystals

For $\mathrm{S} = 5.9 \pm 0.1\,\mu\mathrm{m}$ this leads to $P_{\mathrm{av}} = 7.48 \pm 0.13\,\mu\mathrm{m}$ which is in excellent agreement with the lattice constant $\bar{d}$ observed in our experiments (Fig. 5.6(b), Fig. 5.8). Qualitatively, PAS formation in our experiments is the result of the combination of particle-particle and particle substrate interactions. While the pair interaction favors a uniform spacing, the light field aims to impose quasiperiodic order on the colloidal strings. Accordingly, the PAS can be considered as an intermediate phase since it requires only minimal particle displacements relative to a perfect periodic or quasiperiodic lattice. As a result, the width of the particle distance distributions $p(d)$ in a PAS should be somewhat larger than that in a conventional crystal. In addition, the symmetry of $p(d)$ will be different as shown in Fig. 5.10. While distance

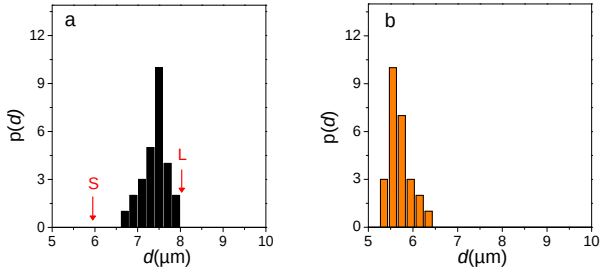

Figure 5.10: *Comparison of $p(d)$ of a PAS for $L = 8.0\,\mu m$, $S = 5.9\,\mu m$, $a = 7.2\,\mu m$ shown in a) (see also Fig. 5.8(c)), and a conventional two-dimensional colloidal crystal b), the latter formed at smaller mean particle distance $a = 6.0\,\mu m$ in the absence of a quasiperiodic substrate potential. Both structures are formed at $V_0 = 1.5\ k_B T$.*

histograms of entirely electrostatically-stabilized colloidal crystals are always strongly asymmetric and fall off more rapidly towards smaller distances due to the exponential distance dependence of $u(r)$ (Fig. 5.10b), this is not the case

in the histograms of the PAS (Fig. 5.10a and Fig. 5.8). This is because particle distances larger than L do not occur in PAS leading to a sharp cutoff in $p(d)$ towards larger distances. As a result, the skewness of the distance histograms of crystals and PAS are opposite. The complete phase behavior of a colloidal

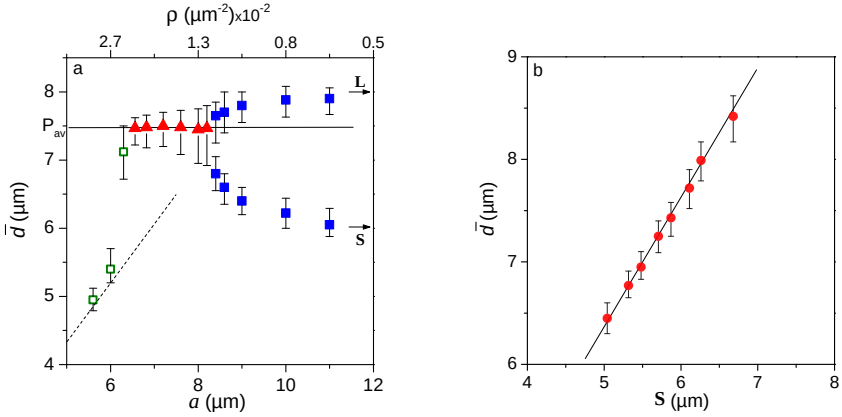

Figure 5.11: *a) Line distance $\bar{d}$ as a function of density ρ and the mean particle distance a. The parameters of the quasiperiodic substrate are $V_0 = 1.5 k_B T$, $L = 8.0\,\mu m$ and $S = 5.9\,\mu m$, respectively. With increasing particle distance (or decreasing the density) we find a triangular crystal (green squares, dashed line), a one-dimensional PAS (red triangles) and a one-dimensional quasicrystal (blue squares). The horizontal line corresponds to the predicted lattice constant of the PAS. b) Experimentally determined periodicity $\bar{d}$ of the PAS with $a = 7.4\,\mu m$ ($\rho = 0.017\,\mu m^{-2}$) as a function of the absolute length scale of the quasiperiodic sequence (red circles). The solid line is the prediction according to Eq.(5.1). The error bars correspond to the halfwidth of the line distance histograms.*

monolayer on a one-dimensional quasiperiodic substrate as a function density ρ and the mean particle distance a is shown in Fig. 5.11a. To distinguish different phases, we have used $\bar{d}$ as the order parameter. For $a \leq 6.0\,\mu m$ ($\rho \geq 0.027\,\mu m^{-2}$), the particle pair interaction is more than 50 times stronger than the substrate potential. Under such conditions, the quasiperiodic light field provides only a small perturbation and we observe an undistorted two-dimensional triangular crystal with lattice constant a which is aligned along the y-direction. Accordingly, the spacing between colloidal strings is $\bar{d} = \frac{\sqrt{3}}{2} a$ in agreement with our data (green symbols, dashed line). In the range

$6.5\,\mu m < a < 8.2\,\mu m$, i.e $0.011\,\mu m^{-2} < \rho < 0.022\,\mu m^{-2}$, the line spacing remains rather constant around $\bar{d} = 7.47\,\mu m$ (red symbols).

As already mentioned, this value agrees with the periodicity of the PAS obtained from Eq. (5.1) (horizontal line). Further increase of the particle distance to $a > 8.2\,\mu m$ finally leads to the dominance of the substrate potential and the colloids follow the quasiperiodic light potential pattern (blue symbols). Then, the histogram $p(d)$ exhibits a double-peaked structure with the peak positions approaching L and S for increasing mean particle distance. The transition between the crystal and the quasicrystal appears to be rather smooth which suggests a continuous phase transition which is consistent with the absence of hysteresis effects in our experiments. To demonstrate the robustness of PAS against variations in the length scale of the Dodecanacci sequence, we also varied L and S with $L/S = (1 + \sqrt{3})/2$ as before. This is shown in Fig. 5.11b where we plotted $\bar{d}$ vs. S for $a = 7.4\,\mu m$ ($\rho = 0.017\,\mu m^{-2}$) and $V_0 = 1.5\ k_B T$. The measured data (symbols) are in excellent agreement with Eq. (5.1) (solid line).

Periodic average structures are also predicted for other quasiperiodic symmetries [164, 10, 163]. Therefore, we performed experiments where the laser pattern was modulated according to a Fibonacci sequence ($LSLLSL...$). Here, the ratio of the length scales L/S and that of the corresponding frequencies $N_L : N_S$ is given by the golden mean $\tau_{\mathrm{F}ib} = (1+\sqrt{5})/2$. Accordingly, the periodicity of the associated PAS is given by $P_{\mathrm{av}} = (3-\tau_{\mathrm{F}ib})S$ [10]. Fig. 5.12 shows the particle density distribution of a colloidal monolayer with $a = 7.0\,\mu m$ ($\rho = 0.02\,\mu m^{-2}$) when exposed to a Fibonacci light pattern with $V_0 = 1.5\ k_B T$ and $L = 8.7\,\mu m$. Again, the colloids arrange in a periodic one-dimensional pattern with spacing $\bar{d} = 7.4\,\mu m$ which is in good agreement with the periodicity of the corresponding periodic average structure $P_{\mathrm{av}} = 7.46 \pm 0.14\,\mu m$. Due to the larger L/S ratio, the formation of PAS requires larger relative particle displacements than in the case of a Dodecanacci sequence [165]. Accordingly, the range of particle densities, where the PAS is observed is much smaller under such conditions. Although, PAS can arise for different types of line sequences, it should be realized, that it is not possible to find a PAS for any arbitrary lattice. This is easily seen by considering the example of a line distribution of two length scales L and S where $L = 3S$ and the corresponding frequencies N_L and N_S are equal. Since the number of vertices must be identical (1-1 mapping), in case there exists a PAS for this sequence, its periodicity must be $P_{av} = 2S$. This, however, would require particle shifts of $P_{av} - S = S$ which is impossible since the quasiperiodic ordering requires a bounded fluctuation of the particles about their positions. For more details see the discussions made by Aubry *et al.* [166].

The concept of PAS finds also use in higher-dimensional quasicrystalline

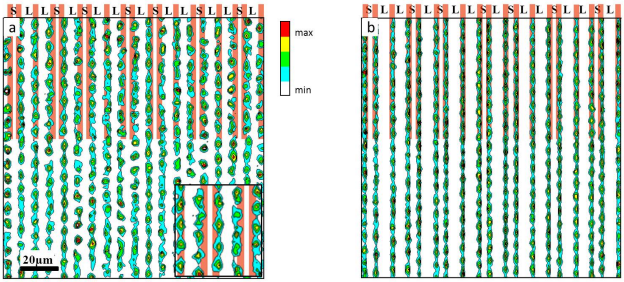

Figure 5.12: *Contour plot of the colloidal particle density in the presence of a Fibonacci sequence (vertical red lines) with $L = 8.7\,\mu m$ and potential depth a) $V_0 = 1.5\ k_BT$ where the particles rather form colloidal lines with periodic spacing $7.4\,\mu m$ which is in quantitative agreement with the periodicity of the PAS related to the Fibonacci sequence. b) V_0=16 k_BT, the particles follow the potential wells and form a quasiperiodic sequence. The inset in a) shows a magnified area.*

structures [10, 28] which can be experimentally achieved e.g. by interference of five laser beams [52]. Because in two-dimensional systems there is no simple 1-1 mapping between periodic and quasiperiodic structures[163], colloidal experimental studies will provide direct information how crystal to quasicrystal transitions are achieved under such conditions. Since the formation of PAS only requires small particle displacements, they may also form during atomic hetero-epitactic monolayers on quasicrystalline surfaces to minimize elastic strain with the substrate. Such monolayers are currently considered for the development of new materials and devices [167, 165].

Comparison between the Dodecanacci and the Fibonacci models

With such two-length scale light potentials we try to understand the effect of quasiperiodic order on 2D systems which, in principle form periodic arrangements in favour of minimal free energy. Therefore we make a comparison between the two models addressed above, based on the structural and thermodynamical properties of the decagonal and dodecagonal quasicrystals.

1. Stable Dodecagonal structure has been reported in soft matter systems [46, 49, 168, 51, 50] while decagonal structures are more frequent in hard metal systems [1]. On the other hand particles might prefer the square and triangular order since they are more stable than other geometrical configurations like pentagons and heptagons.

2. From both models, we calculate the histogram of the particle distribution in the Dodecagonal and the Decagonal tilings. Comparing the number density per line, we see from Fig. 5.13 that a Dodecanacci sequence has less discrepancies among the line pattern than the Fibonacci.

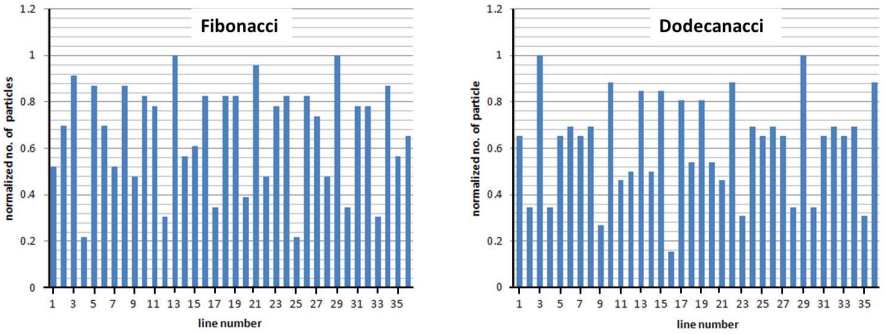

Figure 5.13: *Particle line density histograms for a) Fibonacci and b) Dodecanacci pattern of 35 lines each.*

3. The ratio of the length scales in the Dodecanacci is 1.368... which is smaller than that of the Fibonacci. This means two things: (i) $L - S$ is larger in the Fibonacci sequence and this means that achieving such spacings would require larger energies for the particles to adapt to such configuration. This can be seen during phase transformations from crystals to quasicrystals where the particles shift required for the Fibonacci is are much larger. (ii) due to experimental constrains from the laser line width which is limited to $5\,\mu m$, smaller spacing of the substrate potential cannot be achieved. In our experiments colloidal phase transformations are studied for mean particle distances ranging from 6-8 μm. For example a Fiboanacci sequence with $L = 8\,\mu m$, i.e $S = 4.9\,\mu m$ could raise experimental errors due to the potential well overlaps. Therefore a Fibonacci sequence is used for $L > 8\,\mu$m, while for the Dodecanacci a larger range of its length scales can be used.

As a result we have initiated our experimental study with the Dodecanacci light pattern and extended to other quasiperiodic ones.

5.5 Summary and outlook

In summary, our experiments demonstrate that a smooth transition between one-dimensional crystals to quasicrystals is possible by the formation of a

periodic average structure which is remarkably stable with respect to parameter variations. Obviously, the formation of PAS does not require complex or even anisotropic pair potentials as this is typically encountered in atomic quasicrystalline systems. Rather PAS can be generally expected in situations where periodic and quasiperiodic ordering principles compete against each other.

Finally, it should be mentioned, that in addition to the phases observed here, other structures can form. For example, at higher particle concentrations and smaller Debye screening lengths, phases with interstitial particle strings between the quasiperiodic lines should be observed.

6 Summary and outlook

We experimentally investigate under real space conditions, crystalline and quasicrystalline colloidal assemblies in the presence of one dimensional light field potentials. By using scanning optical tweezers, such potential landscapes can in contrast to interference patterns be controlled in situ without realignment of optical components.

In this thesis we have reported on the creation of colloidal crystalline phases in one-dimensional periodic potential landscapes. We use a suspension of silica particles and bromobenzene in order to realize a wide range of line spacings relative to the lattice constant. Such a suspension is characterized by low electrical polarity and therefore the Debye screening length of the system is about 4.6 µm. This large distance as compared to aqueous suspensions, results in the formation of crystals with lattice constants up to 20 µm. In the presence of the laser pattern, a rich variety of crystal-crystal and crystal-disordered structures are observed. The observed phases are stabilized by the competition of optical and electrostatic forces and thus strongly depend on both the periodicity and the laser intensity of the light field. As for future plans it finds use to understand how would an initially formed liquid monolayers of such a system interact with the periodic light field and evolve for a range $\boldsymbol{d/a}$ larger or smaller than that discussed here.

In the second part of the thesis our experiments demonstrate that a smooth transition between one-dimensional crystals to quasicrystals is possible by the formation of a periodic average structure (PAS) on 1D quasiperiodic substrate potential. This intermediate phase is robust with respect to parameter variations. Contrary to atomic quasicrystals, the formation of PAS does not require complex or even anisotropic pair potentials. Obviously, PAS can be generally expected in situations where periodic and quasiperiodic ordering principles compete against each other.

PAS of higher-dimensional quasicrystalline structures [28, 29, 10], can be experimentally achieved e.g. in decagoconal colloidal monolayers formed in the presence of five interfering beams. In contrast to the 1D case, two-dimensional systems have no simple 1-1 mapping between periodic and quasiperiodic structures [30], hence experimental colloidal studies will provide direct information how crystal to quasicrystal transitions are achieved under such conditions.

Finally, it should be mentioned, that in addition to the phases observed here, other structures can form. For example, at higher particle concentra-

tions and smaller Debye screening lengths, phases with interstitial particle strings between the quasiperiodic or periodic lines should be observed. In addition, inverse tweezing with quasiperiodic light potentials is also applicable for such colloidal systems. And it would be interesting to understand how such colloidal monolayers respond to an external one dimensional quasiperiodic ordering for a wide range of $\boldsymbol{L/a}$.

Acknowledgement

Deepest gratitude goes to Prof. Bechinger, whom without his continuous support and generosity this thesis would have not existed. The time he dedicated in discussions, the ideas and the lessons he taught me are priceless. His enthusiasm and interest in my projects were a driving force and huge motivation!! Above all, I am very grateful to him for giving me not only a chance to advance in the scientific field but also a life changing opportunity.

I am sincerely grateful to Dr. Jules Mikhael who has been supportive and generous during the first stage of my projects.

Special thanks goes to Dr. Thomas Bohlein who was supportive during all my PhD period. He was always present for discussions, assistance in experimental work and data analysis.

With pleasure I acknowledge Dr. Johannes Roth, Dr. Roland Roth, Prof. Christian Holm, Dr. Axel Arnold and Kai Kratzer for enriching our experimental results with their theoretical work and supporting simulations.

My gratitude goes also to those who invested time reading my thesis carefully, specially Prof. Bechinger and Prof. Hans-Reiner Trebin. In addition I am thankful to the generous colleagues who revised parts of the thesis: Daniel Hirneise, Torsten Brazda and Frank Wirner.

I thank Dr. Hans-Jürgen Kümmerer for the technical assistance and the efficiency in finding solutions for experimental problems as well as providing data analysis programs. I also Thank Uwe Rau for providing mechanical equipments for building the experimental set up and Christa Mayer for her advice and help in chemical preparations of colloidal samples.

Special thanks to Mrs. Ulrike Offenbeck who was always available for any administrative issue. Both her kindness and efficiency made handling paper work easy. She has been very supportive and encouraging through out my whole studies.

I also thank Frank Wirner, Dr. Jacob Mehl, Dr. Christian Scholz, Dr. laurent Helden, Dr. Ruben Gomez and Dr. Celia Lozano for their helpful contributions and for creating a motivating working environment.

I thank all former and new members for their contributions in one way or the other.

I would like to thank the Marie Curie Network "Comploids" for the Grant which funded the first three years in my PhD. I am very grateful for the network coordinator Prof. Christos Likos and the organizers for providing a

wonderful and rich Ph.D program which included conferences and training courses in different countries across the continent. That provided lots of opportunities to meet research fellows in the field and establish collaborations and connections.

I would like also to thank the Max Plank Institute for funding my Ph.D studies in its last stage, and providing administrative assistance.

I would like to thank my good friends Giulia Foffano, Gayatry Das, and the Lebanese people I met in Stuttgart.

Special thanks to Mrs. Elke Rahlfs whose endless support to me during my stay in Germany entitles her to be my German mother. Her generosity and kindness helped me learn and appreciate the German culture.

Finally, my endless appreciation goes to priceless parents, wonderful sister and brothers, and special friends whom their unconditional love and support carried me to this point of my life. I dedicate this thesis to my parents.

Bibliography

[1] D. Shechtman, I. Blech, D. Gratias, and J. W. Cahn, "Metallic phase with long-range orientational order and no translational symmetry," *Physical Review Letters*, vol. 53, no. 20, pp. 1951–1953, 1984.

[2] D. Levine and P. J. Steinhardt, "Quasicrystals: a new class of ordered structures," *Physical Review Letters*, vol. 53, no. 26, p. 2477, 1984.

[3] K.-h. Lin, J. C. Crocker, V. Prasad, A. Schofield, D. A. Weitz, T. Lubensky, and A. Yodh, "Entropically driven colloidal crystallization on patterned surfaces," *Physical Review Letters*, vol. 85, no. 8, p. 1770, 2000.

[4] A. Van Blaaderen, R. Ruel, and P. Wiltzius, "Template-directed colloidal crystallization," *Nature*, vol. 385, no. 6614, pp. 321–324, 1997.

[5] V. Fournée, T. Cai, A. Ross, T. A. Lograsso, J. W. Evans, and P. A. Thiel, "Nucleation and growth of ag films on a quasicrystalline alpdmn surface," *Physical Review B*, vol. 67, no. 3, p. 033406, 2003.

[6] S. Curtarolo, W. Setyawan, N. Ferralis, R. D. Diehl, and M. W. Cole, "Evolution of topological order in xe films on a quasicrystal surface," *Physical Review Letters*, vol. 95, no. 13, p. 136104, 2005.

[7] A. Chowdhury, B. J. Ackerson, and N. A. Clark, "Laser-induced freezing," *Physical Review Letters*, vol. 55, no. 8, p. 833, 1985.

[8] V. Berezinskii, "Destruction of long-range order in one-dimensional and two-dimensional systems having a continuous symmetry group i. classical systems," *Sov. Phys. JETP*, vol. 32, no. 3, pp. 493–500, 1971.

[9] Q. Lu, C. O. Reichhardt, and C. Reichhardt, "Reversible vortex ratchet effects and ordering in superconductors with simple asymmetric potential arrays," *Physical Review B*, vol. 75, no. 5, p. 054502, 2007.

[10] W. Steurer and T. Haibach, "The periodic average structure of particular quasicrystals," *Acta Crystallographica Section A: Foundations of Crystallography*, vol. 55, no. 1, pp. 48–57, 1999.

[11] M. Honal, T. Haibach, and W. Steurer, "Geometrical model of the phase transformation of decagonal al-co-ni to its periodic approximant," *Acta Crystallographica Section A: Foundations of Crystallography*, vol. 54, no. 4, pp. 374–387, 1998.

[12] D. Levine and P. J. Steinhardt, "Quasicrystals. i. definition and structure," *Physical Review B*, vol. 34, no. 2, p. 596, 1986.

[13] P. De Wolff, "The pseudo-symmetry of modulated crystal structures," *Acta Crystallographica Section A: Crystal Physics, Diffraction, Theoretical and General Crystallography*, vol. 30, no. 6, pp. 777–785, 1974.

[14] A. Janner and T. Janssen, "Symmetry of periodically distorted crystals," *Physical Review B*, vol. 15, no. 2, p. 643, 1977.

[15] A. Janner and T. Janssen, "Superspace groups," *Physica A: Statistical Mechanics and its Applications*, vol. 99, no. 1, pp. 47–76, 1979.

[16] T. Janssen, G. Chapuis, and M. De Boissieu, *Aperiodic crystals: from modulated phases to quasicrystals*. No. LCR-BOOK-2007-001, Oxford: Oxford University Press, 2007, 2007.

[17] T. Janssen, "Fifty years of aperiodic crystals," *Acta Crystallographica Section A: Foundations of Crystallography*, vol. 68, no. 6, pp. 667–674, 2012.

[18] R. Penrose, "Set of tiles for covering a surface," Jan. 9 1979. US Patent 4,133,152.

[19] J. E. Socolar and P. J. Steinhardt, "Quasicrystals. ii. unit-cell configurations," *Physical Review B*, vol. 34, no. 2, p. 617, 1986.

[20] N. De Bruijn, "Algebraic theory of penrose's non-periodic tilings of the plane. i," in *Indagationes Mathematicae (Proceedings)*, vol. 84, pp. 39–52, Elsevier, 1981.

[21] A. Herpin, P. Meriel, and J. Villain, "Structure magnetique de lalliage mnau2," *Comptes Rendus Hebdomadaires des Seances de l'Academie des Sciences*, vol. 249, no. 15, pp. 1334–1336, 1959.

[22] W. Koehler, J. Cable, E. Wollan, and M. Wilkinson, "Neutron diffraction study of magnetic ordering in thulium," *Journal of Applied Physics*, vol. 33, no. 3, pp. 1124–1125, 1962.

[23] E. Brouns, J. Visser, and P. De Wolff, "An anomaly in the crystal structure of na2co3," *Acta Crystallographica*, vol. 17, no. 5, pp. 614–614, 1964.

[24] G. Dubbledam and P. De Wolff, "The average crystal structure of-na2co3," *Acta Crystallographica Section B: Structural Crystallography and Crystal Chemistry*, vol. 25, no. 12, pp. 2665–2667, 1969.

[25] V. Daniel and H. Lipson, "An x-ray study of the dissociation of an alloy of copper, iron and nickel," *Proceedings of the Royal Society of London. Series A. Mathematical and Physical Sciences*, vol. 181, no. 987, pp. 368–378, 1943.

[26] M. Hargreaves, "Modulated structures in some copper-nickel-iron alloys," *Acta Crystallographica*, vol. 4, no. 4, pp. 301–309, 1951.

[27] H. Sato and R. S. Toth, "Effect of additional elements on the period of cuau ii and the origin of the long-period superlattice," *Physical Review*, vol. 124, no. 6, p. 1833, 1961.

[28] M. Duneau and C. Oguey, "Displacive transformations and quasicrystalline symmetries," *Journal de Physique*, vol. 51, no. 1, pp. 5–19, 1990.

[29] C. Godrèche and C. Oguey, "Construction of average lattices for quasiperiodic structures by the section method," *Journal de Physique*, vol. 51, no. 1, pp. 21–37, 1990.

[30] W. Steurer, "The quasicrystal-to-crystal transformation. i. geometrical principles," *Zeitschrift für Kristallographie*, vol. 215, p. 323, 2000.

[31] A. Baumgarte, J. Schreuer, M. Estermann, and W. Steurer, "X-ray diffraction study of decaprismatic al-co-ni crystals as a function of composition and temperature," *Philosophical Magazine A*, vol. 75, no. 6, pp. 1665–1675, 1997.

[32] M. Audier, P. Guyot, M. De Boissieu, and N. Menguy, "Crystal-to-quasicrystal transformations," *Journal of Non-Crystalline Solids*, vol. 153, pp. 591–594, 1993.

[33] L. Zaidouny, T. Bohlein, J. Roth, and C. Bechinger, "Periodic average structures of colloidal quasicrystals," *Soft matter*, vol. 10, no. 43, pp. 8705–8710, 2014.

[34] R. Penrose, "Tilings and quasi-crystals; a non-local growth problem," *Introduction to the Mathematics of Quasicrystals*, vol. 2, 1989.

[35] J. Hermisson, C. Richard, and M. Baake, "A guide to the symmetry structure of quasiperiodic tiling classes," *Journal de Physique I*, vol. 7, no. 8, pp. 1003–1018, 1997.

[36] J. E. Socolar, "Simple octagonal and dodecagonal quasicrystals," *Physical Review B*, vol. 39, no. 15, p. 10519, 1989.

[37] A.-P. Tsai, A. Inoue, and T. Masumoto, "A stable quasicrystal in al-cu-fe system," *Japanese Journal of Applied Physics*, vol. 26, no. 9A, p. L1505, 1987.

[38] A. P. Tsai, "Icosahedral clusters, icosaheral order and stability of quasicrystals-a view of metallurgy," *Sci. Technol. Adv. Mater*, vol. 9, no. 013008, p. 013008, 2008.

[39] W. Steurer, "Twenty years of structure research on quasicrystals. part i. pentagonal, octagonal, decagonal and dodecagonal quasicrystals," *Zeitschrift für Kristallographie*, vol. 219, no. 7/2004, pp. 391–446, 2004.

[40] M. de Boissieu, "Stability of quasicrystals: energy, entropy and phason modes," *Philosophical Magazine*, vol. 86, no. 6-8, pp. 1115–1122, 2006.

[41] C. Henley, "Clusters, phason elasticity and entropic stabilization: a theoretical perspective," *Philosophical Magazine*, vol. 86, no. 6-8, pp. 1123–1129, 2006.

[42] X. Zeng, G. Ungar, Y. Liu, V. Percec, A. E. Dulcey, and J. K. Hobbs, "Supramolecular dendritic liquid quasicrystals," *Nature*, vol. 428, no. 6979, pp. 157–160, 2004.

[43] A. Takano, W. Kawashima, A. Noro, Y. Isono, N. Tanaka, T. Dotera, and Y. Matsushita, "A mesoscopic archimedean tiling having a new complexity in an abc star polymer," *Journal of Polymer Science Part B: Polymer Physics*, vol. 43, no. 18, pp. 2427–2432, 2005.

[44] A. Denton and H. Löwen, "Stability of colloidal quasicrystals," *Physical Review Letters*, vol. 81, no. 2, p. 469, 1998.

[45] R. Lifshitz and H. Diamant, "Soft quasicrystals–why are they stable?," *Philosophical Magazine*, vol. 87, no. 18-21, pp. 3021–3030, 2007.

[46] K. Barkan, H. Diamant, and R. Lifshitz, "Stability of quasicrystals composed of soft isotropic particles," *Physical Review B*, vol. 83, no. 17, p. 172201, 2011.

[47] M. Engel and H.-R. Trebin, "Self-assembly of monatomic complex crystals and quasicrystals with a double-well interaction potential," *Physical Review Letters*, vol. 98, no. 22, p. 225505, 2007.

[48] G. J. Pauschenwein and G. Kahl, "Zero temperature phase diagram of the square-shoulder system," *The Journal of chemical physics*, vol. 129, no. 17, p. 174107, 2008.

[49] C. R. Iacovella, A. S. Keys, and S. C. Glotzer, "Self-assembly of soft-matter quasicrystals and their approximants," *Proceedings of the National Academy of Sciences*, vol. 108, no. 52, pp. 20935–20940, 2011.

[50] T. Dotera, T. Oshiro, and P. Ziherl, "Mosaic two-lengthscale quasicrystals," *Nature*, vol. 506, no. 7487, pp. 208–211, 2014.

[51] S. Fischer, A. Exner, K. Zielske, J. Perlich, S. Deloudi, W. Steurer, P. Lindner, and S. Förster, "Colloidal quasicrystals with 12-fold and 18-fold diffraction symmetry," *Proceedings of the National Academy of Sciences*, vol. 108, no. 5, pp. 1810–1814, 2011.

[52] J. Mikhael, J. Roth, L. Helden, and C. Bechinger, "Archimedean-like tiling on decagonal quasicrystalline surfaces," *Nature*, vol. 454, no. 7203, pp. 501–504, 2008.

[53] J. Zhang and F. S. Bates, "Dodecagonal quasicrystalline morphology in a poly (styrene-b-isoprene-b-styrene-b-ethylene oxide) tetrablock terpolymer," *Journal of the American Chemical Society*, vol. 134, no. 18, pp. 7636–7639, 2012.

[54] C. Xiao, N. Fujita, K. Miyasaka, Y. Sakamoto, and O. Terasaki, "Dodecagonal tiling in mesoporous silica," *Nature*, vol. 487, no. 7407, pp. 349–353, 2012.

[55] P. Pusey, J. Hansen, D. Levesque, and J. Zinn-Justin, "Liquids, freezing and the glass transition," 1991.

[56] H. Takakura, A. Sato, A. Yamamoto, and A. Tsai, "Crystal structure of a hexagonal phase and its relation to a quasicrystalline phase in zn-mg-y alloy," *Philosophical Magazine Letters*, vol. 78, no. 3, pp. 263–270, 1998.

[57] M. Oxborrow and C. L. Henley, "Random square-triangle tilings: A model for twelvefold-symmetric quasicrystals," *Physical Review B*, vol. 48, no. 10, p. 6966, 1993.

[58] W. Poon, "Colloids as big atoms," *Science*, vol. 304, no. 5672, pp. 830–831, 2004.

[59] D. McQuarrie, "Statistical mechanics, 1976," *Happer and Row, New York*.

[60] L. S. Ornstein and F. Zernike, "Accidental deviations of density and opalescence at the critical point of a single substance," in *Proc. Akad. Sci.(Amsterdam)*, vol. 17, p. 793, 1914.

[61] N. D. Mermin and H. Wagner, "Absence of ferromagnetism or antiferromagnetism in one-or two-dimensional isotropic heisenberg models," *Physical Review Letters*, vol. 17, no. 22, p. 1133, 1966.

[62] N. D. Mermin, "Crystalline order in two dimensions," *Physical Review*, vol. 176, no. 1, p. 250, 1968.

[63] J. M. Kosterlitz and D. J. Thouless, "Ordering, metastability and phase transitions in two-dimensional systems," *Journal of Physics C: Solid State Physics*, vol. 6, no. 7, p. 1181, 1973.

[64] J. Kosterlitz and D. Thouless, "Long range order and metastability in two dimensional solids and superfluids.(application of dislocation theory)," *Journal of Physics C: Solid State Physics*, vol. 5, no. 11, p. L124, 1972.

[65] D. R. Nelson and B. Halperin, "Dislocation-mediated melting in two dimensions," *Physical Review B*, vol. 19, no. 5, p. 2457, 1979.

[66] A. Young, "Melting and the vector coulomb gas in two dimensions," *Physical Review B*, vol. 19, no. 4, p. 1855, 1979.

[67] A. Yethiraj, "Tunable colloids: control of colloidal phase transitions with tunable interactions," *Soft Matter*, vol. 3, no. 9, pp. 1099–1115, 2007.

[68] A. Ashkin, "Optical trapping and manipulation of neutral particles using lasers," *Proceedings of the National Academy of Sciences*, vol. 94, no. 10, pp. 4853–4860, 1997.

[69] D. G. Grier, "A revolution in optical manipulation," *Nature*, vol. 424, no. 6950, pp. 810–816, 2003.

[70] C. Reichhardt and C. Olson, "Novel colloidal crystalline states on two-dimensional periodic substrates," *Physical Review Letters*, vol. 88, no. 24, p. 248301, 2002.

[71] N. Casic, N. Quintero, R. Alvarez-Nodarse, F. G. Mertens, L. Jibuti, W. Zimmermann, and T. M. Fischer, "Propulsion efficiency of a dynamic self-assembled helical ribbon," *Physical Review Letters*, vol. 110, no. 16, p. 168302, 2013.

[72] J. Ge, Y. Hu, and Y. Yin, "Highly tunable superparamagnetic colloidal photonic crystals," *Angewandte Chemie*, vol. 119, no. 39, pp. 7572–7575, 2007.

[73] V. Blickle, J. Mehl, and C. Bechinger, "Relaxation of a colloidal particle into a nonequilibrium steady state," *Physical Review E*, vol. 79, no. 6, p. 060104, 2009.

[74] C. E. Espinosa, Q. Guo, V. Singh, and S. H. Behrens, "Particle charging and charge screening in nonpolar dispersions with nonionic surfactants," *Langmuir*, vol. 26, no. 22, pp. 16941–16948, 2010.

[75] R. K. Iler *et al.*, "The chemistry of silica." John Wiley & Sons USA, 1979.

[76] E. J. W. Verwey, J. T. G. Overbeek, and J. T. G. Overbeek, *Theory of the stability of lyophobic colloids*. Courier Dover Publications, 1999.

[77] M. Brunner, C. Bechinger, W. Strepp, V. Lobaskin, and H. von Grünberg, "Density-dependent pair interactions in 2d," *EPL (Europhysics Letters)*, vol. 58, no. 6, p. 926, 2002.

[78] B. Halperin, "Physics of low-dimensional systems," *Proc. Kyoto Summer Institute*, p. 53, 1979.

[79] D. C. Nelson, DR. and L. JL, "Defect mediated phase transitions," *Academic Press, London*, vol. 7, 1983.

[80] G. Subramania, K. Constant, R. Biswas, M. Sigalas, and K.-M. Ho, "Optical photonic crystals fabricated from colloidal systems," *Applied Physics Letters*, vol. 74, no. 26, pp. 3933–3935, 1999.

[81] E. Yablonovitch, "Optics: Liquid versus photonic crystals," *Nature*, vol. 401, no. 6753, pp. 539–541, 1999.

[82] P. Tierno, T. M. Fischer, T. H. Johansen, and F. Sagués, "Colloidal assembly on magnetically vibrated stripes," *Physical Review Letters*, vol. 100, no. 14, p. 148304, 2008.

[83] M. Holgado, F. Garcia-Santamaria, A. Blanco, M. Ibisate, A. Cintas, H. Miguez, C. Serna, C. Molpeceres, J. Requena, A. Mifsud, *et al.*, "Electrophoretic deposition to control artificial opal growth," *Langmuir*, vol. 15, no. 14, pp. 4701–4704, 1999.

[84] N. Denkov, O. Velev, P. Kralchevsky, I. Ivanov, H. Yoshimura, and K. Nagayama, "Two-dimensional crystallization," 1993.

[85] P. Pusey and W. Van Megen, "Phase behaviour of concentrated suspensions of nearly hard colloidal spheres," *Nature*, vol. 320, no. 6060, pp. 340–342, 1986.

[86] Q.-H. Wei, C. Bechinger, D. Rudhardt, and P. Leiderer, "Experimental study of laser-induced melting in two-dimensional colloids," *Physical Review Letters*, vol. 81, no. 12, p. 2606, 1998.

[87] E. Frey, D. R. Nelson, and L. Radzihovsky, "Light-induced melting of colloidal crystals in two dimensions," *Physical Review Letters*, vol. 83, no. 15, p. 2977, 1999.

[88] L. Zaidouny, T. Bohlein, R. Roth, and C. Bechinger, "Light-induced phase transitions of colloidal monolayers with crystalline order," *Soft Matter*, vol. 9, no. 38, pp. 9230–9236, 2013.

[89] J. E. Curtis, B. A. Koss, and D. G. Grier, "Dynamic holographic optical tweezers," *Optics Communications*, vol. 207, no. 1, pp. 169–175, 2002.

[90] M. Mijalkov and G. Volpe, "Sorting of chiral microswimmers," *Soft Matter*, vol. 9, no. 28, pp. 6376–6381, 2013.

[91] A. Kaiser, H. Wensink, and H. Löwen, "How to capture active particles," *Physical Review Letters*, vol. 108, no. 26, p. 268307, 2012.

[92] V. Blickle and C. Bechinger, "Realization of a micrometre-sized stochastic heat engine," *Nature Physics*, vol. 8, no. 2, pp. 143–146, 2012.

[93] A. Ashkin, "Optical trapping and manipulation of neutral particles using lasers," *Proceedings of the National Academy of Sciences*, vol. 94, no. 10, pp. 4853–4860, 1997.

[94] J. Mikhael, J. Roth, L. Helden, and C. Bechinger, "Archimedean-like tiling on decagonal quasicrystalline surfaces," *Nature*, vol. 454, no. 7203, pp. 501–504, 2008.

[95] M. M. Burns, J.-M. Fournier, and J. A. Golovchenko, "Optical matter: crystallization and binding in intense optical fields," *Science*, vol. 249, no. 4970, pp. 749–754, 1990.

[96] Y. Roichman and D. Grier, "Holographic assembly of quasicrystalline photonic heterostructures," *Optics express*, vol. 13, no. 14, pp. 5434–5439, 2005.

[97] T. Palberg, W. Härtl, U. Wittig, H. Versmold, M. Würth, and E. Simnacher, "Continuous deionization of latex suspensions," *The Journal of Physical Chemistry*, vol. 96, no. 20, pp. 8180–8183, 1992.

[98] K. Loudiyi and B. J. Ackerson, "Direct observation of laser induced freezing," *Physica A: Statistical Mechanics and its Applications*, vol. 184, no. 1, pp. 1–25, 1992.

[99] J. C. Crocker and D. G. Grier, "Methods of digital video microscopy for colloidal studies," *Journal of Colloid and Interface Science*, vol. 179, no. 1, pp. 298–310, 1996.

[100] A. Ashkin, "Acceleration and trapping of particles by radiation pressure," *Physical Review Letters*, vol. 24, no. 4, p. 156, 1970.

[101] C. Bechinger and E. Frey, "Phase behaviour of colloids in confining geometry," *Journal of Physics: Condensed Matter*, vol. 13, no. 20, p. R321, 2001.

[102] K. Loudiyi and B. J. Ackerson, "Monte carlo simulation of laser induced freezing," *Physica A: Statistical Mechanics and its Applications*, vol. 184, no. 1, pp. 26–41, 1992.

[103] M. Schmiedeberg, J. Roth, and H. Stark, "Freezing and melting of a colloidal adsorbate on a 1d quasicrystalline substrate," *Physical Review Letters*, vol. 97, no. 15, p. 158304, 2006.

[104] C. Das and H. Krishnamurthy, "Laser-induced quasicrystalline order in charge-stabilized colloidal systems," *Physical Review B*, vol. 58, no. 10, p. R5889, 1998.

[105] R. Lück, "Basic ideas of ammann bar grids," *International Journal of Modern Physics B*, vol. 7, no. 06n07, pp. 1437–1453, 1993.

[106] J. Chakrabarti, H. Krishnamurthy, A. Sood, and S. Sengupta, "Reentrant melting in laser field modulated colloidal suspensions," *Physical Review Letters*, vol. 75, no. 11, p. 2232, 1995.

[107] L. Radzihovsky, E. Frey, and D. R. Nelson, "Novel phases and reentrant melting of two-dimensional colloidal crystals," *Physical Review E*, vol. 63, no. 3, p. 031503, 2001.

[108] J. Baumgartl, M. Brunner, and C. Bechinger, "Locked-floating-solid to locked-smectic transition in colloidal systems," *Physical Review Letters*, vol. 93, no. 16, p. 168301, 2004.

[109] T. Nattermann, S. Scheidl, S. E. Korshunov, and M. S. Li, "Absence of reentrance in the two-dimensional xy-model with random phase shift," *Journal de Physique I*, vol. 5, no. 5, pp. 565–572, 1995.

[110] M.-C. Cha and H. Fertig, "Disorder-induced phase transitions in two-dimensional crystals," *Physical Review Letters*, vol. 74, no. 24, p. 4867, 1995.

[111] C. Bechinger, M. Brunner, and P. Leiderer, "Phase behavior of two-dimensional colloidal systems in the presence of periodic light fields," *Physical Review Letters*, vol. 86, no. 5, p. 930, 2001.

[112] P. P. Lele and E. M. Furst, "Assemble-and-stretch method for creating two-and three-dimensional structures of anisotropic particles," *Langmuir*, vol. 25, no. 16, pp. 8875–8878, 2009.

[113] A. Yethiraj and A. van Blaaderen, "A colloidal model system with an interaction tunable from hard sphere to soft and dipolar," *Nature*, vol. 421, no. 6922, pp. 513–517, 2003.

[114] K. Mangold, P. Leiderer, and C. Bechinger, "Phase transitions of colloidal monolayers in periodic pinning arrays," *Physical Review Letters*, vol. 90, no. 15, p. 158302, 2003.

[115] M. Brunner and C. Bechinger, "Phase behavior of colloidal molecular crystals on triangular light lattices," *Physical Review Letters*, vol. 88, no. 24, p. 248302, 2002.

[116] S. H. Behrens and D. G. Grier, "The charge of glass and silica surfaces," *The Journal of Chemical Physics*, vol. 115, no. 14, pp. 6716–6721, 2001.

[117] P. Thiessen *et al.*, "Höhere und niedere kieselsäuren definierter zusammensetzung," *Zeitschrift für anorganische und allgemeine Chemie*, vol. 189, no. 1, pp. 168–173, 1930.

[118] G. Zhang and I. Hua, "The impact of particulates on the aqueous sonication of bromobenzene," *Chemosphere*, vol. 46, no. 1, pp. 59–66, 2002.

[119] P. C. Van der Hoeven and J. Lyklema, "Electrostatic stabilization in non-aqueous media," *Advances in Colloid and Interface Science*, vol. 42, pp. 205–277, 1992.

[120] R. Evans, "The nature of the liquid-vapour interface and other topics in the statistical mechanics of non-uniform, classical fluids," *Advances in Physics*, vol. 28, no. 2, pp. 143–200, 1979.

[121] R. Roth, K. Mecke, and M. Oettel, "Communication: Fundamental measure theory for hard disks: Fluid and solid," *The Journal of Chemical Physics*, vol. 136, no. 8, p. 081101, 2012.

[122] J. Hansen and I. McDonald, "Theory of simple fluids," *New York*, 1986.

[123] F. Preparata and M. Shamos, "Computational geometry springer," *New York*, 1985.

[124] J. Mikhael, G. Gera, T. Bohlein, and C. Bechinger, "Phase behavior of colloidal monolayers in quasiperiodic light fields," *Soft Matter*, vol. 7, no. 4, pp. 1352–1357, 2011.

[125] V. Volterra, "Sur l'équilibre des corps élastiques multiplement connexes," in *Annales scientifiques de l'Ecole Normale superieure*, vol. 24, pp. 401–517, Société mathématique de France, 1907.

[126] I. Guillamón, R. Córdoba, J. Sesé, J. De Teresa, M. Ibarra, S. Vieira, and H. Suderow, "Enhancement of long-range correlations in a 2d vortex lattice by an incommensurate 1d disorder potential," *Nature Physics*, 2014.

[127] D. McDermott, C. Reichhardt, and C. Reichhardt, "Stripe systems with competing interactions on quasi-one dimensional periodic substrates," *arXiv preprint arXiv:1406.0015*, 2014.

[128] C. Janot, "Quasicrystals: A primer, 1994."

[129] J. M. Dubois, "Quasicrystals," *Journal of Physics: Condensed Matter*, vol. 13, no. 34, p. 7753, 2001.

[130] K. Hiraga, W. Sun, and F. J. Lincoln, "Structural change of al-cu-co decagonal quasicrystal studied by high-resolution electron microscopy," *Japanese Journal of Applied Physics*, vol. 30, no. Part 2, No. 2B, pp. L302–L305, 1991.

[131] E. Abe and A. P. Tsai, "Quasicrystal-crystal transformation in zn-mg–rare-earth alloys," *Physical Review Letters*, vol. 83, no. 4, p. 753, 1999.

[132] M. Sanyal, V. Sahni, and G. Dey, "Evidence for endothermic quasicrystalline–crystalline phase transitions in al6cumg4," *Nature*, vol. 328, pp. 704 – 706, 1987.

[133] T. Watanuki, A. Machida, T. Ikeda, K. Aoki, H. Kaneko, T. Shobu, T. J. Sato, and A. P. Tsai, "Pressure-induced phase transitions in the cd-yb periodic approximant to a quasicrystal," *Physical Review Letters*, vol. 96, no. 10, p. 105702, 2006.

[134] J. Reyes-Gasga, G. R Garcia, and M. Jose-Yacaman, "Electron-beam-induced structure transformation of the quasicrystalline phases of the al¡ sub¿ 62¡/sub¿ cu¡ sub¿ 20¡/sub¿ co¡ sub¿ 15¡/sub¿ si¡ sub¿ 3¡/sub¿ alloy," *Radiation Physics and Chemistry*, vol. 45, no. 2, pp. 283–291, 1995.

[135] B. Grushko, D. Holland-Moritz, R. Wittmann, and G. Wilde, "Transition between periodic and quasiperiodic structures in al–ni–co," *Journal of Alloys and Compounds*, vol. 280, no. 1, pp. 215–230, 1998.

[136] W. Steurer and T. Haibach, "The periodic average structure of particular quasicrystals," *Acta Crystallographica Section A: Foundations of Crystallography*, vol. 55, no. 1, pp. 48–57, 1999.

[137] B. Grushko and D. Holland-Moritz, "Quasicrystals and related structures in al-ni-co," *Journal of Alloys and Compounds*, vol. 262, pp. 350–355, 1997.

[138] B. Bolliger, M. Erbudak, D. Vvedensky, M. Zurkirch, and A. Kortan, "Surface structural transitions on the icosahedral quasicrystal al70pd20mn10," *Physical Review Letters*, vol. 80, no. 24, p. 5369, 1998.

[139] Y. Weisskopf, S. Burkardt, M. Erbudak, and J.-N. Longchamp, "The quasicrystal–crystal interface between icosahedral al–pd–mn and deposited co: Evidence for the affinity of the quasicrystal structure to the cscl structure," *Surface Science*, vol. 601, no. 2, pp. 544–551, 2007.

[140] M. Erbudak, T. Flückiger, A. Kortan, and R. Lüscher, "Crystal-quasicrystal interfaces on al-pd-mn," *Progress in Surface Science*, vol. 75, no. 3, pp. 161–175, 2004.

[141] Z. Luo, S. Zhang, Y. Tang, and D. Zhao, "Quasicrystals in as-cast mg-zn-re alloys," *Scripta metallurgica et materialia*, vol. 28, no. 12, pp. 1513–1518, 1993.

[142] B. A. Niikura, A. Tsai, A. Inoue, and T. Masumoto, "Stable zn [sbnd] mg [sbnd] rare [sbnd] earth face-centred icosahedral alloys with pentagonal dodecahedral solidification morphology," *Philosophical magazine letters*, vol. 69, no. 6, pp. 351–355, 1994.

[143] A. Singh, E. Abe, and A. Tsai, "A hexagonal phase related to quasicrystalline phases in zn-mg-rare-earth system," *Philosophical magazine letters*, vol. 77, no. 2, pp. 95–104, 1998.

[144] A. Le Lann and J. Devaud, "Structural transformation from the alcufe icosahedral phase to the 1/1 cubic (alsi) cufe approximant phase; three dimensional models of translation defects," *The European Physical Journal B-Condensed Matter and Complex Systems*, vol. 15, no. 2, pp. 235–246, 2000.

[145] M. Döblinger, R. Wittmann, and B. Grushko, "Initial stages of the decomposition of the decagonal phase in the system al–ni–fe," *Journal of Alloys and Compounds*, vol. 360, no. 1, pp. 162–167, 2003.

[146] Y. Qin, R. Wang, Q. Wang, Y. Zhang, and C. Pan, "Ar+-ion-irradiation-induced phase transformations in an al70co15ni15 decagonal quasicrystal," *Philosophical Magazine Letters*, vol. 71, no. 2, pp. 83–90, 1995.

[147] H. Zhang and K. Urban, "Radiation-induced transformation from the decagonal quasicrystalline phase to a cscl-type phase in al-cu-co (-si)," *Philosophical Magazine Letters*, vol. 66, no. 4, pp. 209–215, 1992.

[148] N. Mukhopadhyay, G. Murthy, B. Murty, and G. Weatherly, "Transformation of the decagonal quasicrystalline phase to a b2 crystalline phase in the al-cu-co system by high-energy ball milling," *Philosophical Magazine Letters*, vol. 82, no. 7, pp. 383–392, 2002.

[149] W. Steurer, "Structural phase transitions of decagonal quasicrystals," in *MRS Proceedings*, vol. 553, p. 159, Cambridge Univ Press, 1998.

[150] W. Steurer, "Structural phase transitions from and to the quasicrystalline state," *Acta Crystallographica Section A: Foundations of Crystallography*, vol. 61, no. 1, pp. 28–38, 2004.

[151] A. Tsai, A. Niikura, A. Inoue, T. Masumoto, Y. Nishida, K. Tsuda, and M. Tanaka, "Highly ordered structure of icosahedral quasicrystals in zn-mg-re systems," *Philosophical Magazine Letters*, vol. 70, no. 3, pp. 169–175, 1994.

[152] A. Tsai, J. Guo, E. Abe, H. Takakura, and T. Sato, "Alloys: A stable binary quasicrystal," *Nature*, vol. 408, no. 6812, pp. 537–538, 2000.

[153] A. Yamamoto, "Electron density of icosahedral zn-mg-y quasicrystals determined by a six-dimensional maximum entropy method," *Philosophical Magazine Letters*, vol. 73, no. 5, pp. 247–254, 1996.

[154] A. Tsai, A. Niikura, A. Inoue, and T. Masumoto, "Stoichiometric icosahedral phase in the zn-mg-y system," *Journal of Materials Research*, vol. 12, no. 06, pp. 1468–1471, 1997.

[155] L. X. He, Y. Wu, and K. Kuo, "Decagonal quasicrystals with different periodicities along the tenfold axis in rapidly solidified al 65 cu 20 m 15 (m= mn, fe, co or ni)," *Journal of Materials Science Letters*, vol. 7, no. 12, pp. 1284–1286, 1988.

[156] Y. He, H. Chen, X. Meng, S. Poon, and G. Shiflet, "Stability investigation of a decagonal alcuco quasicrystal," *Philosophical Magazine Letters*, vol. 63, no. 4, pp. 211–216, 1991.

[157] G. Coddens, C. Soustelle, R. Bellissent, and Y. Calvayrac, "Study of phason hopping in perfect icosahedral alfecu quasi-crystals by inelastic neutron scattering," *EPL (Europhysics Letters)*, vol. 23, no. 1, p. 33, 1993.

[158] S. Song, E. Ryba, and G. Gray III, "Orientation relationship and partial lattice match between the decagonal alcocu phase and a (cscl) crystalline alco (cu) phase," *Materials Science and Engineering: A*, vol. 219, no. 1, pp. 66–70, 1996.

[159] R. R. Netz and H. Orland, "Beyond poisson-boltzmann: Fluctuation effects and correlation functions," *The European Physical Journal E*, vol. 1, no. 2-3, pp. 203–214, 2000.

[160] M. Brunner, J. Dobnikar, H.-H. von Grünberg, and C. Bechinger, "Direct measurement of three-body interactions amongst charged colloids," *Physical Review Letters*, vol. 92, no. 7, p. 078301, 2004.

[161] H.-J. Limbach, A. Arnold, B. A. Mann, and C. Holm, "Espressoan extensible simulation package for research on soft matter systems," *Computer Physics Communications*, vol. 174, no. 9, pp. 704–727, 2006.

[162] A. Yamamoto, "Crystallography of quasiperiodic crystals," *Acta Crystallographica Section A: Foundations of Crystallography*, vol. 52, no. 4, pp. 509–560, 1996.

[163] W. Steurer and S. Deloudi, *Crystallography of quasicrystals*, vol. 126. Springer, 2009.

[164] J. Wolny, "Average unit cell of the fibonacci chain," *Acta Crystallographica Section A*, vol. 54, no. 6-2, pp. 1014–1018, 1998.

[165] D. Sutter-Widmer, S. Deloudi, and W. Steurer, "Periodic average structures in phononic quasicrystals," *Philosophical Magazine*, vol. 87, no. 18-21, pp. 3095–3102, 2007.

[166] S. Aubry, C. Godrèche, and F. Vallet, "Incommensurate structure with no average lattice: an example of a one-dimensional quasicrystal," *Journal de Physique*, vol. 48, no. 3, pp. 327–334, 1987.

[167] H. Sharma, M. Shimoda, and A. Tsai, "Quasicrystal surfaces: structure and growth of atomic overlayers," *Advances in Physics*, vol. 56, no. 3, pp. 403–464, 2007.

[168] T. Asari, S. Arai, A. Takano, and Y. Matsushita, "Archimedean tiling structures from aba/cd block copolymer blends having intermolecular association with hydrogen bonding," *Macromolecules*, vol. 39, no. 6, pp. 2232–2237, 2006.